論文 / 著書情報
Article / Book Information

題目(和文)	単分子膜モットＦＥＴの作製と室温動作
Title(English)	Fabrication and operation of monolayer Mott FET at room temperature
著者(和文)	楊帆
Author(English)	Fan Yang
出典(和文)	学位:博士(理学), 学位授与機関:東京工業大学, 報告番号:甲第10694号, 授与年月日:2017年12月31日, 学位の種別:課程博士, 審査員:冨田 育義,山本 浩史,真島 豊,小泉 武昭,稲木 信介,山下 敬郎
Citation(English)	Degree:Doctor (Science), Conferring organization: Tokyo Institute of Technology, Report number:甲第10694号, Conferred date:2017/12/31, Degree Type:Course doctor, Examiner:,,,,,
学位種別(和文)	博士論文
Type(English)	Doctoral Thesis

Fabrication and operation of monolayer Mott FET at room temperature

A Doctoral Thesis

2017

Fan Yang

Department of Electronic Chemistry,
Interdisciplinary Graduate School of Science and Engineering,
Tokyo Institute of Technology

Contents

Part 1 Introduction

1.1 Organic semiconductor material 3
1.1.1 General Introduction 3
1.1.2 Organic Semiconductors 3
1.1.3 Organic Field-Effect transistors 4
1.1.4 Operation of Organic Thin Film Transistors 5
1.1.5 Performance of Organic Thin film Transistors 7
1.2 Mott Insulator and Mott FET 9
1.2.1 General introduction 9
1.2.2 Mott FET 11
1.2.3 A brief history of organic conductors 11
1.2.4 κ-type BEDT-TTF Electrolytic Crystals 17
1.3 Monolayer 21
1.3.1 Self-assembled monolayer 21
1.3.2 Langmuir-Blodgett 23
1.3.3 Conductance-controlled evaporation 23
1.3.4 Coating techniques 23
1.4 Purpose and constitution of this thesis 24
1.5 References 26

Part 2 Molecular design, synthesis and monolayer fabrication

2.1 Molecular design 29
2.2 Molecular synthesis 31
2.3 Monolayer fabrication 32
2.3.1 10^{-3} M EDT-DMT-TTF-C_9-PA solution 33
2.3.2 10^{-2} M EDT-DMT-TTF-C_9-PA solution 36
2.3.3 EDT-DMT-TTF-C_9-PA solution with TCNQ 37
2.3.4 EDT-DMT-TTF-C_9-PA solution with F_4TCNQ 39
2.4 Summary 41
2.5 Experimental section 42
2.6 References 46

Part 3 FET property without doping

3.1 FET property of monolayer device fabricated by pure solution 47
3.2 Monolayer device fabricated with TCNQ 49

3.3 Monolayer device fabricated with F_4TCNQ 51
3.4 Summary 52
3.5 Reference 52

Part 4 F4TCNQ Doping by spin coating method

4.1 Introduction 53
4.2 Doping effect on device made by donor's pure solution 53
4.2.1 Doping by 0.05 g/L F_4TCNQ solution 53
4.2.2 Doping by 0.1 g/L F_4TCNQ solution 54
4.2.3 Doping by 0.25 g/L F_4TCNQ solution 56
4.2.4 Doping by 0.5 g/L F_4TCNQ solution 59
4.2.5 Doping by 1 g/L F_4TCNQ solution 60
4.2.6 Doping by 5 g/L F_4TCNQ solution 62
4.3 Doping by 0.5 g/L F4TCNQ solution on monolayer device made with TCNQ 64
4.4 Discussion 65
4.5 Summary 69
4.6 Reference 70

Part 5 Temperature dependence

5.1 General introduction 71
5.1.1 Arrhenius plot and Meyer-Neldel rule 71
5.2 Temperature dependence 73
5.3 Results of Arrhenius plot and Meyer-Neldel rule 75
5.3.1 Results of Arrhenius plot and Meyer-Neldel rule in p-type region 75
5.3.2 Result of Arrhenius plot and Meyer-Neldel rule in n-type region 77
5.3.3 Activation energy and conductivity limit 79
5.4 Discussion 81
5.5 Summary 83
5.6 Reference 84

Part 6 Concluding remarks

List of publications **87**

Acknowledgement **88**

Part 1 Introduction

1.1 Organic semiconductor material

1.1.1 General Introduction

In the past decades, human life has been revolutionary changed by application of semiconductors. Moore's law successfully predicted development of semiconductor industry in the past half-century. By reducing the size of basic electronic devices, improvements in switching speed, density, functionality was realized. For every 18 to 24 months, the number of transistors in an integrated circuit has doubled approximately. After half-century of clockwork, Moore's law finally has come close to the theoretical limit[10].

On the other hand, mass production of inorganic semiconductors requires highly-energy consuming manufacturing process, harsh production conditions and huge investment in equipment. In order to address these issues, developments of new materials, new structures, new production processes and even new semiconductor device-working mechanisms are being seriously discussed. Organic materials are expected to raise new possibilities by creating new opportunities such as flexible and light-weight electronics, bio-adaptive electronics, and nano-scale molecular electronics.

1.1.2 *Organic Semiconductors*

In the year 2000 three professors who studied conductive polymers were awarded Nobel Prize in Chemistry, as their research stimulated long-time study of organic electronics. Semiconductor properties could be observed on organic small molecule or polymer with π-conjugated structure. Inorganic semiconductor materials are assembled together by covalent bond between atoms, holding the material together tightly. On the other hand, organic semiconductor materials only have weak van der Waals interaction between molecules. This difference makes organic semiconductors soft and special materials, which is different from inorganic counterparts. Such a property brings about relatively low mobility and sensitivity against water and oxygen at the same time.

However, organic semiconductor materials can be much more diverse in our life compared to inorganic ones, even though the performance at present cannot be compared to those of inorganics. Advantages of organic semiconductor lie in its flexibility, low-weight and suitable for large area mass production. These factors make

them potentially favorable to replace inorganic materials in some application areas.

Some of organic semiconductors devices have already been commercially used widely, such as the AMOLED screen in large-screen smart cellular phones. Take the advantages of Organic Light-Emitting Diode (OLED), low power consumption and designed flexible screen makes it very popular among customers.

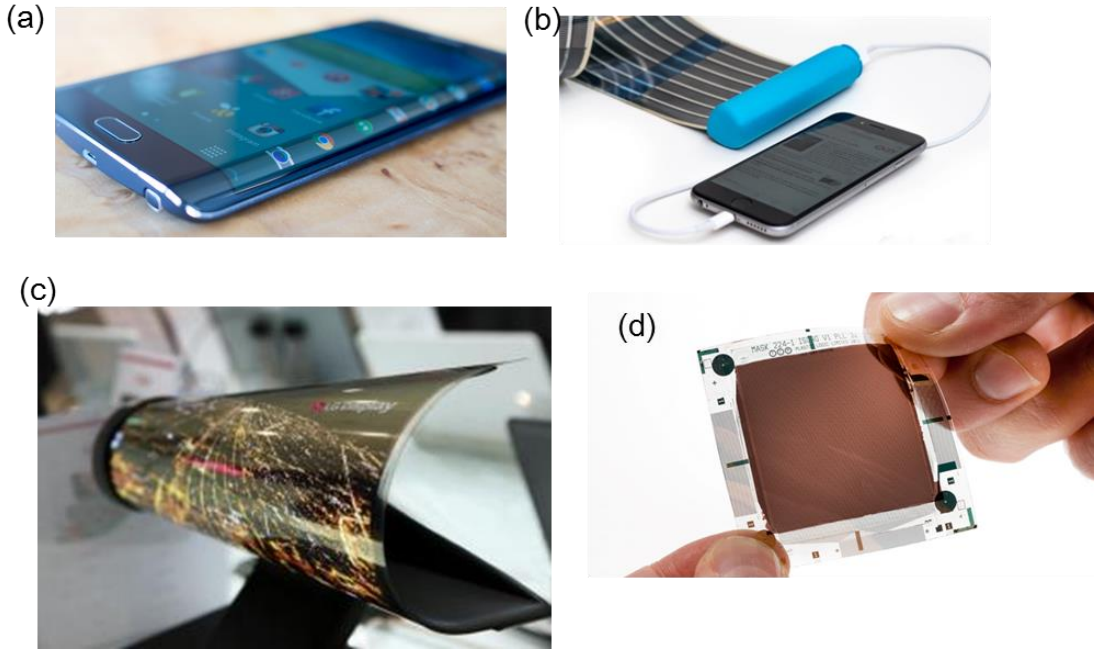

Figure 1.1.2.1: (a) Samsung Galaxy Note Edge smart cell phone, which have an OLED flexible screen bending at the edge of the cell phone. (b) HeLi-on solar charger made by infinityPV, which has a printed organic solar cell. (c) LGD 18" rollable OLED television prototype showed in CES2016. (d) Organic image sensor on plastic developed by ISORG and Plastic logic.

1.1.3 Organic Field-Effect transistors

Generally speaking, Field-effect transistor (FET) is a type of switching device with 3 electrodes, *i.e.* source, drain and gate. By modifying the gate voltage, the on and off state of the device can be controlled. As the name implies, OFET (= Organic FET) is kind of FET device using organic materials as active material. Study on field effect of organic materials started no later than 1960s[11] but not until 1980s FET device based on organic materials became reality. Ebisawa *et al*[12] and Kudo *et al*[13] reported field effect properties on polyacetylene/polysiloxane interface and merocyanine dyes, respectively. Soon, in the year 1986 Tsumura *et al*[14] at Mitsubishi Chemical reported the first OFET

device using polythiophenes. Tang *et al* reported an organic hetero-junction solar cell[15] in the same year, followed by the study of an organic light emitting diode in the next year.[16]

These breakthroughs on organic electronics draw researchers' much attention, and until now, vast amount of reports of new compounds and new fabrication processes have been reported.[17] The advantages and application prospects are making them competitive with inorganic thin film transistors

Most OFETs are designed based on the structure of thin film transistor (TFT) which was first introduced by Weimer in 1962[18]. Structure is shown in figure 1.1.3.1. For both top contact type and bottom contact type devices, source and drain electrodes contact the organic conducting channel directly to form ohmic contacts (when energy levels are matching). This type of bottom-gate transistor is the most commonly used structure for OTFTs. For top-contact case, deposition of organic semiconductor layer is followed by those for source and drain electrode. For bottom-contact case, they come for an opposite order as electrodes come first and semiconductor layer follows. The substrates are not limited to hard and flat ones. Flexible substrates can also be used in this type of device.

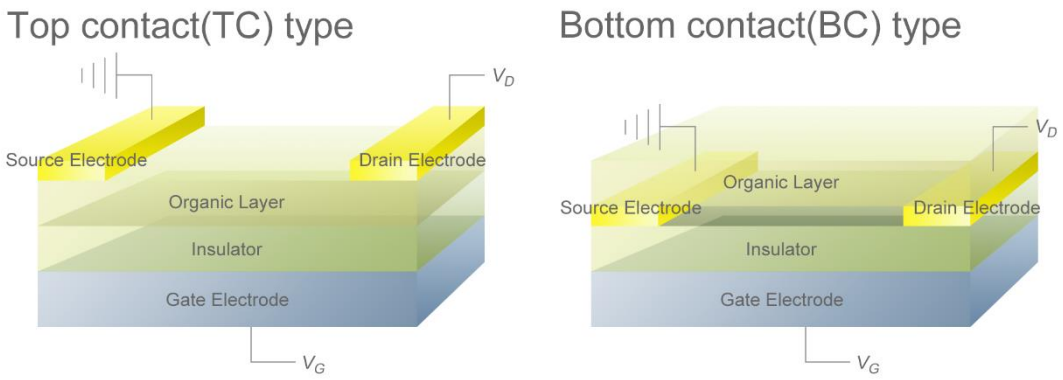

Figure 1.1.3.1: Structure of top contact type and bottom contact type organic thin film transistors.

1.1.4 Operation of Organic Thin Film Transistors

Besides grounded source electrode, there are 2 electrodes left to modify operation of OTFT. The most important one is a gate electrode which controls the "on" and "off" state of the device by applying a gate voltage. When the device is at "off" state, current cannot flow between source electrode and drain electrode. When the device is turned "on", current flows through the semiconductor channel. The working mechanism for a normal OFET device is explained in figure 1.1.4.1 by electronic energy level diagrams.

At first, HOMO (Highest occupied molecular orbital) and LUMO (lowest unoccupied molecular orbital) of the organic semiconductor channel are located at their original levels when no gate voltage applied. No carriers are accumulated in the channel so that no current would be induced even if the drain voltage was applied. On the other hand, for p-type semiconductor materials, when negative gate voltage was applied on the gate electrode, electric field at the interface between organic semiconductor and insulator layer will shift the HOMO and LUMO levels up, relatively to the Fermi level. If the applied gate voltage is large enough to shift the HOMO level close to a resonance with the Fermi level electrons in the electrodes, then holes can flow from HOMO to the drain electrode and current flows when voltage applied on drain electrode. For n-type semiconductor materials, since the carriers are electrons with negative charge, positive gate voltage should be applied and LUMO will be lifted down. Then the electrons flow from LUMO to drain electrode. Notice that carriers always flow from source electrode to drain electrode regardless of the type of carriers. However, this is a very simplified

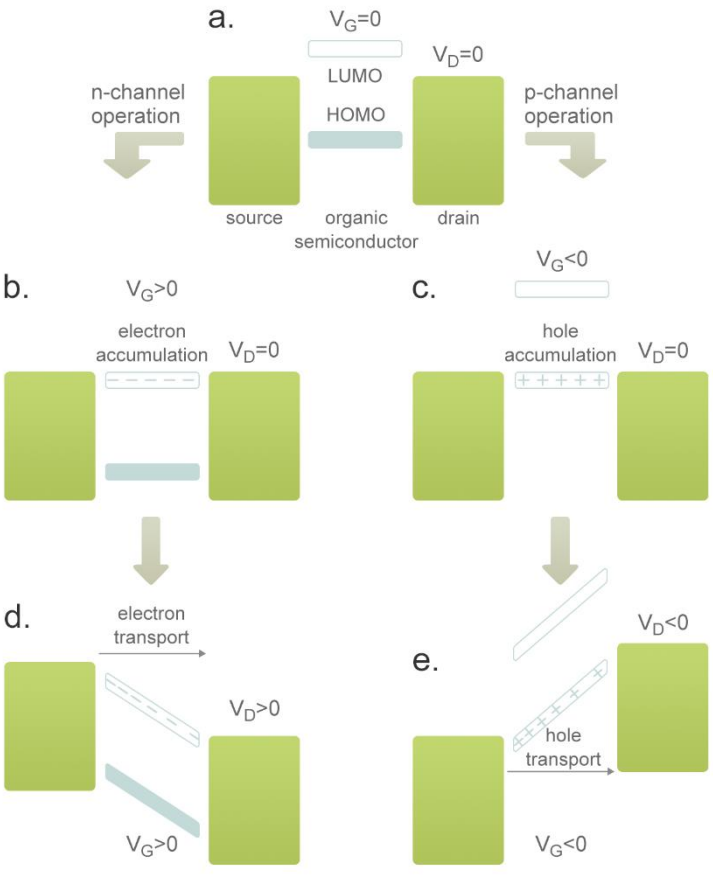

Figure 1.1.4.1: (a) Idealized energy diagram of OFET at $V_G = V_D = 0$. (b) At $V_G > 0$ and $V_D = 0$ (c) At $V_G > 0$ and $V_D > 0$ (d) at $V_G < 0$ and $V_D = 0$ (e) at $V_G < 0$ and $V_D < 0$.

explanation for ideal cases of normal OFETs based on semiconductor materials and cannot not fully explain other type of organic FETs such as Mott FETs.

1.1.5 Performance of Organic Thin film Transistors

In a given FET device, performance such as mobility and threshold voltage can be influenced by many factors, both intrinsic and extrinsic ones. The performance could be influenced by device structure, electrode configuration, insulating layer quality, fabrication process, and so on.

When gate voltage V_G was applied, carriers are accumulated at the interface between the semiconductor and the insulating layer, forming a channel with p- or n-type carriers. The existence of this channel will decrease the resistance between source and drain electrodes. When $V_G > V_{th}$, this channel will become conductive, and application of drain voltage V_D will induce source-drain current described as:

$$I_D = \frac{WC_i\mu}{L}\left\{(V_G - V_{th})V_D - \frac{V_D^2}{2}\right\} \quad (1)$$

where W is channel width, L is channel length, C_i is the capacitance of the unit-area insulating layer, μ is the field-effect mobility and V_{th} is threshold voltage for the measured device, as shown in figure 1.4.1 a. At this region, an increase of drain voltage V_D will induce the increase of drain current I_D. Field-effect mobility μ can be calculated with this equation.

However, when V_D becomes high enough to satisfy a condition$V_G - V_{th} < V_D$, pinch-off occurs (figure 1.1.4.1 b) and I_D will not increase anymore. Then, the field-induced current can be rewritten as:

$$I_D = \frac{WC_i\mu}{2L}(V_G - V_{th})^2 \quad (2)$$

In this equation, the drain current I_D has no relationship with drain voltage V_D and shows a constant value for a constant gate voltage V_D. This state is called saturation regime. Field-effect mobility μ for this region could be calculated with this equation. Different equations can be applied for two different regions to calculate the field-effect mobility μ in two ways for a given single devices.

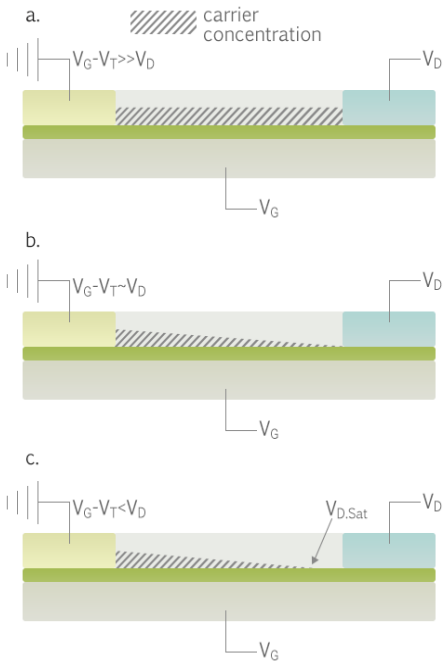

Figure 1.1.4.1: (a) Carrier concentration profile of OFET in the linear regime. (b) Pinch-off occurs when V_D~V_G-V_{th} (c) Carrier concentration profile of OFET in the saturation regime.

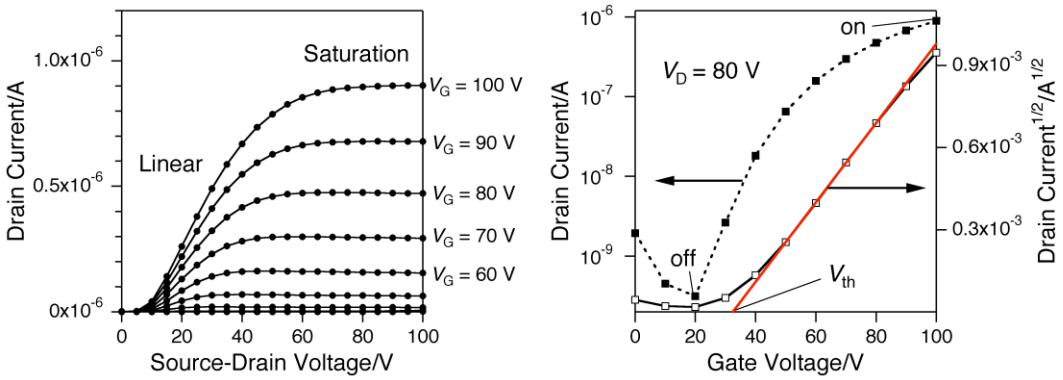

Figure 1.1.4.2: Output characteristics curves (left) and transfer characteristics (right) for a typical OFET device.

1.2 Mott Insulator and Mott FET

1.2.1 General introduction

Band theory explained and predicted the difference among metal, semiconductor and insulator (figure 1.2.1.1). However, some materials that are predicted to be metal are known to experimentally show an insulating behavior. For example, in CoO (Cobalt(II) oxide), the number of outer electrons for cobalt and oxygen atoms are 9 and 6, respectively. For CoO molecule, with 15 outer electrons, it should be a metal under an assumption of band theory since the highest energy band is half-filled. But in reality, it shows insulator behavior upon cooling. This unexpected phenomenon in terms of band theory was explained by *Nevill Mott* in 1937[19] , by an adjunction of the Coulomb interaction between electrons which is expected to be well screened in the band theory. This type of materials were named after *Nevill Mott* and called Mott insulator. Generally speaking, when the Coulomb repulsion is large enough to create an energy gap so called Mott-Hubbard gap in a half-filled band, a material will become a Mott insulator.

As shown in figure 1.2.1.1, the overlapping modes between valence band and conduction band will make a difference among metal, semiconductor and insulators. In a Mott insulator case, due to the Coulomb repulsion *U*, a half-filled conduction band is separated into empty UHB (upper Hubbard band) and filled LHB (lower Hubbard band) (figure 1.2.1.2). Electrons cannot move from LHB to UHB without additional energy. But if a doping to a Mott insulator material is done, it will become metallic. And a change of a band structure should be observed since the Coulomb repulsion is effectively reduced by incommensurate charge filling. In an ideal case, A FET device

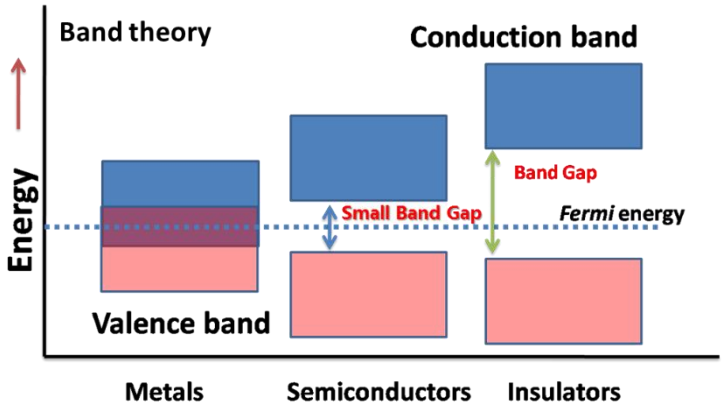

Figure 1.2.1.1: Differences between Metals, semiconductors and insulators according to band theory.

made of Mott insulator can theoretically be transferred between insulator and metal by applying gate voltage.

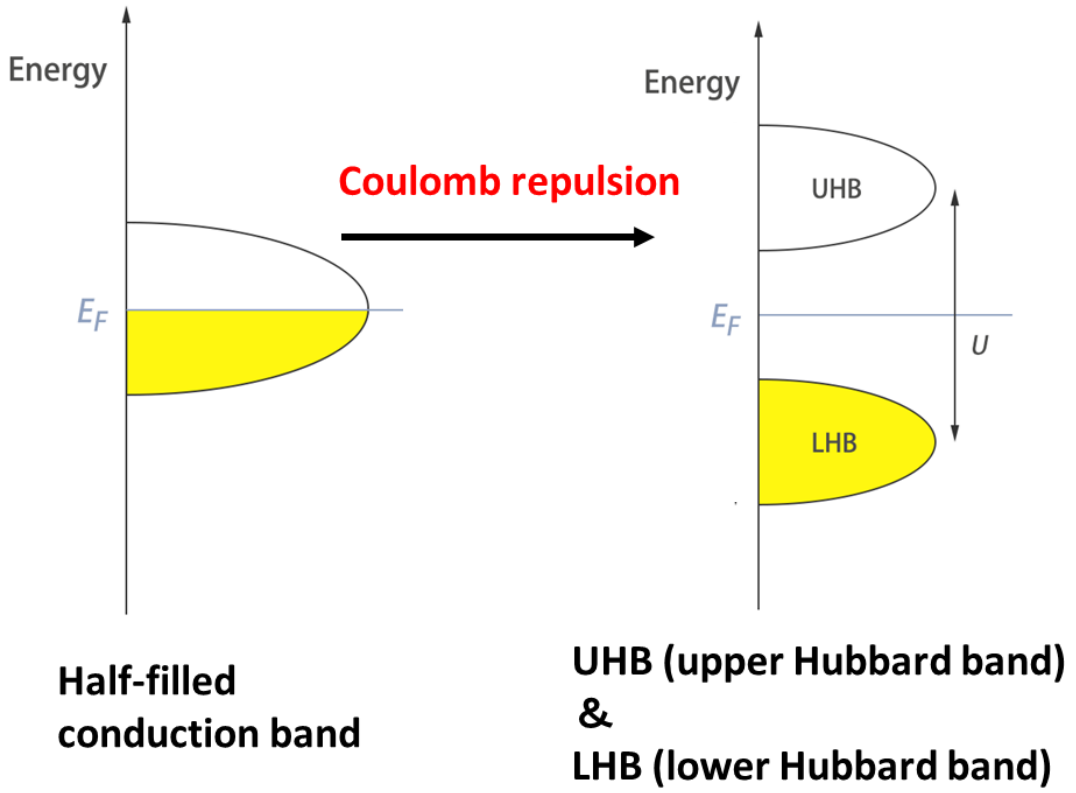

Figure 1.2.1.2: Half-filled conduction band separates into upper Hubbard band and lower Hubbard band because of Coulomb repulsion, creating Mott insulator.

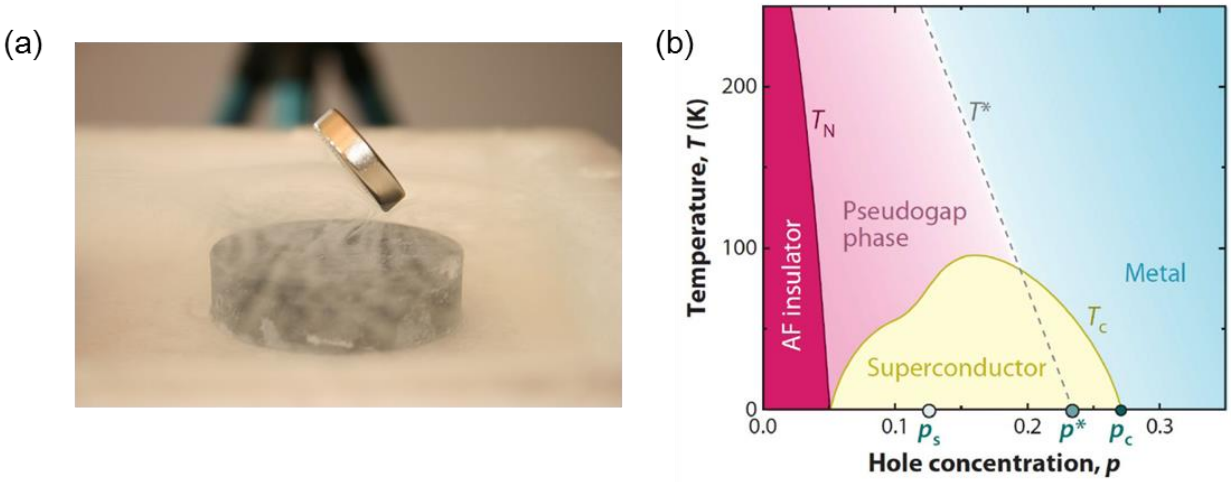

Figure 1.2.1.3: a) Superconducting Maglev of YBCO. b) Phase diagram of YBCO[1].

On the other hand, Mott insulators such as YBCO ($YBa_2Cu_3O_{(7-x)}$) is a high-temperature superconductor with critical temperature (T_c) over 77 K[20], which is exceeding the boil point of liquid nitrogen. This critical temperature is higher than McMillan limit 39 K[21] which is the theoretical limit of the critical temperature allowed by BCS theory (Bardeen–Cooper–Schrieffer theory). By controlling the amount of oxygen dopants, this inorganic Mott insulator can turn into metal, insulator or superconductor. But the mechanism of this superconductivity is still remain unknown even a lot of superconductors with much higher T_c have already been fabricated and reported. The research on Mott insulator itself is also very important in order to find the proper theory to explain the mechanism of this type of superconductivity and to guide further research.

1.2.2 Mott FET

Mott FET is a FET-like switching device using Mott insulator materials instead of traditional semiconductor materials. Theoretically, a Mott FET device channel is insulator at "off" state and transfers into metal at "on" state by different concentration of electron doping. Since both holes and electrons flows when a Mott FET device is turned "on", a typical Mott FET should be ambipolar. With different conducting mechanism, Mott FET hopefully overcomes the theoretical limits of normal semiconductor materials such as short channel effects, dopant number fluctuations, and tunneling effect[22,23,24,25]. In Mott FETs, these demerits of semiconductor might not exist anymore. It is possible to reach a channel length less than 10 nm and sub-threshold swing less than 60 mV $decade^{-1}$ without facing fundamental theory problems, as is the case with TFET (Tunneling field-effect transistor). Notice that Intel has been stopped at 14 nm node in its ultra-fine process for over 3 years since Jan. 2014. Research on FET devices with new conducting mechanism is very important if we want to extend Moore's law one more second.

Newns *et al.* have successfully fabricated a prototype Mott FET with $Y_{1-x}Pr_xBa_2Cu_3O_{7-\delta}$ (YPBCO) with STO (Strontium titanate) dielectric layer on an Nb doped STO substrate[26]. Iwasa *et al.* also reported a prototype Mott FET by VO_2, where metal-insulator transition was achieved by applying gate voltage.[27]

1.2.3 A brief history of organic conductors

Early study of organic conductor has been done by Eley and Vartanian in 1948 on phthalocyanine compounds. In 1954, Inokuchi, Matsunaga and Akamatsu reported

perylene–bromine complex with resistivity of only 10 Ω·cm, which is very close to the resistivity of inorganic semiconductors such as Ge. Since then, carrier doping by oxidation or reduction of π-electronic compounds became a hot research topic.

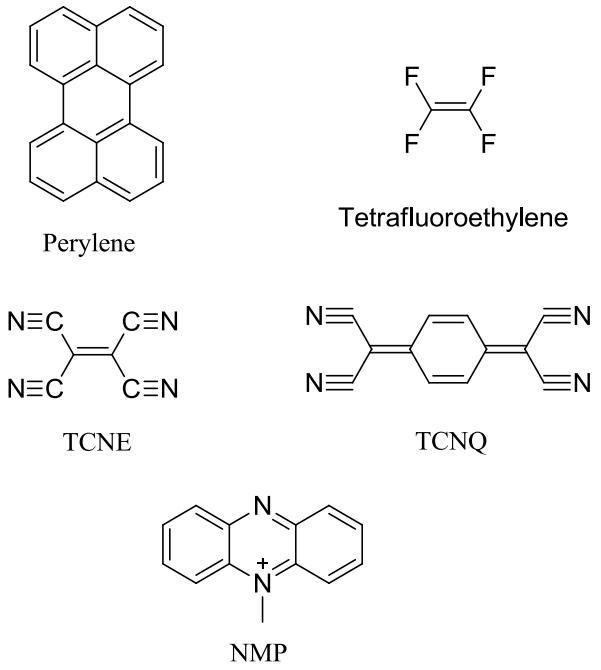

Figure1.2.3.1: Molecular structures of perylene, tetrafluoroethylene, TCNE, TCNQ and NMP. (= N-Methyle….)

Apart from molecular conductivity, studies on tetrafluoroethylene analogues were quite active after commercial success of DuPont who synthesized Telfon® from this molecule. Since halogen atoms work as electron-withdrawing groups, chemists tried its substitution by another well-known electron-withdrawing group, cyano group. Attempts to use four cyano groups instead of four fluorine atoms in tetrafluoroethylene led to the design of TCNE (Tetracyanoethylene or Ethenetetracarbonitrile). However the result of polymerization was not as successful as tetrafluoroethylene. Further attempt is to insert a benzene ring into the position of the carbon-carbon double bond to get TCNQ (7,7,8,8-tetracyanoquinodimethane)[28]. For DuPont, either of those works were not successful because TCNE or TCNQ did not give polymers that work like Telfon®. But it was a big surprise for scientists to observe the electronic activities of these molecules. TCNQ molecule contains 4 cyano groups and shows strong electron accepting behavior. Mixing TCNQ with electron donating compounds will induce charge-transfer and results in high-conductivity material whose resistivity is comparable to or even less than perylene–bromine complex. For instance, NMP-TCNQ (N-methyl-phenazinium-7,7,8,8,-tetracyanoquinodimethanide) exhibits conductivity

as high as 200 S/cm with a metallic behavior from room temperature to about 200 K[29].

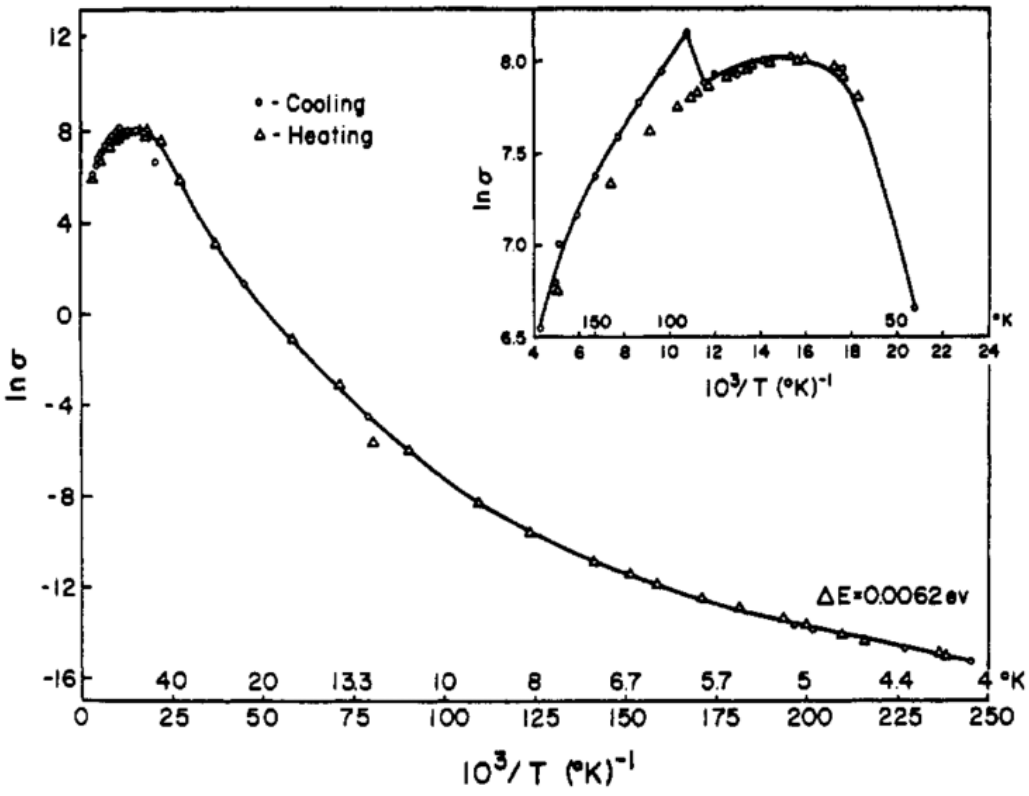

Figure 1.2.3.2: Temperature dependent conductivity of TTF-TCNQ charge transfer complex[4].

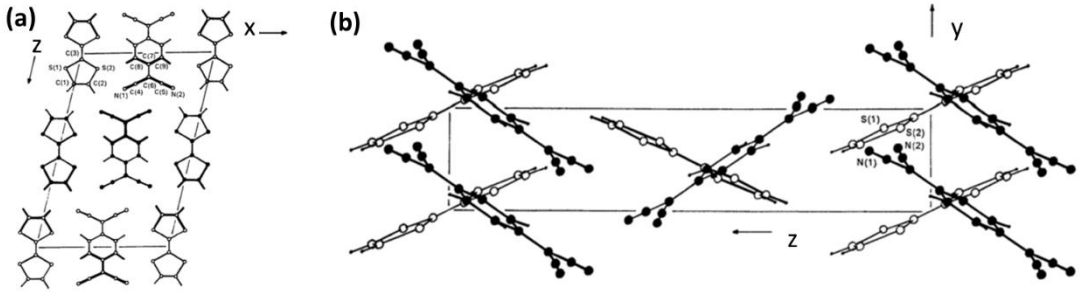

Figure 1.2.3.3: Single crystal structure of TTF-TCNQ. a) A view along y axis. b) A view along x axis. Both TTF and TCNQ showed one-dimensional stacking independently in single crystal.[7]

Back to 1957, BCS theory (Bardeen–Cooper–Schrieffer theory) explained the mechanism of superconductivity by introducing the idea of Copper pair (or BCS pair) which is produced by electron-phonon interaction[30]. An electron in crystal lattice will gather a little positive charges nearby and this charge will attract another electron with opposite spin and bound them together to form a so called Copper pair under very low temperature. All the pairs have the same total momentum and travel in the whole material without energy consumption. The BCS theory successfully predicted a relationship between superconducting transition temperature T_c and atomic mass, known as

$$T_2/T_1 = \sqrt{M_1/M_2}$$

Where M_1, M_2 are ionic masses and T_1, T_2 are critical temperatures. An obvious conclusion of this equation indicate that lighter mass will result in relatively higher critical temperature.

These facts led to a suggestion that conduction carriers in an organic conductor with surrounding electrons that can move perpendicular to the carrier motion will attract each other to form Cooper pairs. This idea is theoretically discussed by W. A. Little[31]. If this idea works, superconductivity will appear at high temperature because electron mass is much smaller than those of ions in any ordinary superconductors. Unfortunately, there is no proper material found until now, but his idea has stimulated many organic chemists and made them try to synthesize candidate materials.

The research on TTF (Tetrathiafulvalene) started in 1972, when F. Wudl *et al* reported a resistivity of about 10^{12} Ω·cm on neutral TTF under room temperature[32]. This value is far better than the resistivity of anthracene which is 10^{22} Ω • cm and ferrocene which is 10^{14} Ω·cm. Later research discovered that TTF·Cl is an excellent organic semiconductor at room temperature with a resistivity of only 3.7±1 Ω·cm. From then on, different TTF salts were synthesized and measured.

When TTF was mixed with TCNQ, TTF molecules hand over electrons to the TCNQ molecules and form TTF·TCNQ charge transfer salt. This salt was found to be a good conductor[4]. In the crystal, both TTF and TCNQ form one-dimensional conducting column independently. Each molecule forms a very simple one-dimensional π-stacking structure. Surprisingly, this type of crystal showed metallic behavior over a wide range of temperature. At the beginning, superconducting behavior was expected to some extent because this type of material has almost the same structure as Little's design. Unfortunately, however, TTF-TCNQ charge-transfer complex turned into insulator when temperature was decreased to about 60 K. Later research attribute this metal-insulator transition to Peierls distortion which is typical phenomenon for one-dimensional conductors.

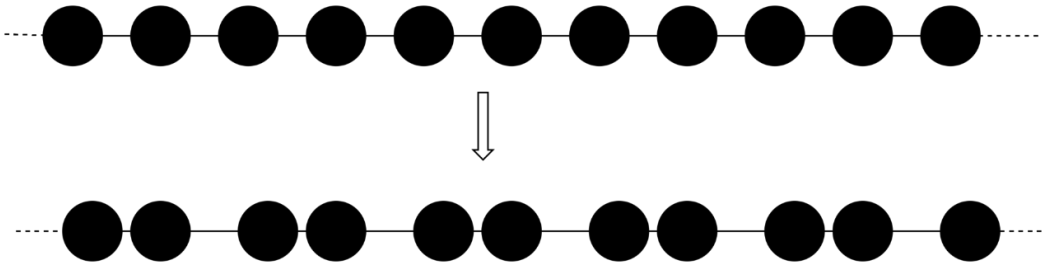

Figure 1.2.3.4: A brief scheme of Peierls distortion along one-dimensional chain. Filled black circle stands for crystal lattice. At first, each lattic have the same distance from neighboring one. If Peierls distortion occurs, dimerization of lattice will make crystal lattice far from eachother and this disorder will create insulator phase.

R. Peierls asserted in 1930s that a metallic state in one-dimensional equally spaced chain is unstable. In TTF-TCNQ, molecules in the crystal rearrange slightly and result in distortion to form a new band gap. Then, energy is required for the carrier transport, creating an insulating phase.

TTF is so excellent that a lot of scientists are fascinated in it. TTF-TCNQ showed a spontaneous charge-transfer without external aids. On the other hand, scientists also found it possible to make charge-transfer crystal with different anions under electrochemical process which lead to another series of organic conductors. Some of donor molecules are oxidized while others remain neutral. Most of the case they are forming oligomers to share the charge and lattice, as can be presented as $D^{+}+nD^{0}\rightarrow D_{n+1}^{+}$. These are so called mix-valent salts and this type of material is still under intense research as molecular conductors like κ-type BEDT-TTF crystals.

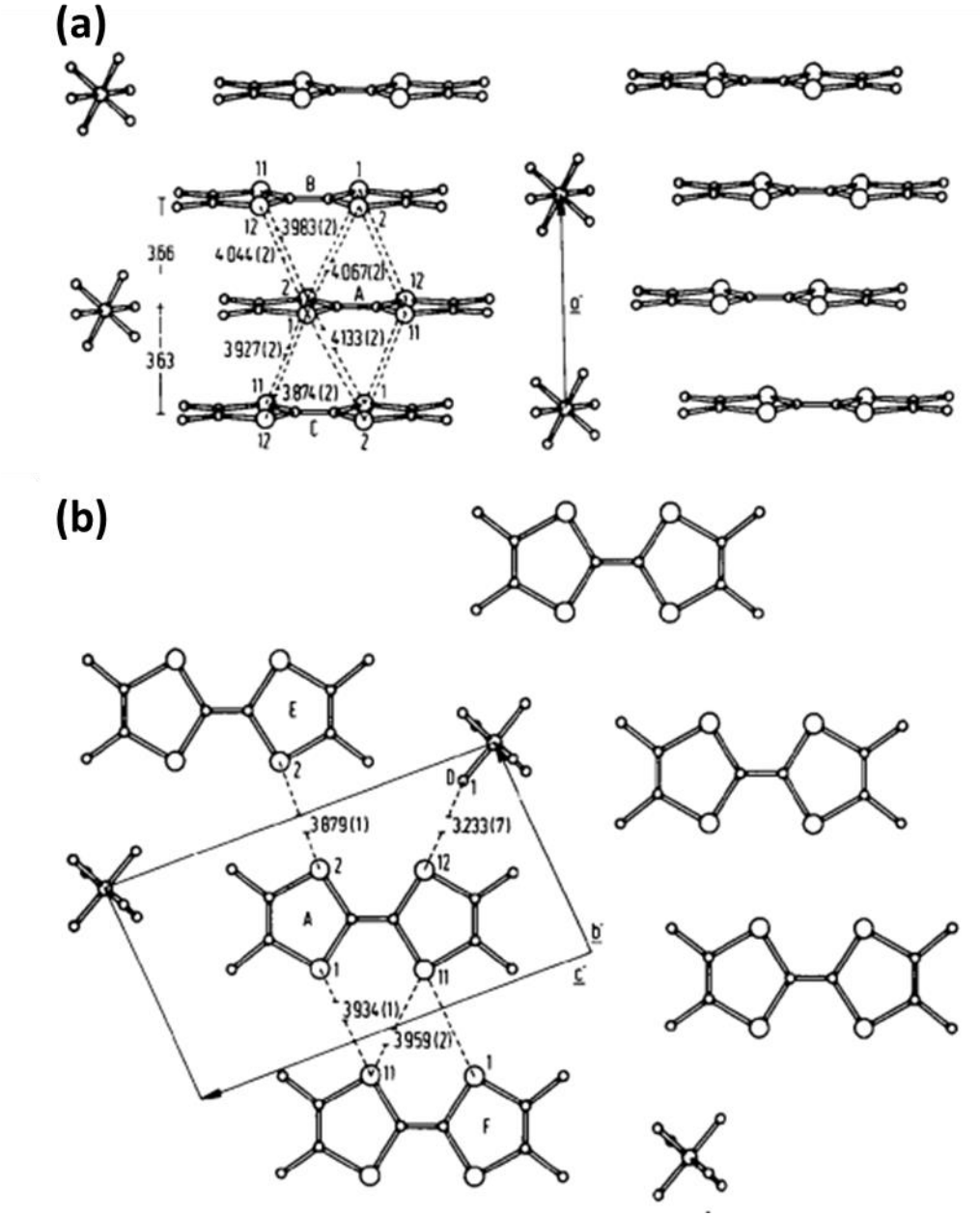

Figure 1.2.3.5: Single crystal structure of $(TMTSF)_2PF_6$. a) Side view of the quasi one-dimensional conducting column. b) View along the quasi one-dimensional conducting column.[8]

In 1980, the first organic superconductor was realized with TMTSF (Tetramethyltetraselenafulvalene). This TTF derivative is designed by introducing four methyl groups and four selenium atoms. By the former improvement, not only solubility, but also the crystal packing was improved. The substitution of the sulfur atoms by selenium atoms can increase the molecular orbital overlap both in the intra- and inter-conducting column interactions because the selenium atoms have bigger molecule

radius (and thus orbital size). This molecule was designed to overcome the insulating behavior of purely one-dimensional system and to reach superconducting phase.

K. Bechgaard synthesized the first organic superconductor salt $(TMTSF)_2PF_6$. As a quasi-one dimensional material, $(TMTSF)_2PF_6$ became insulator at low temperature. But when pressure was applied，the denser crystal packing allowed carriers to transfer and superconductivity was realized at 1.6 K with a pressure of 6 kbar. To remember his contribution, this salt was named as Beahgaard Salt.

In the next stage of research, scientists replaced PF_6 anion by other anion such as BF_4^-, ClO_4^-, AsF_6^- and SbF_6^- with relatively bigger sizes that will affect the crystal lattice. Such a substitution creates similar effect to the application of pressure. As a result, $(TMTSF)_2ClO_4$ showed superconductivity at 1 K even at normal pressure.

In a Bechgaard Salt $(TMTSF)_2PF_6$, every two TMTSF molecules virtually hand over one electron to PF_6 anion to form a dimer. Since each HOMO energy level of one molecule has been occupied by two electrons, one dimer of TMTSF originally possesses four electrons at HOMO level, and those electrons are accommodated in antibonding- and bonding-combination of HOMO orbitals. Since the electrons occupy the orbitals from the lowest energy level, one electron at higher energy level (the antibonding-orbital in this case) will be lost at the oxidation, to leave a half-filled antibonding-orbital and full-filled bonding orbital.

Scientists have realized superconductivity in quasi one-dimensional materials such as TMTSF-based Beahgaard salt. Considering the unfavorable effect brought by Peierls distortion, it seems better to introduce non-planar organic moiety connected to the outer part of the TTF structure in order to create two-dimensional conducting pathways. From then on, a lot of compounds were synthesized and measured. The most representative one is BEDT-TTF (bis(ethylenedithio)tetrathiafulvalene). BEDT-TTF can also show charge-transfer with TCNQ and create metal-like behavior automatically. But due to the non-plane structure of BEDT-TTF, BEDT-TTF molecules always stack with an angle, which made the conducting channel change from one-dimensional to two-dimensional. These type of BEDT-TTF crystals are separated into different type marked by Greek alphabet such as α, β and κ according to their molecular arrangements.

1.2.4 κ-type BEDT-TTF Electrolytic Crystals

κ-type $(BEDT\text{-}TTF)_2X$ (X stands for acceptor anion) crystals were studied as organic conductors very well. Just like Beahgaard salts such as $(TMTSF)_2ClO_4$ or $(TMTSF)_2PF_6$, every two BEDT-TTF molecules form a dimer and give out 1 electron to the acceptor anion, forming a layer-by-layer structure. But what was not expected is that κ-type $(BEDT\text{-}TTF)_2X$ crystals was accidently found to be Mott insulator. This is

quite an amazing coincidence because Mott insulator sometimes gives superconductivity; this result is quite exciting.

For instance, in a typical Mott-insulating crystal such as (BEDT-TTF)$_2$Cu[N(CN)$_2$]Br[33], two BEDT-TTF molecules give one electron to the acceptor anion Cu[N(CN)$_2$]Br. For each dimer, HOMO is separated into half-filled antibonding orbital and fully-filled bonding orbital. Due to the Coulomb repulsion, the half-filled antibonding orbital splits into UHB and LHB to form an insulator phase as shown in figure 1.2.4.1. By comparing the on-site Coulomb energy *U* with kinetic energy of carriers *t*, this type of band splitting can be discussed. When *U* > t, carriers cannot move

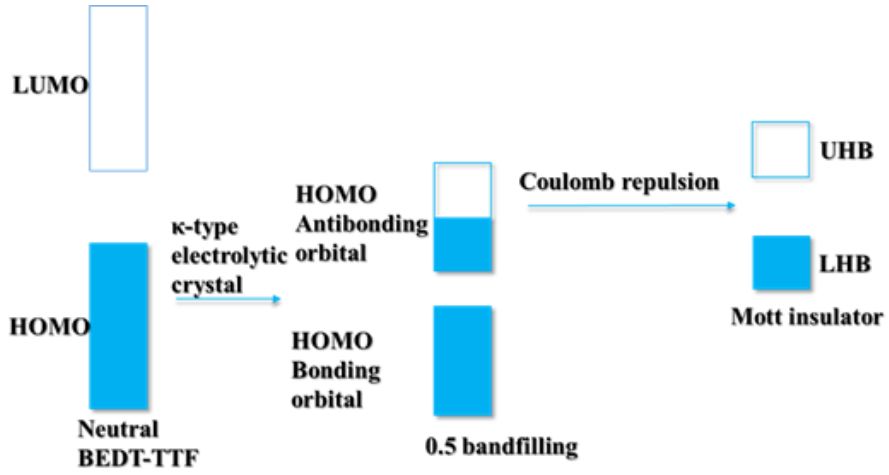

Figure 1.2.4.1: Band filling of κ-type BEDT-TTF electrolytic crystal appears as Mott insulator

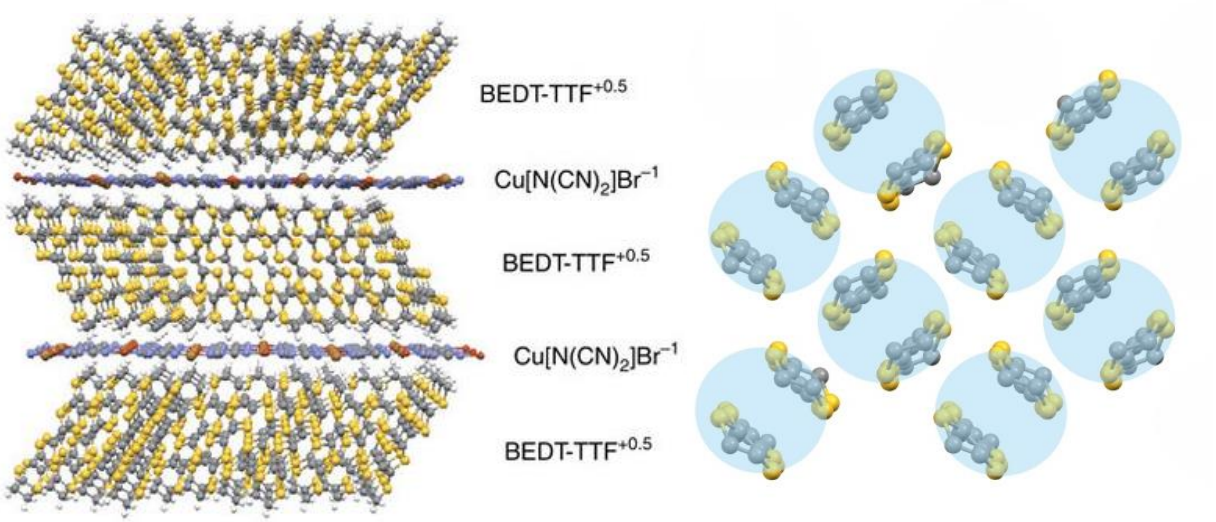

Figure1.2.4.2: Crystal structure and band filling of κ-Br (left)[9] and BEDT-TTF dimer (right).

from one dimer to another, which is insulator, but when $U < t$, carriers can move from one dimer to another, which is metal. Since it is difficult to control U or t independently, control the ratio of U/t is often used as a control parameter for this type of Mott insulator.

What is amazing is that κ-$(BEDT\text{-}TTF)_2Cu[N(CN)_2]Br$ (abbreviated as κ-Br hereafter) crystals showed superconductivity at ambient pressure with critical temperature of 10.4 K. This temperature is much higher than $(TMTSF)_2ClO_4$. Since $(TMTSF)_2ClO_4$ is a quasi-one dimensional superconductor and is not a Mott insulator, the conductivity of this two different type of crystals mush be different. In any case, the pressure still influences the superconducting behavior in κ-Br crystals. For example, if the bromine atom is replaced by chlorine atom, the κ-Cl ($(BEDT\text{-}TTF)_2Cu[N(CN)_2]Cl$) crystal remains Mott insulator under ambient pressure when temperature decreases. This is because the size of chlorine atom is smaller than bromine atom, and this atom substitution decreases the internal pressure of crystal lattice and increases the U/t. Therefore, metallic behavior and superconducting phase disappeared. However, κ-Cl will transfer into metal phase that is followed by a superconducting phase under high pressure.[34,35] Phase diagram of different $(BEDT\text{-}TTF)_2X$ crystals are shown in figure 1.2.4.3[36]. There are various possibilities for us to get fascinating devices by synchronously controlling U/t. For example, with different substrate, strain from the substrate modified by temperature can demonstrate a shift between superconductivity and Mott insulator by influencing the U/t [9]. By taking advantages of spiropyran, which

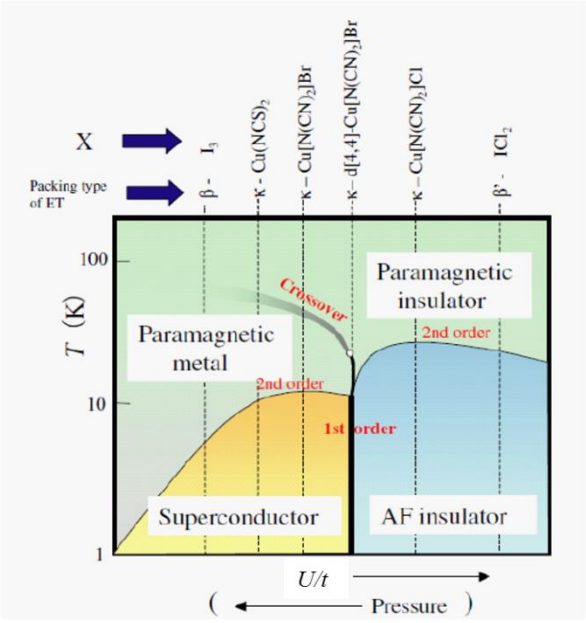

Figure 1.2.4.3: Phase diagram of different $(BEDT\text{-}TTF)_2X$ crystals. U/t and pressure could be used to modify the material to be metal, insulator or even superconductor. [3]

is a photochromic compound with charge separation, a κ-Br device can turn between

on and off states of superconductivity[37,38].

Unfortunately, however, the conductivity of these crystals cannot be ignored at room temperature since the Mott-Hubbard band is relatively small. As the field-induced carriers accumulates only in the first few layers[39], most of the BEDT-TTF layers appears as bulk layers offering a relatively high bulk current to mask the pure FET function. Pure FET behaviors can only be observed under low temperature.

Under this situation, it is a natural corollary to think about two-dimensional monolayer device if one wishes to measure the FET behavior only in the active layer.

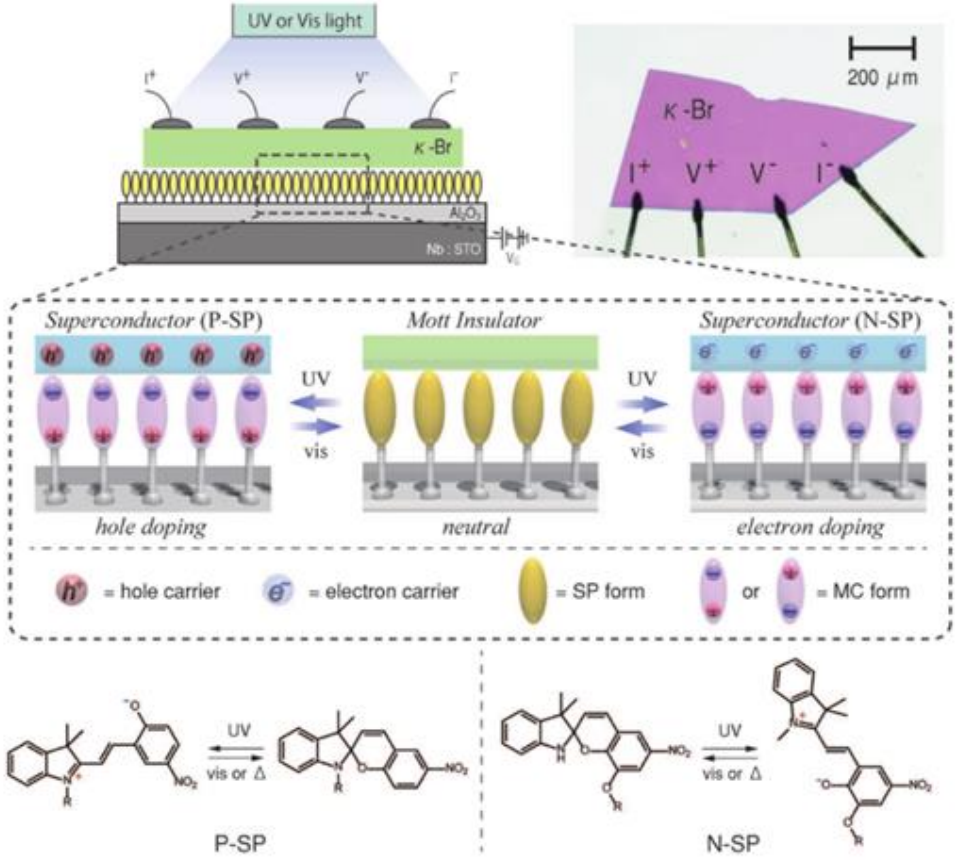

Figure1.2.4.4: P- and n-type superconductivity device using κ-Br single crystal. Spiropyran monolayer was used to control the carriers doping[6].

1.3 Monolayer

Generally speaking, monolayer is a thin film arranged as only one layer of molecules or atoms. So far, several processes have been reported to fabricate monolayer devices, such as self-assembled monolayer (SAM), Langmuir-Blodgett (LB) film, and some other special coating techniques.

1.3.1 Self-assembled monolayer

Self-assembled monolayer was introduced by W. A. Zisman *et al*[40] as a concept, but not until the year 1978 it became reality with a good quality[41,42]. By creation of chemical bond between the substrate and functional molecule, monolayer can be formed on different substrates such as metal, metal oxide, silicon or silicon oxide and even polymer. The covalent bond that anchors the monolayer to the substrate can be optimized by modifying reacting group. Most of the reports on monolayer semiconductors are concentrated on hydroxyl groups, carboxylic acids, chlorosilanes and phosphoric acid derivatives. Among them, chlorosilanes and phosphoric acid derivatives are most reported for monolayer OFETs.

- *Chlorosilanes*

Chlorosilanes are among the first choices for reacting groups suitable for SAM[43]. A number of monolayers formed by chlorosilanes have been reported as a part of dielectric layer[44,45,46]. With more chlorine atoms, the reactivity for functional groups increases. This fact makes the most popular reagent to be trichlorosilanes. The first monolayer FET example, oligothiophene semiconductor, was reported by S.A. Ponomarenko *et al*[47]. The formation of this type monolayer generally follows the equation:

$$\text{Si-Cl} + \text{Si-OH} \rightleftharpoons \text{Si-O-Si} + \text{HCl}$$
$$\text{Si-Cl} + \text{H}_2\text{O} \rightleftharpoons \text{Si-O-Si} + \text{HCl}$$
$$\text{Si-OH} + \text{Si-OH} \rightleftharpoons \text{Si-O-Si} + \text{H}_2\text{O}$$

According to this equation, the formation of this monolayer requires a hydroxylated substrate surface on metal oxide and during monolayer formation, hydrochloric acid, which is not preferred for electron donating functional group, will be formed. These silanes are very sensitive to water and self-condensation of silanes also remains as a

problem. These demerits drive the urge for better anchor groups.

- *Phosphonic acid derivitives*

The phosphonic acid derivatives were investigated without the above shortcomings described in chlorosilanes. E.L. Hanson reported a SAM on a surface of silicon oxide anchored by phosphoric acid moiety in 2003[48]. By immersing the substrate into a functional solution, monolayer can be realized very easily with a good quality. Further report by H. Klauk *et al.* showed that the SAM density is higher than trichlorosilane derivatives[49] . This report led to the explosive growth of publications on monolayer devices made by phosphoric acid derivatives. Monolayer FETs based on quaterthiophene (4T)[50], pentathiophene (5T)[51], BTBT(benzothieno[3,2-b][1]benzothiophene)[52], fullerene[50] and PTCDI(3,4,9,10-perylenedicarboximide)[53] were reported in a short time. Compare to silanes, reaction situation of phosphoric acid derivatives are not so strict and can be used on metal-oxide surfaces. The compound itself does not have the problem of self-condensation like silanes and is not so sensitive to moisture. These merits make it very attractive for monolayer fabrication and compound storage.

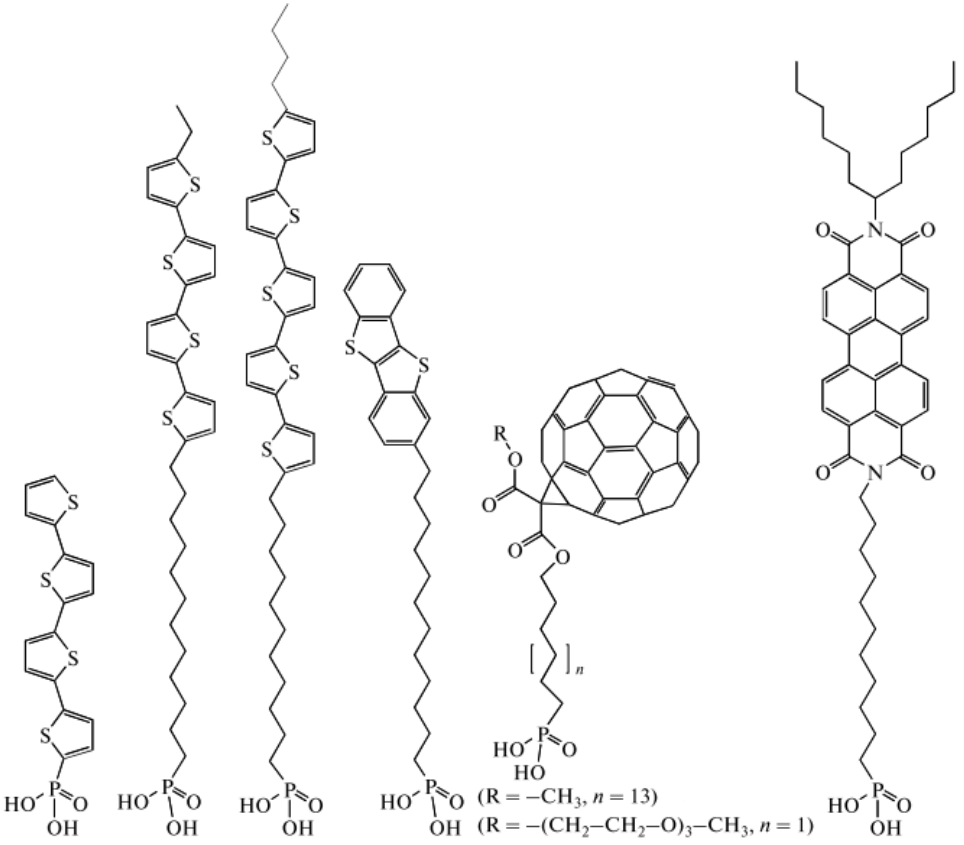

Figure1.3.1.1: Some reported monolayer organic FET materials with phosphonic acid group as anchor.[2]

1.3.2 Langmuir-Blodgett

Langmuir-Blodgett technique can also form a monolayer by an amphiphilic molecule solved homogeneously in the interface of two immiscible solutions (or solution and air)[54,55,56]. A molecule should contain a "head" part which should be highly hydrophilic and a "tail" part which is necessary to be hydrophobic in order to form a monolayer in the interface. Physical deposition of this monolayer on a solid substrate can give a highly-ordered thin film. This technique was named after Irving Langmuir and Katharine B. Blodgett, who invented the technique. This technique is one of the most popular methods for preparing thin films including monolayer but it is quite hard to control because of the difficulty in finding appropriate solvent and condition for monolayer raising.

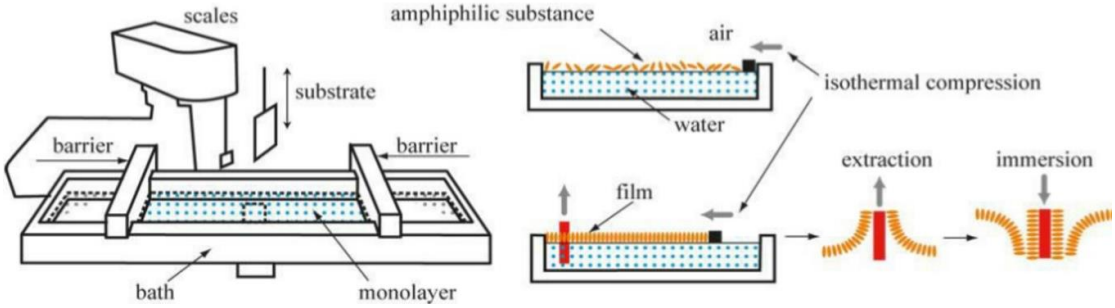

Figure 1.3.2.1: Thin film formation process of Langmuir-Blodgett film (monolayer).

1.3.3 Conductance-controlled evaporation

Conductance-controlled evaporation can be achieved by controlling the evaporation speed of molecule to form a monolayer. This method requires high vacuum and precise operation[57]. It is a highly technical process and may not be suitable for all the materials.

1.3.4 Coating techniques

Coating processes that directly or indirectly form a monolayer on the substrate is also very popular; dip coating, spin coating and inkjet printing.

- *Dip-coating*

Dip-coating by immersing the substrate in a solution of the coating material and lifting it at a constant speed can make a thin film. By adjusting the concentration of

solution and lifting speed, fabrication of monolayer become possible[58,59].

- *Spin coating*

Spin coating is also reported a lot. By adjusting the spin speed, solvent and concentration of solution, a lot of semiconductor compounds such as 5T[60], 7T(septithiophene)[61] can be made into monolayer devices. It is also possible to create nonplanar monolayer devices by brickwork arrangement[62]. The disadvantages are just the same with dip-coating: the conditions are quite material-dependent and require highly-sophisticated technique that also depends on materials. This is not suitable for large area deposition, either.

- *Inkjet printing*

Inkjet printing is a little bit different from dip-coating and spin coating. By printing a solution of a semiconductor and a poor solvent for the semiconductor individually on top of substrate will form a micro liquid intermixture. Optimized printing condition is possible to control the formation of crystalline thin film and molecularly flat surfaces can be achieved.[5]

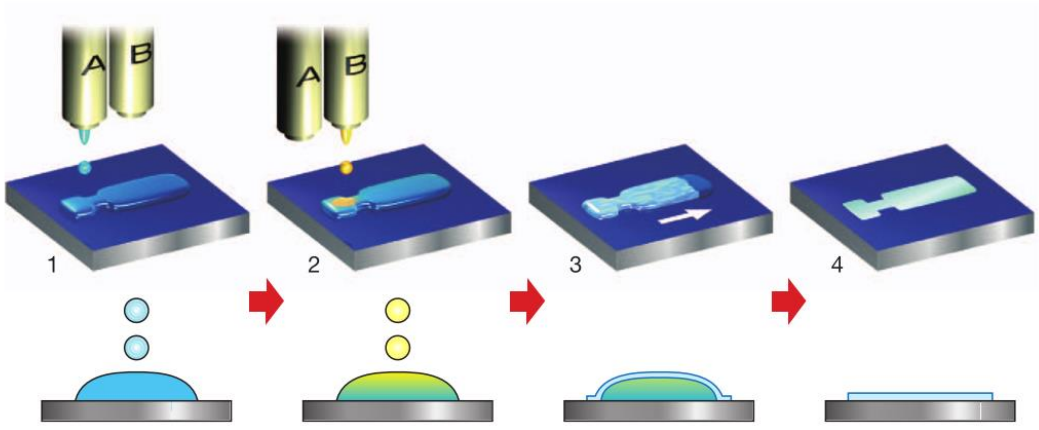

Figure 1.3.4.1: Process of inkjet printing with two different solutions[5].

1.4 Purpose and constitution of this thesis

As discussed above, in order to get a Mott FET that works at room temperature, it is necessary to remove additional layers of a κ-type BEDT-TTF crystal to avoid the electric conduction which comes from the upper layers. Comprehensive consideration about the requirements for our target monolayer leads to the following idea: a densely packed monolayer with proper oxidation potential will result in a monolayer Mott-FET with reduced *U/t*. SAM using phosphonic acid is employed for the monolayer

deposition due to the relatively high monolayer density and easier fabrication.

This thesis consists of six parts including the present part that is reviewing the background of this research. This research is concentrated on achieving a monolayer FET device with two-dimensional conductivity. Further doping turns this FET device into a two- dimensional Mott FET device.

In the second part, the molecular design and synthesis are discussed. With the help of introduced phosphonic acid group which anchors the molecule to the substrate, a monolayer is achieved. Monolayer fabricated by solution with different concentration and dopants are discussed in this part.

In the third part, the monolayer FET performance without doping is discussed.

In the fourth part, the monolayer FET is doped by spin coating F_4TCNQ solutions with different concentration, and the FET performances of these doped monolayer device will be measured at room temperature.

In the fifth part, temperature dependence is checked and further analysis is applied to discuss the conducting mechanism of this type of monolayer device.

In the last part, summary of this thesis will be described and conducting mechanism of this monolayer device will be reviewed.

1.5 References

(1) Taillefer, L. *Annu. Rev. Condens. Matter Phys.* **2010**, *1*, 51.

(2) Borshchev, O. V.; Ponomarenko, S. A. *Polymer Science Series C* **2014**, *56*, 32.

(3) Kanoda, K. *J Phys Soc Jpn* **2006**, *75*, 051007.

(4) Ferraris, J.; Cowan, D.; Walatka, V. t.; Perlstein, J. *J Am Chem Soc* **1973**, *95*, 948.

(5) Minemawari, H.; Yamada, T.; Matsui, H.; Tsutsumi, J. y.; Haas, S.; Chiba, R.; Kumai, R.; Hasegawa, T. *Nature* **2011**, *475*, 364.

(6) Suda, M.; Takashina, N.; Namuangruk, S.; Kungwan, N.; Sakurai, H.; Yamamoto, H. M. *Adv Mater* **2017**.

(7) Kistenmacher, T. J.; Phillips, T. E.; Cowan, D. O. *Acta Crystallographica Section B: Structural Crystallography and Crystal Chemistry* **1974**, *30*, 763.

(8) Thorup, N.; Rindorf, G.; Soling, H.; Bechgaard, K. *Acta Crystallographica Section B: Structural Crystallography and Crystal Chemistry* **1981**, *37*, 1236.

(9) Yamamoto, H. M.; Nakano, M.; Suda, M.; Iwasa, Y.; Kawasaki, M.; Kato, R. *Nat Commun* **2013**, *4*, 2379.

(10) Castell, M. R.; Muller, D. A.; Voyles, P. M. *Nature Materials* **2003**, *2*, 129.

(11) Heilmeier, G. H.; Zanoni, L. A. *J Phys Chem Solids* **1964**, *25*, 603.

(12) Ebisawa, F.; Kurokawa, T.; Nara, S. *J Appl Phys* **1983**, *54*, 3255.

(13) Kudo, K.; Yamashina, M.; Moriizumi, T. *Jpn J Appl Phys* **1984**, *23*, 130.

(14) Tsumura, A.; Koezuka, H.; Ando, T. *Appl Phys Lett* **1986**, *49*, 1210.

(15) Tang, C. W. *Appl Phys Lett* **1986**, *48*, 183.

(16) Tang, C. W.; VanSlyke, S. A. *Appl Phys Lett* **1987**, *51*, 913.

(17) Wang, C.; Dong, H.; Hu, W.; Liu, Y.; Zhu, D. *Chem Rev* **2012**, *112*, 2208.

(18) Weimer, P. K. *Proceedings of the IRE* **1962**, *50*, 1462.

(19) Mott, N.; Peierls, R. *Proceedings of the Physical Society* **1937**, *49*, 72.

(20) Wu, M.-K.; Ashburn, J. R.; Torng, C. J.; Hor, P. H.; Meng, R. L.; Gao, L.; Huang, Z. J.; Wang, Y.; Chu, a. *Phys Rev Lett* **1987**, *58*, 908.

(21) McMillan, W. *Physical Review* **1968**, *167*, 331.

(22) Taur, Y.; Mii, Y.-J.; Frank, D. J.; Wong, H.-S.; Buchanan, D. A.; Wind, S. J.; Rishton, S. A.; Sai-Halasz, G.; Nowak, E. J. *Ibm J Res Dev* **1995**, *39*, 245.

(23) Frank, D.; Laux, S.; Fischetti, M. *IEEE T Electron Dev* **1993**, *40*, 2103.

(24) Agrawal, B.; De, V.; Pimbley, J.; Meindl, J. *IEEE J Solid-st Circ* **1994**, *29*, 122.

(25) Fiegna, C.; Iwai, H.; Wada, T.; Saito, M.; Sangiorgi, E.; Ricco, B. *IEEE T Electron Dev* **1994**, *41*, 941.

(26) Newns, D.; Misewich, J.; Tsuei, C.; Gupta, A.; Scott, B.; Schrott, A. *Appl Phys Lett* **1998**, *73*, 780.

(27) Nakano, M.; Shibuya, K.; Okuyama, D.; Hatano, T.; Ono, S.; Kawasaki, M.; Iwasa, Y.; Tokura, Y. *Nature* **2012**, *487*, 459.
(28) Acker, D.; Harder, R.; Hertler, W.; Mahler, W.; Melby, L.; Benson, R. E.; Mochel, W. *J Am Chem Soc* **1960**, *82*, 6408.
(29) Siemons, W.; Bierstedt, P.; Kepler, e. R. *The Journal of Chemical Physics* **1963**, *39*, 3523.
(30) Bardeen, J.; Cooper, L. N.; Schrieffer, J. R. *Physical Review* **1957**, *108*, 1175.
(31) Little, W. *Physical Review* **1964**, *134*, A1416.
(32) Wudl, F.; Wobschall, D.; Hufnagel, E. J. *J Am Chem Soc* **1972**, *94*, 670.
(33) Kini, A. M.; Geiser, U.; Wang, H. H.; Carlson, K. D.; Williams, J. M.; Kwok, W.; Vandervoort, K.; Thompson, J. E.; Stupka, D. L. *Inorg Chem* **1990**, *29*, 2555.
(34) Ito, H.; Ishiguro, T.; Kubota, M.; Saito, G. *J Phys Soc Jpn* **1996**, *65*, 2987.
(35) Schultz, A.; Geiser, U.; Wang, H.-H.; Williams, J.; Finger, L.; Hazen, R. *Physica C: Superconductivity* **1993**, *208*, 277.
(36) Y. Iwasa, K. M., T. Koda, Y. Tokura, and G. Saito, Phys.; Rev. B 49, S., Masatoshi; Sakuma, H.; Ito, Y.; Saito, A.; Nakamura, M.; Kudo, K. *Phys Rev B* **2007**, *76*, 045111.
(37) Suda, M.; Kato, R.; Yamamoto, H. M. *Science* **2015**, *347*, 743.
(38) Sato, Y.; Kawasugi, Y.; Suda, M.; Yamamoto, H. M.; Kato, R. *nano lett*, **2017**, *17*, 708.
(39) Tajima, N.; Yamauchi, T.; Yamaguchi, T.; Suda, M.; Kawasugi, Y.; Yamamoto, H. M.; Kato, R.; Nishio, Y.; Kajita, K. *Phys Rev B* **2013**, *88*, 075315.
(40) Bigelow, W.; Pickett, D.; Zisman, W. *Journal of Colloid Science* **1946**, *1*, 513.
(41) Polymeropoulos, E.; Sagiv, J. *The Journal of Chemical Physics* **1978**, *69*, 1836.
(42) Sagiv, J. *J Am Chem Soc* **1980**, *102*, 92.
(43) Maoz, R.; Sagiv, J. *J Colloid Interf Sci* **1984**, *100*, 465.
(44) Aswal, D.; Lenfant, S.; Guerin, D.; Yakhmi, J.; Vuillaume, D. *Anal Chim Acta* **2006**, *568*, 84.
(45) Vuillaume, D.; Boulas, C.; Collet, J.; Davidovits, J.; Rondelez, F. *Appl Phys Lett* **1996**, *69*, 1646.
(46) Collet, J.; Tharaud, O.; Chapoton, A.; Vuillaume, D. *Appl Phys Lett* **2000**, *76*, 1941.
(47) Ponomarenko, S. A.; Borshchev, O. V.; Meyer-Friedrichsen, T.; Pleshkova, A. P.; Setayesh, S.; Smits, E. C.; Mathijssen, S. G.; de Leeuw, D. M.; Kirchmeyer, S.; Muzafarov, A. M. *Organometallics* **2010**, *29*, 4213.
(48) Hanson, E. L.; Schwartz, J.; Nickel, B.; Koch, N.; Danisman, M. F. *J Am Chem Soc* **2003**, *125*, 16074.
(49) Klauk, H.; Zschieschang, U.; Pflaum, J.; Halik, M. *Nature* **2007**, *445*, 745.
(50) Novak, M.; Ebel, A.; Meyer-Friedrichsen, T.; Jedaa, A.; Vieweg, B. F.; Yang, G.;

Voitchovsky, K.; Stellacci, F.; Spiecker, E.; Hirsch, A. *nano lett*, **2010**, *11*, 156.
(51) Hutchins, D. O.; Acton, O.; Weidner, T.; Cernetic, N.; Baio, J. E.; Ting, G.; Castner, D. G.; Ma, H.; Jen, A. K.-Y. *Organic Electronics* **2012**, *13*, 464.
(52) Schmaltz, T.; Amin, A. Y.; Khassanov, A.; Meyer‐Friedrichsen, T.; Steinrück, H. G.; Magerl, A.; Segura, J. J.; Voitchovsky, K.; Stellacci, F.; Halik, M. *Adv Mater* **2013**, *25*, 4511.
(53) Ringk, A.; Li, X.; Gholamrezaie, F.; Smits, E. C.; Neuhold, A.; Moser, A.; Van der Marel, C.; Gelinck, G. H.; Resel, R.; de Leeuw, D. M. *Adv Funct Mater* **2013**, *23*, 2016.
(54) Fabiano, S.; Musumeci, C.; Chen, Z.; Scandurra, A.; Wang, H.; Loo, Y. L.; Facchetti, A.; Pignataro, B. *Adv Mater* **2012**, *24*, 951.
(55) Kaur, H.; Yadav, S.; Srivastava, A. K.; Singh, N.; Schneider, J. J.; Sinha, O. P.; Agrawal, V. V.; Srivastava, R. *Scientific Reports* **2016**, *6*.
(56) Hussain, S. A. *arXiv preprint arXiv:0908.1814* **2009**.
(57) Mannebach, E. M.; Spalenka, J. W.; Johnson, P. S.; Cai, Z.; Himpsel, F.; Evans, P. G. *Adv Funct Mater* **2013**, *23*, 554.
(58) Jang, J.; Nam, S.; Im, K.; Hur, J.; Cha, S. N.; Kim, J.; Son, H. B.; Suh, H.; Loth, M. A.; Anthony, J. E. *Adv Funct Mater* **2012**, *22*, 1005.
(59) Li, L.; Gao, P.; Schuermann, K. C.; Ostendorp, S.; Wang, W.; Du, C.; Lei, Y.; Fuchs, H.; Cola, L. D.; Müllen, K. *J Am Chem Soc* **2010**, *132*, 8807.
(60) Chen, H.; Dong, S.; Bai, M.; Cheng, N.; Wang, H.; Li, M.; Du, H.; Hu, S.; Yang, Y.; Yang, T. *Adv Mater* **2015**, *27*, 2113.
(61) Defaux, M.; Gholamrezaie, F.; Wang, J.; Kreyes, A.; Ziener, U.; Anokhin, D. V.; Ivanov, D. A.; Moser, A.; Neuhold, A.; Salzmann, I.; Resel, R.; de Leeuw, D. M.; Meskers, S. C.; Moeller, M.; Mourran, A. *Adv Mater* **2012**, *24*, 973.
(62) Shan, L.; Liu, D.; Li, H.; Xu, X.; Shan, B.; Xu, J. B.; Miao, Q. *Adv Mater* **2015**, *27*, 3418.

Part 2 Molecular design, synthesis and monolayer fabrication

2.1 Molecular design

As discussed in part 1, BEDT-TTF is a derivative of TTF, which was designed in order to increase dimensionality in its charge-transfer salts, and realization of the Mott insulating states in κ–type $(BEDT\text{-}TTF)_2X$ was an unexpected finding. Neutral BEDT-TTF itself has a non-planar structure and when it was oxidized, the shape of BEDT-TTF cation became flat. This behavior requires reorganization energy which limits the mobility of BEDT-TTF neutral molecule as a p-type OFET material. On the other hand, BEDT-TTF cation has a planar structure and carriers on it transfer without consumption of large reorganization energy; it is very important in order to reach a higher performance of device.

These facts raise limitations in the molecular design for self-assembled monolayer. That is, introduction of other atoms into donor core should be avoided and the moiety of BEDT-TTF should be remained as much as possible.

On the other hand, most of the reported SAM OFET devices have an alkyl spacer with around 10 carbon atoms[1-4] between the functional core and phosphonic acid anchor, which is useful to adjust the overlap of the functional groups and to get a better monolayer quality. Such an alkyl spacer group should be connected only to the edge of the functional donor core to avoid influence on the electronic properties of the donor core such as TTF part.

As discussed in part 1, the phosphonic acid derivatives are helpful to give a densely packed monolayer and it is a suitable option for our monolayer.

Alumina was chosen to be the dielectric layer due to the high reactivity with phosphonic acid.

The following summarizes the above descriptions about requirements for molecular design of monolayer:

- The energy level of BEDT-TTF-derivatized donor core should be kept equal to that of BEDT-TTF and the moiety of BEDT-TTF should be remained. The structure should not be changed too much.
- Alkyl chain spacer which enhance the overlap of functional donor core is necessary to realize a good-quality monolayer.
- Phosphonic acid anchor which fix the molecule on the alumina substrate is necessary.

Considering the above all requirements, the molecular design is shown in figure 2.1.1. The structure of donor core derives from that of BEDT-TTF, whose charge-transfer salts have been widely studied as Mott insulators. For easier synthesis, one of the dithiane rings of BEDT-TTF was substituted by alkyl chain while keeping the sulfur atom capped by methyl group, resulting in a structural change of the donor moiety to EDT-DMT-TTF. A C_9 alkyl chain as a spacer was introduced to enhance the overlap of the functional donor core. A phosphonic acid group as the anchor will react and form a covalent bond with the alumina substrate. This covalent bond will fix the EDT-DMT-TTF moiety together with the alkyl spacer tightly on the substrate. Realization of monolayer device with this designed compound is expected.

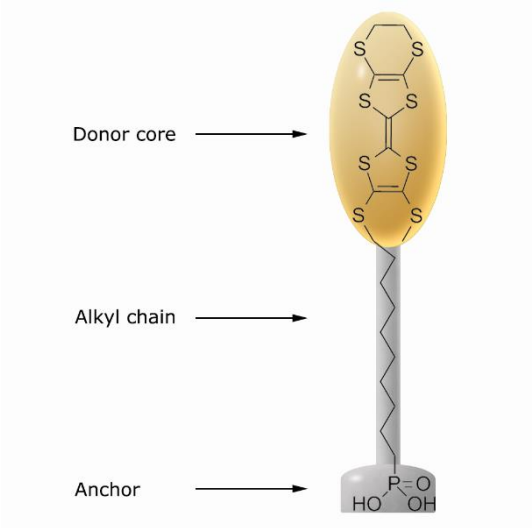

Figure 2.1.1: Molecular design for self-assembled monolayer FET device.

2.2 Molecular synthesis

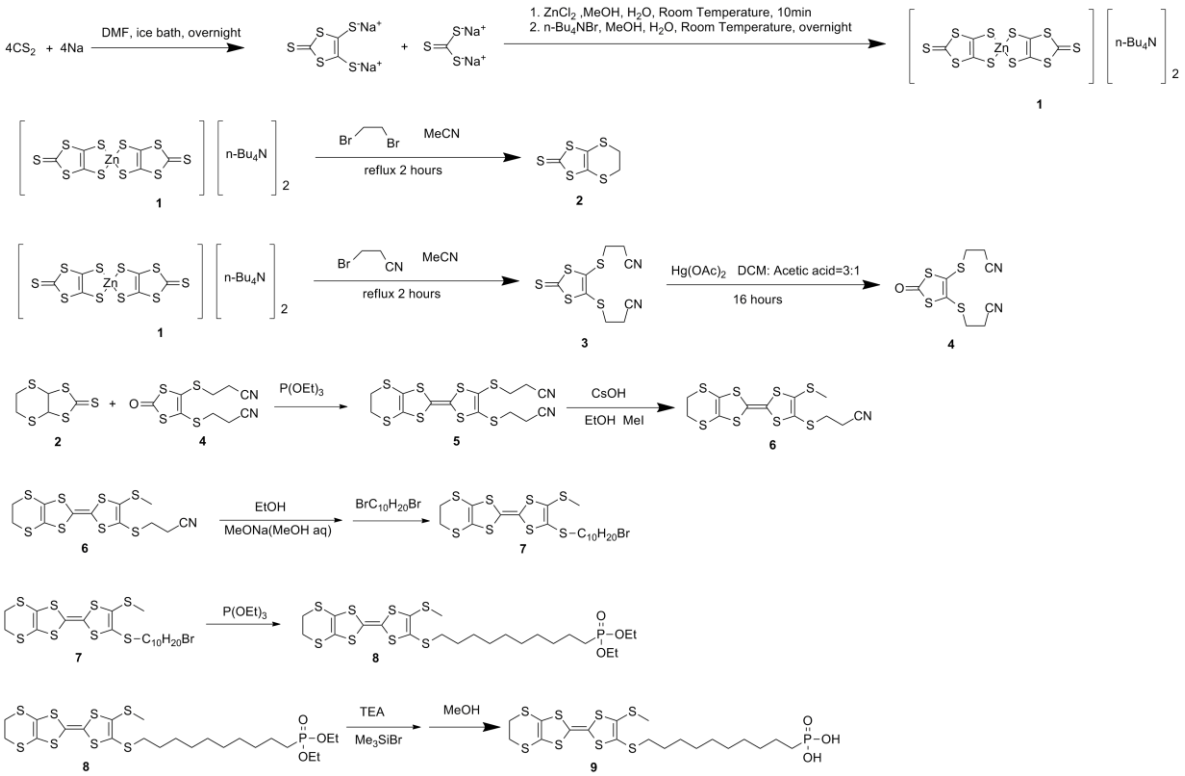

Scheme 2.2.1: Synthetic route for the designed molecule.

Starting from a synthesis of DMIT salt, final compound **9** (EDT-DMT-TTF-C_9-PA) was obtained after 9 step reactions. The entire synthetic route is shown in scheme 2.2.1.

Starting from sodium metal and carbon disulfide, sodium salt of DMIT (l,3-dithiol-2-thione-4,5-dithiolate) could be formed under Ar atmosphere. After Na^{1+} was replaced by Zn^{2+}, tetrabutylammonium anion ($n\text{-}Bu_4N^-$) was used to precipitate the $Zn(DMIT)_2[(n\text{-}Bu_4N)]_2$ salt, to obtain compound **1** with 68% yield. Compound **1** reacted with 1,2-dibromoethane and 3-bromopropionitrile can give compound **2** and **3** independently with yield of 60% and 92%, respectively. The sulfur atom in thioxo group of compound **3** was reacted with Mercury(II) acetate to be substituted by oxygen atom in order to increase the yield of the next coupling reaction: compound **4** was obtained by 74% yield. Cross coupling of compound **2** and **4** gave compound **5** with by-product BEDT-TTF and TCE-TTF (2,3,6,7-Tetra(cyanoethylsulfanyl)tetrathiafulvalene) which are the self-cross coupling products of the raw materials compound **2** and compound **4** (48% yield). By strictly controlling the ratio between CsOH and compound **5** to 1：1, compound **6** could be synthesized with a relatively high yield of 92%. Further synthesis to replace the propiononitrile group by alkyl chain with a bromine atom at the end of alkyl chain afforded compound

7 at 71% yield. By heating compound **7** in triethylphosphite to 140 ℃ overnight, compound **8** was obtained as orange oil (92% yield).

Compound **8** reacted with trimethylbromosilane under Ar atmosphere to give compound **9** through a two-step reaction. During this reaction, hydrochloric acid generated from trimethylbromosilane and the phosphonic acid in the final compound **9** seemed to react with the EDT-DMT-TTF donor core. Therefore, the compound will be destroyed without protecting material such as trimethylamine. On the other hand, pure compound **9** seems to undergo a self-polymerization which makes it hard to be concentrated too much. The purification of compound **9** was not executed because we could not find proper process for purification. Compound **9** was kept as THF solution under Ar atmosphere in a refrigerator and used as soon as possible. The yield was unknown but just assumed as about 70%.

2.3 Monolayer fabrication

On a p-doped silicon wafer which is covered with 300 nm-thick SiO_2 insulating layer, alumina layer with a thickness of 30 nm was grown by ALD (Atomic Layer Deposition). Electrode patterns were formed by photolithography. Ti (1 nm) and Au (20 nm) was then sputtered on the substrate. After the lift-off process with hot acetone, the substrate with the patterned electrodes was obtained with channel length of 5 μm, 10 μm, 15 μm, 25 μm, 50 μm, 100 μm, and 200 μm. Channel width was fixed at 1 mm. Before monolayer fabrication, the substrate was washed by acetone and isopropanol, dried with dry air flow and then treated with 10 W ozone plasma for 3 min to activate the surface. The activated substrate was then immersed in the THF solution of compound **9**. After a certain time, the substrate was transferred to clean THF solution, slightly shaken and then washed with isopropanol. Monolayer was obtained on the substrate after dried with air flow.

During the above process, EDT-DMT-TTF-C_9-PA solution in THF with different concentration was used to fabricate monolayer. TCNQ or F_4TCNQ was contained in some of the solutions. Schematic diagram of the monolayer device is shown in figure 2.3.1.

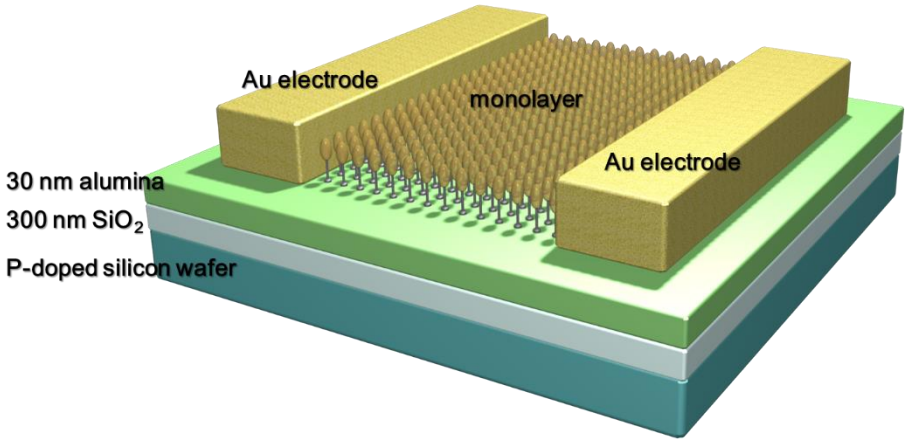

Scheme 2.3.1: Schematic diagram of the monolayer device

2.3.1 10^{-3} M EDT-DMT-TTF-C_9-PA solution

In this research, 10^{-3} M EDT-DMT-TTF-C_9-PA solution was used mostly. Solution at this concentration can offer a monolayer device very stably. AFM images of the surface are shown in figure 2.3.1.1. A basically smooth surface could be observed with a lot of highlight spots which are considered to be aggregates as a result of the intermolecular reaction between the EDT-DMT-TTF donor and protonic phosphonic acid group. Monitoring of the monolayer formation is shown in figure 2.3.1.2. Surface morphology of 1 hour-immersed sample looks crude with maximum height difference of about 2 nm. After 2 hours, the surface roughness decreased to show a maximum height difference of less than 0.5 nm, indicating that the formation of monolayer had finished. Unlike some other reported monolayer devices[4] in which the monolayer grain keep expanding as time flows, this monolayer is much likely to be formed by reaction between the molecule and the substrate without forming large grains. This could probably be attributed to the lack of planar structure of EDT-DMT-TTF donor core which is different from other monolayer.

The internal structure of the formed monolayer was checked by X-ray reflectivity (XRR) by using X-ray with wave length of 1.541867 Å (Cu K-α). Measured reflectivity curve and fitting curve calculated for the monolayer structure are shown in figure 2.3.1.3. The simulated data of the layer thickness, density and roughness for the fitting curve are listed in table 2.3.1.1. The monolayer thickness was fitted at about 2.1nm and separated into a 0.7 nm alkyl-spacer and a 1.4nm TTF core with clearly different density, indicating a regular arrangement on the surface of substrate. On the other hand, an additional layer of about 0.81 nm with a very low density (about 0.24

g/cm^3) was calculated to exist on the surface of monolayer.

The molecular weight for EDT-DMT-TTF core and C_9 alkyl chain without phosphonic acid is 385 and 126, respectively, giving a weight ratio of 3.06. However, the weight ratio calculated from XRR analysis is 3.77. Provided that the additional layer is alkyl chain from inverted molecule inserting into the donor core layer, the above discrepancy can be explained. An inclination angle of about 35 °was estimated for the alkyl chain layer. At the same time, the thickness of 1.41 nm calculated for EDT-DMT-TTF core indicated almost vertical standing of this moiety with respect to surface of the substrate.

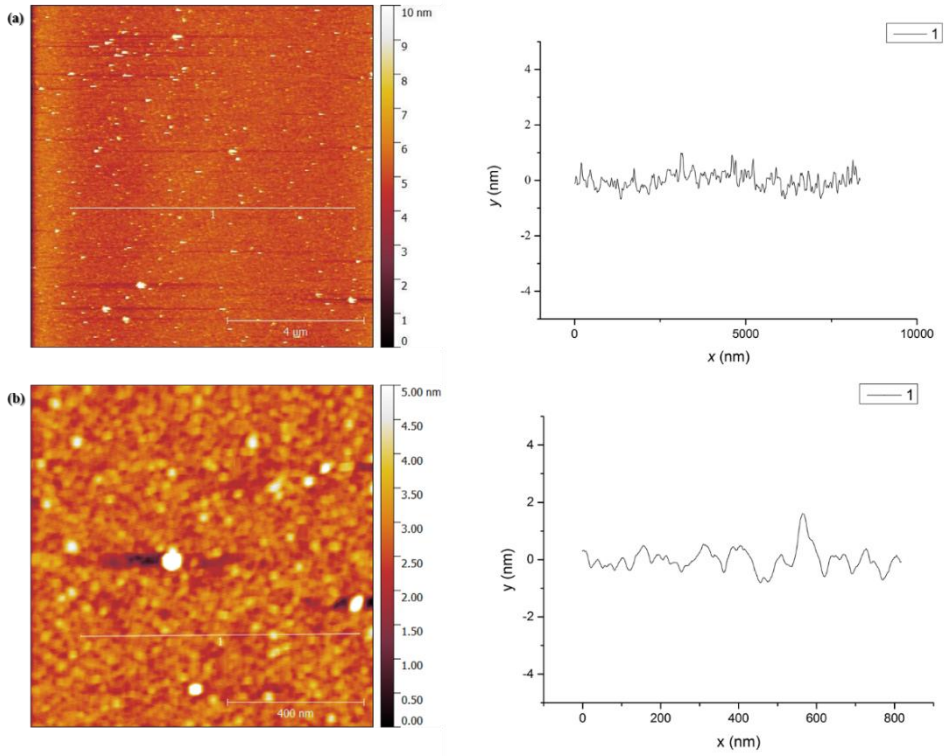

Figure 2.3.1.1: (a) AFM image (10 µm × 10 µm) of monolayer formed on alumina substrate after 2 hours immersion and cross sectional height profile measured along the white line 1 in the AFM image. (b) Expanded AFM image (1 µm × 1 µm) and the cross sectional height profile measured along the white line 1 of the same sample in (a).

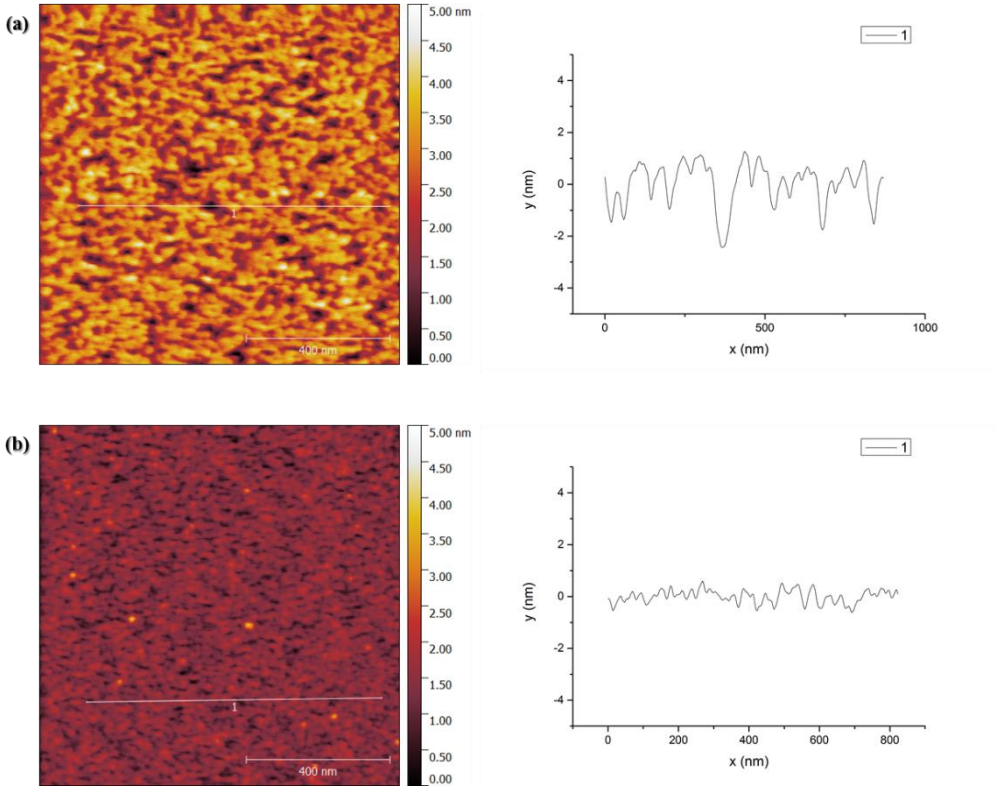

Figure 2.3.1.2: Monitoring of the formation process of the monolayer**.** (a) AFM image (1 μm × 1 μm) of monolayer formed on alumina substrate after 1 hour immersion and cross sectional height profile measured along the white line 1 in the AFM image. (b) AFM image (1 μm × 1 μm) of monolayer formed on alumina substrate after 2 hour immersion and cross sectional height profile measured along the white line 1 in the AFM image.

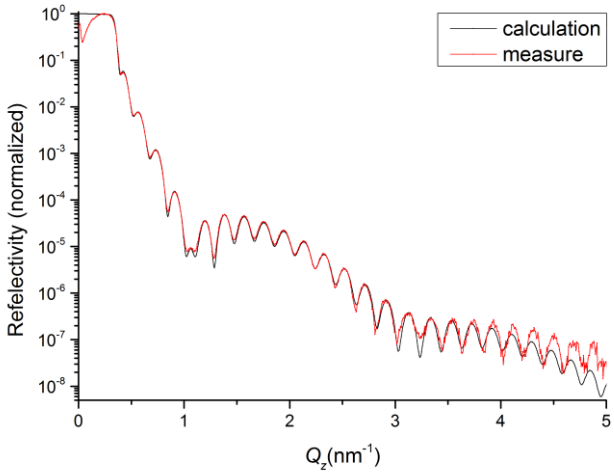

Figure 2.3.1.3: X-ray reflectivity analysis result for fabricated EDT-DMT-TTF-C_9-PA monolayer. Black line is calculated reflectivity from the internal structure listed in table 2.3.1.1. Red line is measured data from XRR.

Table 2.3.1.1: Calculated internal structure of monolayer to fit the XRR analysis result. Layer thickness *d*, density ρ and roughness σ are listed for every layer calculated from fitting data. SiO_2 layer was omitted.

Layer	***d* (nm)**	**ρ (g/cm^3)**	**σ (nm)**
Additional layer	0.8101	0.24	0.11
EDT-MDT-TTF core	1.41	1.85	1.10
C9 alkyl group	0.701	0.7	0.45
Alumina	31.54	2.71	0.68

2.3.2 10^{-2} M EDT-DMT-TTF-C_9-PA solution

Generally speaking, the substrate reacted with 10^{-2} M solution could not be covered by monolayer with good quality. The AFM images of alumina substrates immersed into 10^{-2} M solution of compound **9** for 2 hours and 24 hours are shown in figure 2.3.2.1. For immersion time of 2 hours, the roughness was larger with a maximum height difference of over 1 nm, which shows distinct difference to that of 2 hours immersion in 10^{-3} M solution. This could be caused by the intermolecular self-polymerization of the compound **9**. For the substrate immersed for 24 hours, a bumped surface was observed, indicating the intermolecular self-condensation was enhanced by extending the reaction time. In this concentration, it is hard to obtain a monolayer with good quality.

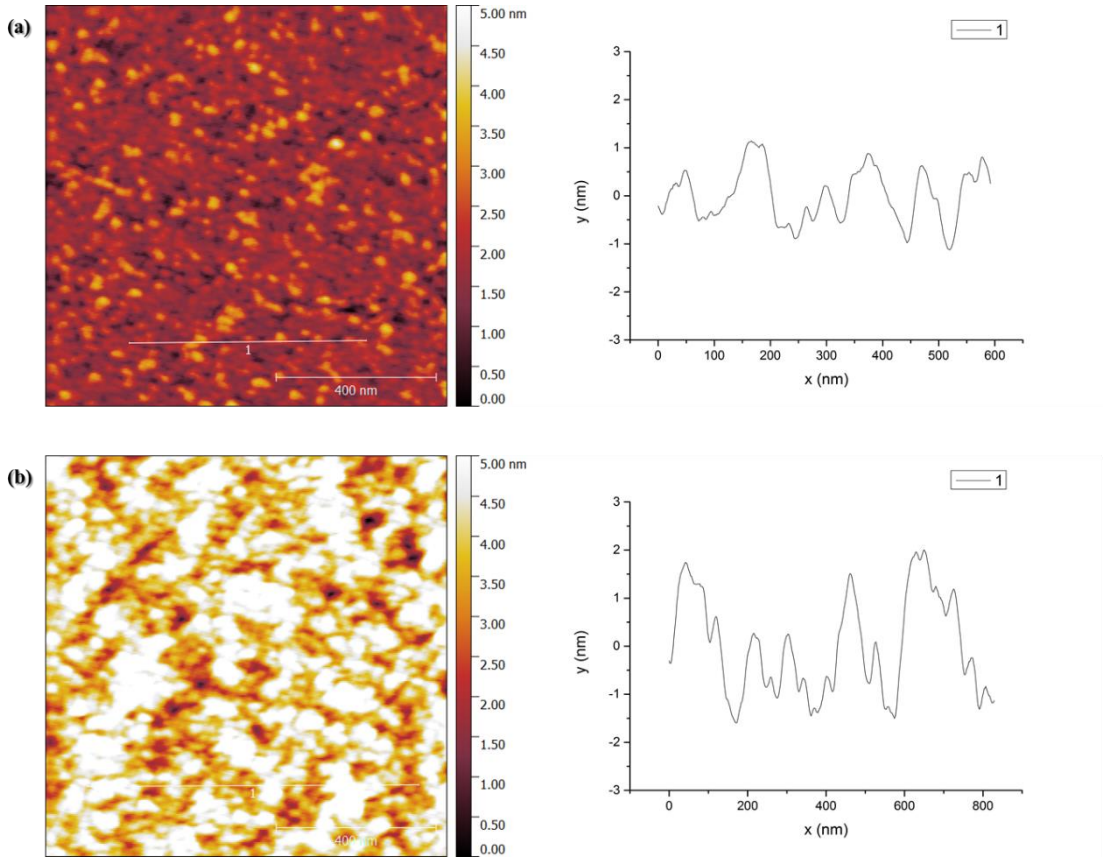

Figure 2.3.2.1: AFM image (1 μm × 1 μm) of monolayer formed on alumina substrate after 2 hours (a) or 24 hours (b) immersion in 10^{-2} M solution and cross sectional height profile measured along the white line 1 in each AFM image.

2.3.3 EDT-DMT-TTF-C_9-PA solution with TCNQ

In $(BEDT\text{-}TTF)_2X$ crystals, the BEDT-TTF donors are not neutral. This fact leaded to the attempt to fabricate a charge-transferred monolayer of EDT-DMT-TTF-C_9-PA. In this experiment, the charge-transferred monolayer was fabricated by immersing a substrate to the EDT-DMT-TTF-C_9-TTF solution under the existence of TCNQ. The AFM image of the substrate immersed in the solution with TCNQ for 2 hours is shown in figure 2.3.3.1. Compared with the monolayer fabricated by pure solution without TCNQ, the images are not so much different. However, the number of high-lighted spots is much smaller than that of the pure monolayer.

10^{-2} M solution with TCNQ was also used to fabricate the monolayer device. AFM images of 2 hours and 24 hours samples are shown in figure 2.3.3.2. In case of the solution with TCNQ, increase of the concentration of EDT-DMT-TTF-C_9-PA to 10^{-2} M

and extension of the reaction time even to 24 hours did not influence the morphology of monolayer, in contrast to the case without TCNQ. The existence of monolayer was confirmed by FET measurement as described in the next part since the AFM images could not give an obvious evidence for the existence of the monolayer.

Considering the above results, addition of TCNQ in the solution could help us to get a flatter surface. This may originate from the charge-transfer of electrons between EDT-DMT-TTF donor core and TCNQ in solution, quenching the reacting point with phosphonic acid group. Addition of TCNQ is helpful to exclude the intermolecular-condensation reaction even with high solution concentration and longer reacting time.

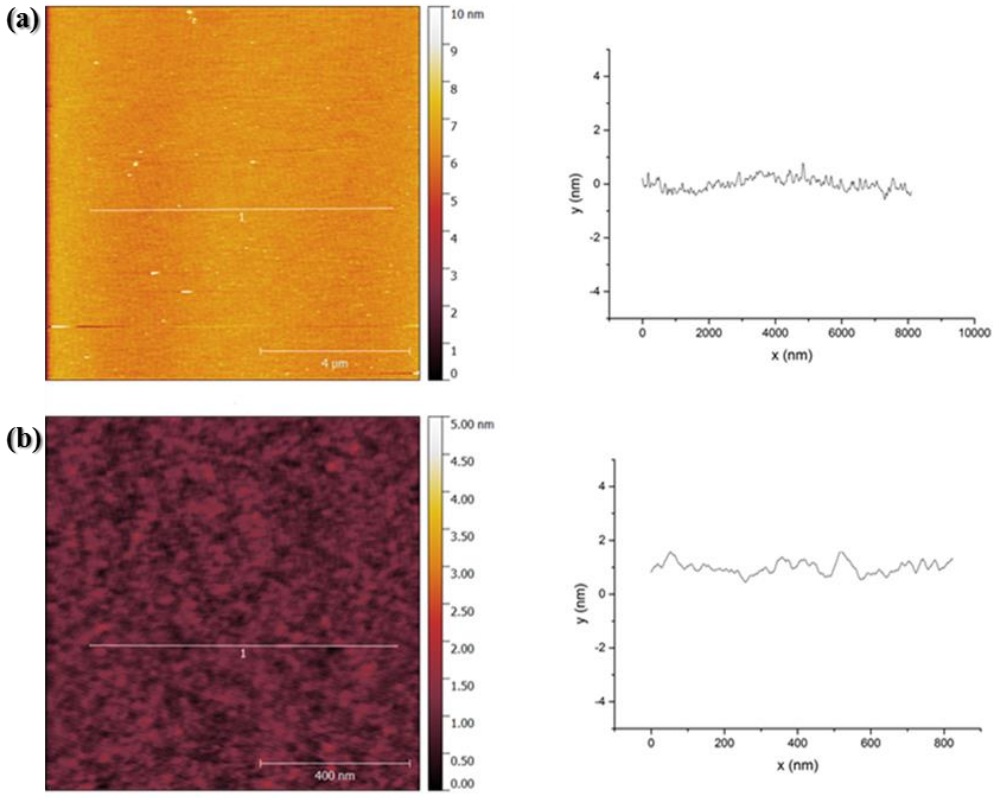

Figure 2.3.3.1: (a) AFM image (10 µm × 10 µm) of monolayer formed on alumina substrate by 10^{-3} M EDT-DMT-TTF-C_9-PA solution with TCNQ after 2 hours and cross sectional height profile measured along the white line 1. (b) AFM image (1 µm × 1 µm) of monolayer formed on alumina substrate by 10^{-3} M EDT-DMT-TTF-C_9-PA solution with TCNQ after 2 hours and cross sectional height profile measured along the white line 1.

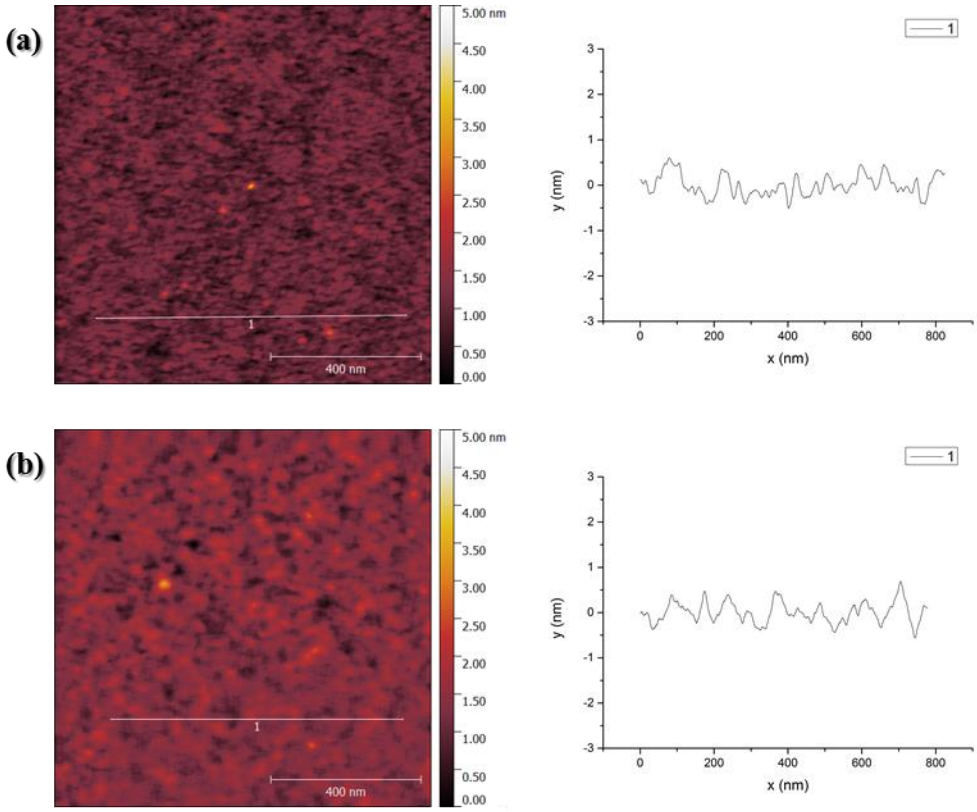

Figure 2.3.3.2: AFM image (1 μm × 1 μm) of monolayer formed on alumina substrate after 2 hours (a) or 24 hours (b) immersion in 10^{-2} M solution with TCNQ and cross sectional height profile measured along the white line 1 in each AFM image.

2.3.4 EDT-DMT-TTF-C_9-PA solution with F_4TCNQ

Generally speaking, immersion of substrates into EDT-DMT-TTF-C_9-PA solution with F_4TCNQ gave a similar result with those with TCNQ-containing solution for short time. However, the obtained monolayer was not so stable when the immersion time was extended in the presence of F_4TCNQ. This result can probably be attributed to the instability of F_4TCNQ in the solution under ambient atmosphere. As shown in figure 2.3.4.1, after 2 hours immersion, a smooth surface without high bumps could be obtained, which is similar to that of the TCNQ-containing ones. After 13 hours, however, some high bumps appeared although the entire surface still remained smooth. After 24 hours immersion, a lot of high bumps came out while the surface of the monolayer could still be recognized. After 38 hours immersion, the sample showed so many bumps at the surface that the surface of the monolayer could no longer be recognized.

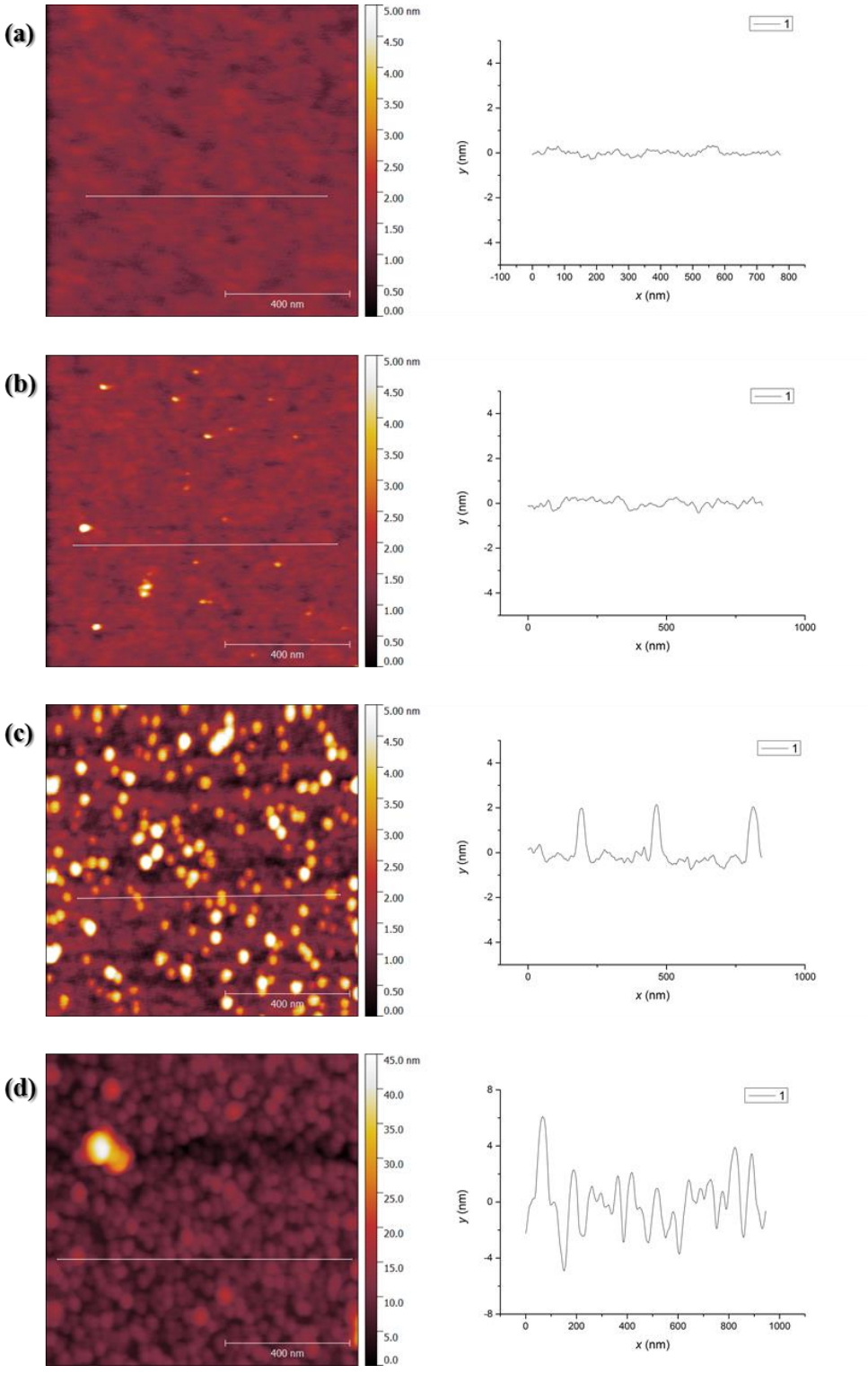

Figure 2.3.4.1: AFM image (1 μm × 1 μm) of monolayer formed on alumina substrate after 2 hours (a), 13 hours (b), 24 hours (c) and 38 hours (d) immersion in 10^{-3} M solution with F_4TCNQ and cross sectional height profile measured along the white line 1 in each AFM image.

This behavior could come from the low LUMO level of F_4TCNQ, which is very easy to be reduced under ambient atmosphere and is not so stable in air. The deterioration of the monolayer after long time immersion could probably be attributable to the instability of F_4TCNQ.

2.4 Summary

EDT-DMT-TTF-C_9-PA was synthesized, which was designed to fabricate a monolayer device. The monolayer could be fixed on alumina substrates under various conditions.

Immersion of the substrate into 10^{-3} M pure solution of EDT-DMT-TTF-C_9-PA for 2 hours could give a monolayer. The internal structure of this monolayer was analyzed by X-ray reflexivity (XRR) measurement, indicating almost vertical standing of TTF moiety with respect to the surface of substrate. By increasing the concentration to 10^{-2} M, the monolayer could not be obtained due to the self-condensation of the molecules. Addition of TCNQ or F_4TCNQ to the solution could stop the self-condensation and the monolayer could be obtained even with high concentration of 10^{-2} M. However, instability of F_4TCNQ in air would damage the monolayer after a long time immersion such as 24 hours.

2.5 Experimental section

All reagents are purchased from commercial sources and used without further purification.

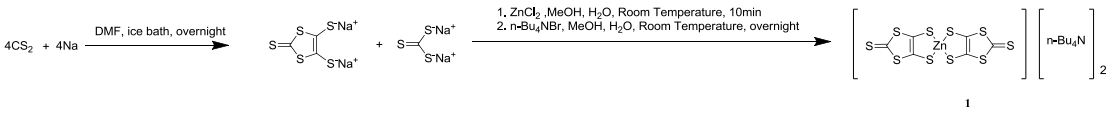

1

11.5 g (0.5 mol) sodium was cut into small cubes and put into a 3-necked flask after washing with hexane followed by vacuum evaporation to remove hexane. 90 mL CS2 was added and the flask was placed in an ice bath. 100 mL DMF was added drop wise during 4 hours while the ice bath was maintained. The reagents turned red during the addition of DMF. After DMF was all added, the suspension was warmed to room temperature slowly and stirred overnight.

The next day the reaction suspension was cooled in an ice bath again and 25 mL MeOH was added drop wise to quench the sodium followed by addition of mixture of 200 mL MeOH and 250 mL DI water. After that, 20 g $ZnCl_2$ was solved in 250 mL ammonium water and added dropwise. 200mL water was then added followed by 200 mL MeOH. Then 40.25 g n-Bu_4NBr was solved in 125mL water and added drop wise during 4 hours to give the precipitate.

The third day, the mixture in the flask was filtered with a glass fiber funnel and washed lightly with water, then 500 mL *i*-PrOH and 200 mL Et_2O. The solid was dried in vacuum to give the compound **1**. (59.497 g, 0.085 mol, 68%)

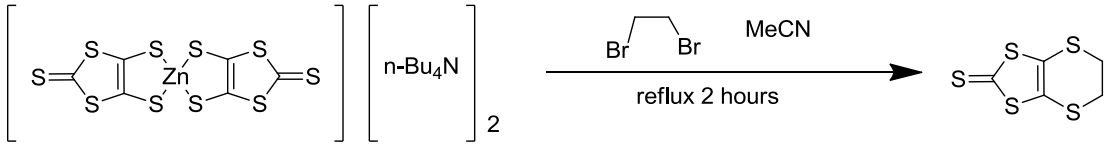

1 **2**

To a 500mL round bottom flask 7.00 g (0.01 mol) zinc salt **1** was added together with 100 mL MeCN. And 4.3 mL 1, 2-dibromoethane (0.05 mol) was added through a syringe. Then the reaction system was heated to reflux for 2 hours. After cooling to room temperature, MeCN was evaporated and the residue was solved in dichloromethane, this solution was washed by water 3 times and dried over $MgSO_4$. The product was recrystallized with dichloromethane and ethanol to give compound **2** as yellow crystal. (2.751 g, 12.3 mmol, 60%)

EIMS (*m/z*): $[M]^+$ calculated for $C_5S_5H_4$, 223.89 g mol^{-1}; found 224 g mol^{-1}.

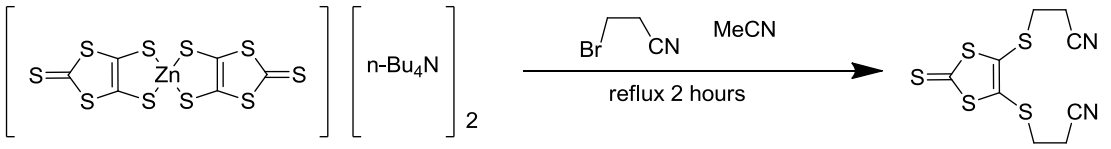

1 3

To a 500 mL round bottom flask 7.00 g (0.01 mol) zinc salt **1** was added together with 100 mL MeCN. 4.1 mL 3-bromopropanenitrile (0.05 mol) was added through a syringe. Then the reaction system was heated to reflux for 2 hours. After cooling to room temperature, MeCN was evaporated and the residue was solved in dichloromethane. This solution was washed by water 3 times and dried over $MgSO_4$. Then dichloromethane was evaporated and the residue was recrystallized with toluene and hexane to give **3** as needle-shaped yellow crystal. (5.622 g, 18.5 mmol, 92%)

EIMS (*m/z*): $[M]^+$ calculated for $C_9S_5H_8N_2$, 303.93 g mol^{-1}; found 304 g mol^{-1}.

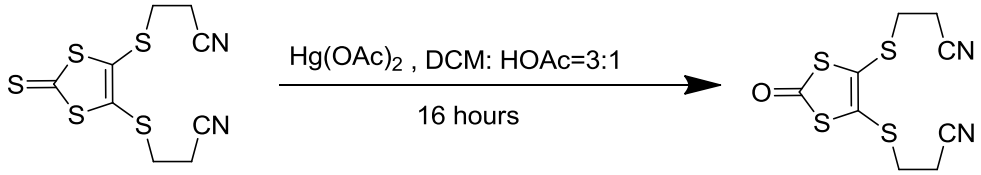

3 4

4.187 g (13.7 mmol) compound **5** was added to a 500 mL round bottom flask together with 8.401 g $Hg(OAc)_2$ (26 mmol). 60 mL Dichloromethane and 20 mL acetic acid was added and stirred at room temperature for 16 hours. The mixture was then filtered using 0.5 μm filter. The filtrate was washed with brine and deionized water several times. After dried over $MgSO_4$ and evaporated solvent, compound **4** was given as light yellow solid. (2.909 g, 10.1 mmol, 74%)

EIMS (*m/z*): $[M]^+$ calculated for $C_9S_4H_8N_2O$, 287.95 g mol^{-1}; found 288 g mol^{-1}.

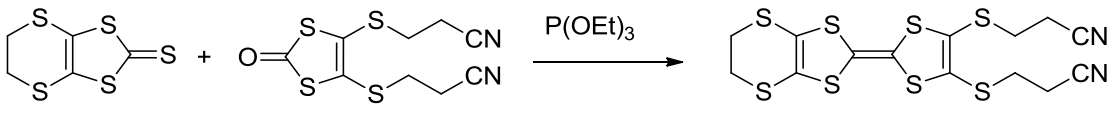

2 4 5

1.251 g compound **4** (5.6 mmol) and 1.677 g compound **6** (5.8 mmol) was added to a 3-necked flask and followed by 25 mL triethylphosphate under Ar atmosphere. The mixture was heated to 120 ℃ for 2 hours. After cooling to room temperature, 100 mL MeOH was added. The following day, the mixture was filtered through a 0.5 μm filter. The precipitate was collected and chromatography column was taken with dichloromethane to give **5** as orange solid. (1.252 g, 2.7 mmol, 48%)

EIMS (*m/z*): $[M]^+$ calculated for $C_{14}S_8H_{12}N_2$, 463.88 g mol^{-1}; found 464 g mol^{-1}.

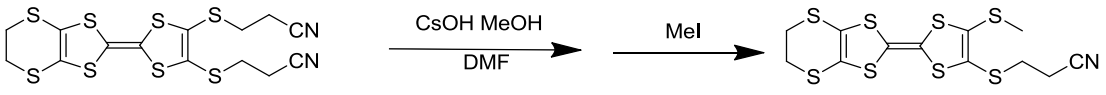

5 6

1.223 g compound **7** (2.6 mmol) in a 200 mL round bottom flask was solved in 50 mL DFM. 0.45 g cesium hydroxide monohydrate (2.6 mmol) was solved in 60 mL MeOH and added drop wise during 30 minutes. The solution was then stirred for another 30 minutes followed by addition of 1.62mL MeI (26 mmol) and stirred for another 2 hours. MeOH was removed together with MeI during rotary evaporation. Then water was added and extracted with dichloromethane. A short column with dichloromethane was able to give pure compound **6** as red solid. (1.056 g, 2.4 mmol, 92%)

EIMS (*m/z*): $[M]^+$ calculated for $C_{12}S_8H_{11}N_2$, 424.87 g mol^{-1}; found 425 g mol^{-1}.

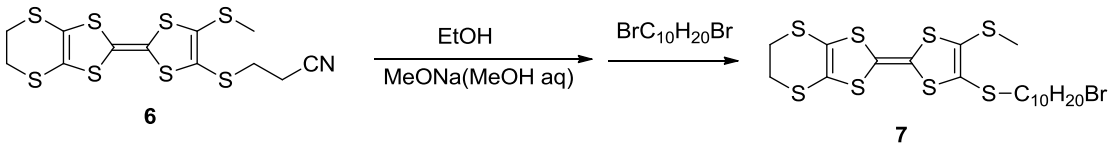

6 7

To a flask filled with 0.474 g compound **8** (1.1 mmol) 80 mL EtOH was added and stirred for 1 hour. 2 mL MeONa (28% MeOH solution) was added slowly and stirred for 4 hours. Then 2.008 g 1, 10-dibromodecane was added and stirred overnight. The next day, all solution was removed by rotary evaporation, 100 mL water was added and extracted by dichloromethane(100 mL×3). Solution was dried over $MgSO_4$ and separated through column chromatography with dichloromethane and hexane (dichloromethane: hexane=1:4). 0.462 g orange oil was collected as compound **7**. (0.462 g, 0.78 mmol, 71%)

EIMS (*m/z*): $[M]^+$ calculated for $C_{19}S_8H_{27}Br$, 591.90 g mol^{-1}; found 592 g mol^{-1}.

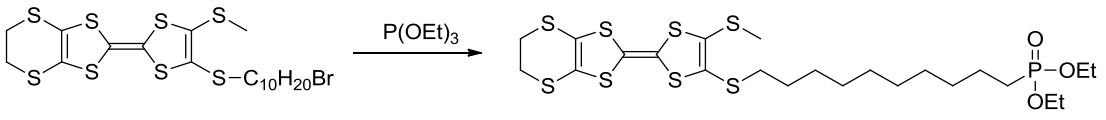

7 8

0.300 g compound **9** (0.51 mmol) was solved in 10 mL triethylphosphite and heated to 140 ℃ overnight. After cooled to room temperature, vacuum distillation was applied to evaporate solvent. The residue was solved in dichloromethane and washed with brine 3 times, dried over $MgSO_4$ and separated with column chromatography by THF and hexane(THF: Hexane=1:5). After rotary evaporation, compound **10** was collected as red oil. (0.306 g, 0.47 mmol, 92%)

EIMS (*m/z*): $[M]^+$ calculated for $C_{23}S_8H_{37}O_3P$, 648.02 g mol^{-1}; found 648 g mol^{-1}.

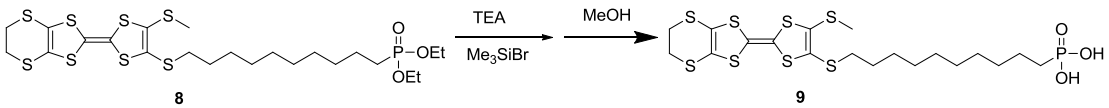

8 9

10 mg compound **10** was added to a 3-necked flask and sealed under Ar atmosphere. 0.5 mL trimethylamine (TEA) and 30 mL dry dichloromethane was added to a drop funnel and bubbled for several minutes. Half of the solution was dropped into the flask and 0.2 mL Me_3SiBr was added to the drop funnel, bubbled for another several minutes and then added to the flask drop wise. The solution was stirred overnight. The next day, 20 mL MeOH was added after vacuum distillation and stirred for additional 4 hours. Dichloromethane was added and the solution was transferred to a separating funnel. The solution was washed by mixture of MeOH and NaH_2PO_4 solution several times and water was removed by azeotropy with benzene to remove water. The compound was stored in diluted solution until use in order to avoid self-polymerization reaction. Finally, the solution was filtered with 0.5 μm filter and used immediately. Yield was considered as 70%.

ESIMS (*m/z*): $[M - H]^-$ calculated for $C_{19}S_8H_{18}O_3P$, 590.95 g mol^{-1}; found 591 g mol^{-1}.

2.6 References

(1) Gholamrezaie, F.; Mathijssen, S. G.; Smits, E. C.; Geuns, T. C.; van Hal, P. A.; Ponomarenko, S. A.; Flesch, H. G.; Resel, R.; Cantatore, E.; Blom, P. W.; de Leeuw, D. M. *Nano Lett* **2010**, *10*, 1998.

(2) Schmaltz, T.; Amin, A. Y.; Khassanov, A.; Meyer‐Friedrichsen, T.; Steinrück, H. G.; Magerl, A.; Segura, J. J.; Voitchovsky, K.; Stellacci, F.; Halik, M. *Adv Mater* **2013**, *25*, 4511.

(3) Ringk, A.; Li, X.; Gholamrezaie, F.; Smits, E. C.; Neuhold, A.; Moser, A.; Van der Marel, C.; Gelinck, G. H.; Resel, R.; de Leeuw, D. M. *Adv Funct Mater* **2013**, *23*, 2016.

(4) Mathijssen, S. G.; Smits, E. C.; van Hal, P. A.; Wondergem, H. J.; Ponomarenko, S. A.; Moser, A.; Resel, R.; Bobbert, P. A.; Kemerink, M.; Janssen, R. A.; de Leeuw, D. M. *Nat. Nanotech.* **2009**, *4*, 674.

Part 3 FET property without doping

3.1 FET property of monolayer device fabricated by pure solution

Since the BEDT-TTF and its derivatives are electron donating semiconductor materials, p-type FET behavior should exist for a monolayer device. FET property was measured on bottom-contact/bottom-gate device with channel length 5 μm and channel width 1 mm under vacuum.

Figure 3.1.1a shows the output characteristic curves, where p-type behavior is observed. Hole mobility was calculated at $5.54 \times 10^{-7}\ cm^2V^{-1}s^{-1}$ with on/off ratio of about 10^4. The mobility is quite poor compared to other reported monolayer FETs[1-4]. Poor aromaticity and electron-conjugation may contribute to this poor performance. Notice that even single crystal BEDT-TTF device only show mobility of $1.7 \times 10^{-3}\ cm^2V^{-1}s^{-1}$ for the corrugated molecular shape at neutral state[5].

Figure 3.1.1b shows the transfer characteristic curves with drain voltage fixed at 50 V. The drain current shows a two-step increase from the OFF state at highly positive gate voltage close to 200 V. The first region can be considered as sub-threshold region, where increase of I_D can probably be attributed to the delocalization of carriers inside grains. Carriers are getting easier to transfer among monolayer grains when gate voltage decrease furthermore. This p-type device was turned “on” at about gate voltage 50 V. Threshold voltage above 0 V for p-type FET can be attributed to a shift of Fermi-level due to the oxygen.

Sheet conductivity was checked with different samples for channel length 5 μm, 10 μm, 15 μm, 25 μm, 50 μm, 100 μm and 200 μm. Gate voltage was fixed on -100 V and drain voltage was fixed on 50 V. Average sheet conductivity with error bar is shown in figure 3.1.2. Generally speaking, the sheet conductivity didn’t change very much during the expansion of channel length. This implies either the domain size of monolayer is much smaller than 5 μm or it does not affect the sheet conductance very much. During this expansion of channel length, the standard deviation of sheet conductivity became very large for channel length longer than 50 μm because of the resolution limit of the measurement system.

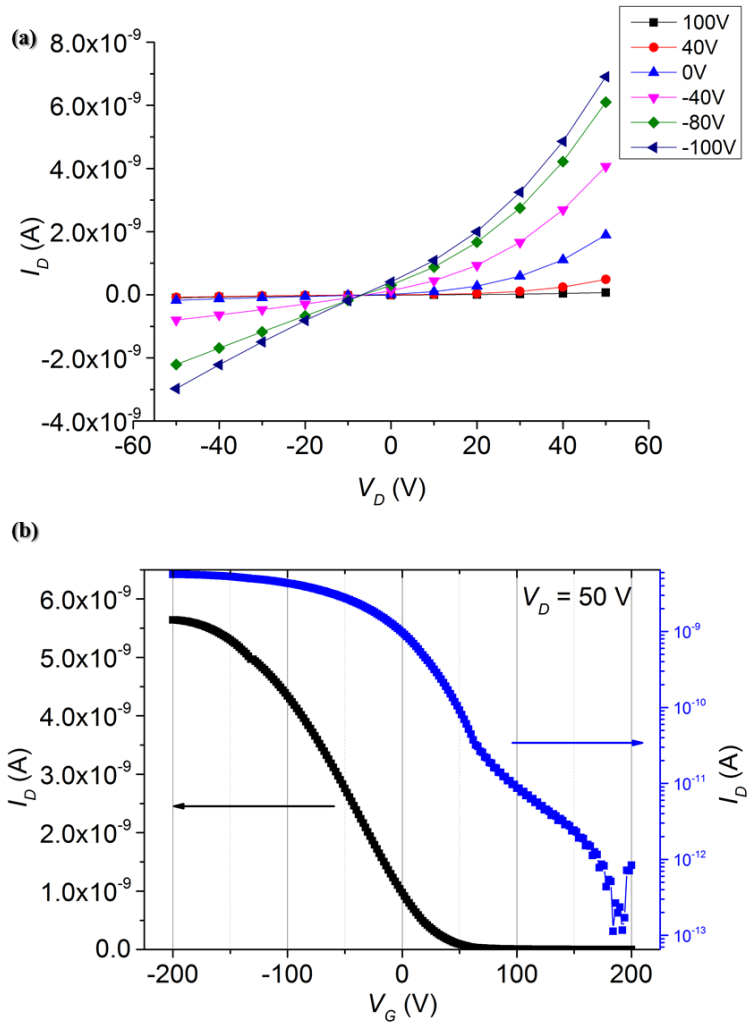

Figure 3.1.1: output characteristic curves (a) and transfer characteristic curves (b) of monolayer device fabricated by 10^{-3} M EDT-DMT-C_9-PA pure solution.

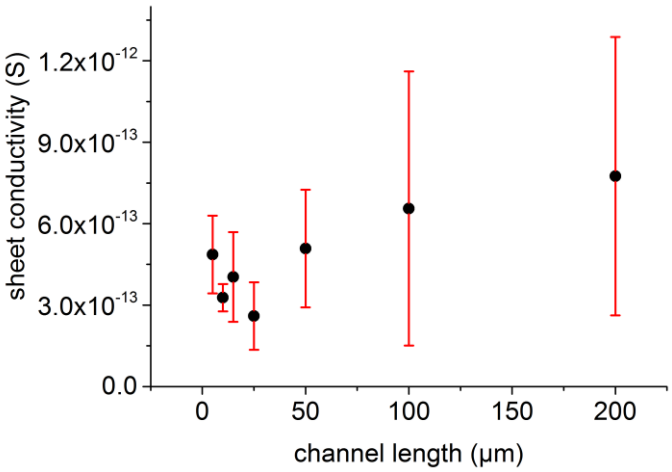

Figure 3.1.2: Channel length related sheet resistance with error bar at gate voltage -100 V and drain voltage 50 V.

3.2 Monolayer device fabricated with TCNQ

Monolayer device was also fabricated by solution containing TCNQ as discussed in Part 2. Output and transfer characteristic curves of device fabricated with TCNQ are shown in figure 3.2.1.

Obviously, the performance is decreased by more than one order of magnitude compared to monolayer devices fabricated by 10^{-3} M solution without TCNQ. Hole mobility was calculated at $2.43 \times 10^{-8}\ cm^2V^{-1}s^{-1}$, which is again lower than those for devices fabricated by pure solution. In transfer characteristic curves, drain current I_D appears slightly negative when gate voltage is higher than 64V and these negative current data are deleted. Relationship between conductivity and channel length was not measured because the current is pretty close to the detection limit.

Solution with TCNQ did not give a monolayer device with higher performance but gave a monolayer with TCNQ existing as impurities inside it, resulting in a decrease of the performance.

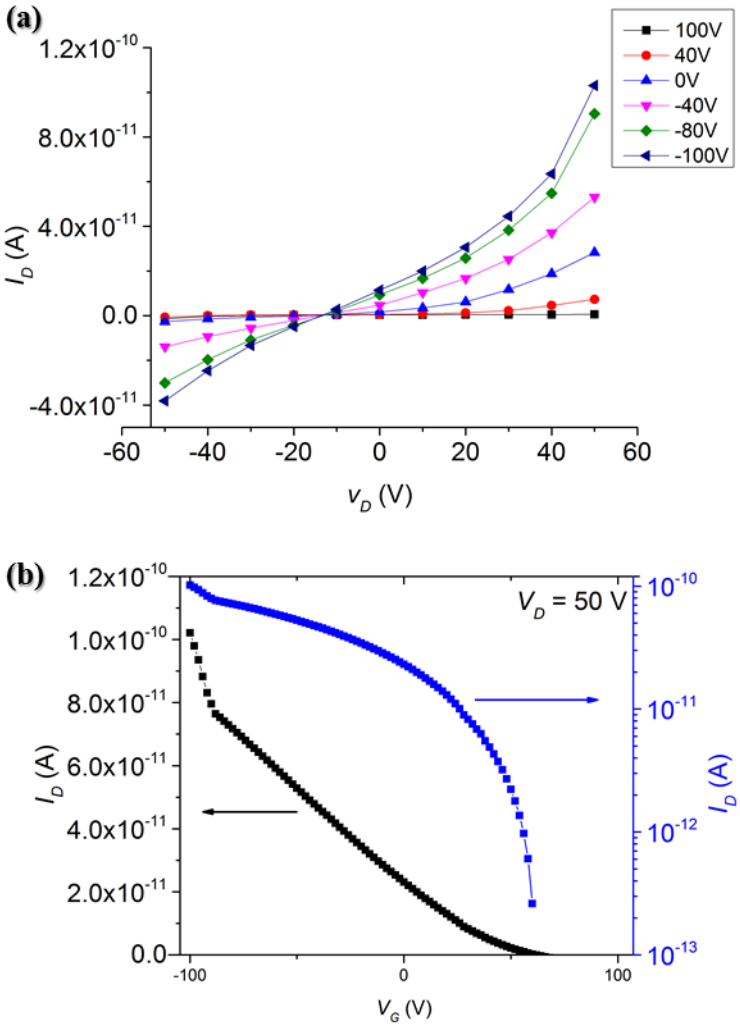

Figure 3.2.1: Output characteristic curves (a) and transfer characteristic curves (b) of monolayer device fabricated by 10^{-3} M EDT-DMT-C_9-PA solution with TCNQ.

3.3 Monolayer device fabricated with F_4TCNQ

Monolayer device could also be fabricated by solution with F_4TCNQ in a short time such as 2 hours, which was discussed in Part 2. Output and transfer characteristic curves of device fabricated by EDT-DMT-TTF-C_9-PA 10^{-3} M solution with F_4TCNQ are shown in figure 3.3.1.

As a p-type FET device, the FET mobility of device fabricated with F_4TCNQ is almost as low as monolayer device fabricated with TCNQ. Hole mobility was calculated to be $3.41 \times 10^{-8}\ cm^2V^{-1}s^{-1}$. This result is very close to the TCNQ ones. The low mobility may be caused by the same reason with TCNQ case.

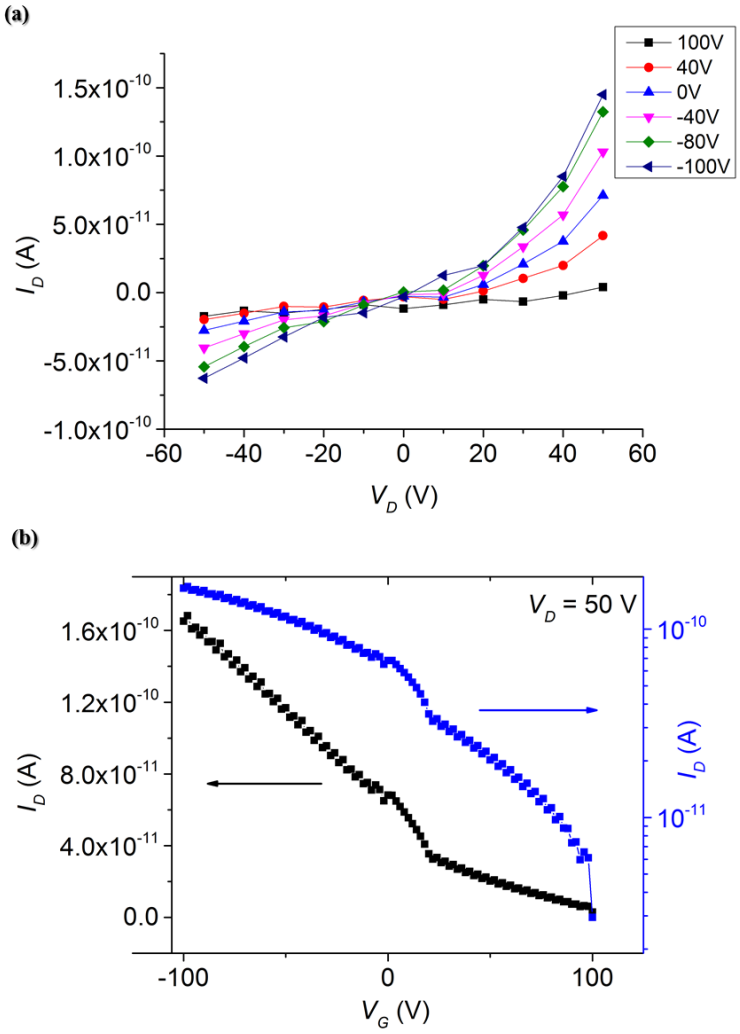

Figure 3.3.1: Output characteristic curves (a) and transfer characteristic curves (b) of monolayer device fabricated by 10^{-3} M EDT-DMT-C_9-PA solution with F_4TCNQ.

3.4 Summary

All monolayer devices fabricated by pure EDT-DMT-TTF-C_9-PA solution, solution with TCNQ and solution with F_4TCNQ were measured and p-type FET behavior could be observed with a relatively low performance. TCNQ or F_4TCNQ containing solutions gave a monolayer device with even lower performance. The decrease of FET performance was attributed to the TCNQ or F_4TCNQ existing as charged impurities.

3.5 Reference

(1) Shan, L.; Liu, D.; Li, H.; Xu, X.; Shan, B.; Xu, J. B.; Miao, Q. *Adv Mater* **2015**, *27*, 3418.

(2) Defaux, M.; Gholamrezaie, F.; Wang, J.; Kreyes, A.; Ziener, U.; Anokhin, D. V.; Ivanov, D. A.; Moser, A.; Neuhold, A.; Salzmann, I.; Resel, R.; de Leeuw, D. M.; Meskers, S. C.; Moeller, M.; Mourran, A. *Adv Mater* **2012**, *24*, 973.

(3) Novak, M.; Ebel, A.; Meyer-Friedrichsen, T.; Jedaa, A.; Vieweg, B. F.; Yang, G.; Voitchovsky, K.; Stellacci, F.; Spiecker, E.; Hirsch, A. *nano lett*, **2010**, *11*, 156.

(4) Ringk, A.; Li, X.; Gholamrezaie, F.; Smits, E. C.; Neuhold, A.; Moser, A.; Van der Marel, C.; Gelinck, G. H.; Resel, R.; de Leeuw, D. M. *Adv Funct Mater* **2013**, *23*, 2016.

(5) Mas-Torrent, M.; Hadley, P.; Bromley, S. T.; Ribas, X.; Tarrés, J.; Mas, M.; Molins, E.; Veciana, J.; Rovira, C. *J Am Chem Soc* **2004**, *126*, 8546.

Part 4 F4TCNQ Doping by spin coating method

4.1 Introduction

As discussed in part 1, in a κ-type BEDT-TTF cation radical crystal, Mott insulating phase can be obtained at band-filling 0.5. Every two BEDT-TTF molecules form a dimer and give out 1 electron, to let the Coulomb repulsion form an electronic solid, or Mott insulator. In this type of crystals, anions virtually accept the electrons from the BEDT-TTF layer. If we can remove electrons from the previously mentioned monolayer, Coulomb repulsion will probably create a Mott gap which will prevent the carriers to move. Chemical doping by acceptor materials was thus considered the most convenient way to remove electrons from these monolayer devices.

Among the organic electron-accepting materials, TCNQ and F_4TCNQ are the most commonly used molecules. Ambipolar FET devices fabricated with (BEDT-TTF)(TCNQ) single crystals, in which metal-like behavior was observed[2], have been reported. Since the EDT-DMT-TTF should have a close HOMO energy level with BEDT-TTF, both TCNQ and F_4TCNQ should be able to dope the monolayer. In experiments, however, the effect of TCNQ doping was not observed while F_4TCNQ showed a significant conductivity change upon doping. In this part, F_4TCNQ doping will be discussed.

All doping processes are conducted by spinning the substrate at 500 r.p.m for 5 seconds followed by 4000 r.p.m for 35 seconds under ambient atmosphere. THF was used as solvent for different concentration of F_4TCNQ. PFA (perfluoroalkoxy copolymer) container was used instead of glass to avoid the reaction between F_4TCNQ and Pyrex® glass.

4.2 Doping effect on device made by donor's pure solution

4.2.1 Doping by 0.05 g/L F_4TCNQ solution

At first, diluted F_4TCNQ solution at a concentration of 0.05g/L was used. Output and transfer characteristic curves are shown in figure 4.2.1.1. Compared to device performance before the doping, the current at on state didn't raise very much, still remaining at 10^{-9} A level. But the off state seems not able to remain in a similar level. This is probably because of the charge-transfer which injected hole carriers into the monolayer. Here ΔI was used to show up the field-induced current, to be defined as

$\Delta I = I_D - I_{min}$. I_D is the drain current and I_{min} is the lowest current value in each I_D-V_G transfer curve, so that ΔI represents only the FET switching current. I_{min} was replaced by 10^{-13}A so that we can mark the point of V_{min} when I_{min} appears with logarithmic y-axis. In figure 4.2.1.1c, with drain voltage 50 V, this device shows only p-type behavior with V_{min} at 100 V. Hole mobility was calculated to be $3.8 \times 10^{-7}\ cm^2V^{-1}s^{-1}$. When drain voltage was fixed on -50 V, a weak n-type behavior seems to exist on highly positive gate voltage region, with V_{min} at 78 V. N-type mobility was not calculated because it was too small and ambiguous.

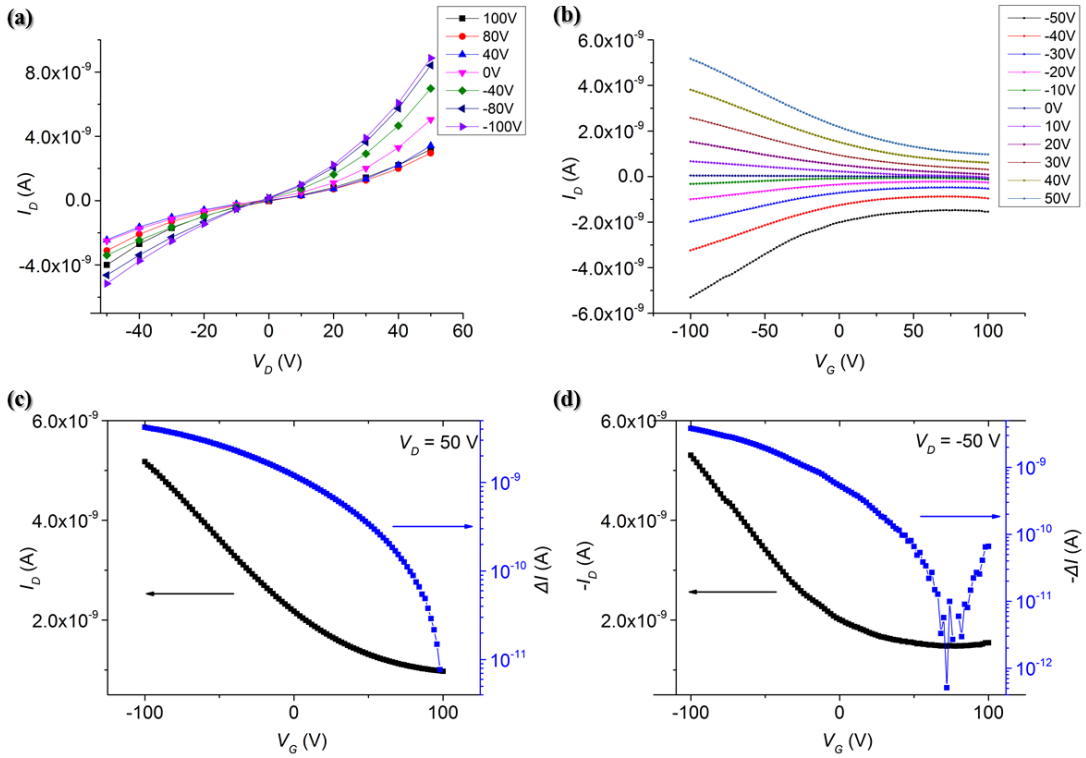

Figure 4.2.1.1: output characteristic curves (a) and transfer characteristic curves (b) of monolayer device fabricated by 10^{-3} M EDT-DMT-C_9-PA pure solution and doped by 0.05 g/L F_4TCNQ solution spin coating. c) I_D-V_G curve (linear scale) and ΔI-V_G curve (log scale) at drain voltage 50 V. d) I_D-V_G curve (linear scale) and ΔI-V_G curve (log scale) at drain voltage -50 V.

4.2.2 Doping by 0.1 g/L F_4TCNQ solution

By increasing the concentration of F_4TCNQ to 0.1 g/L, the current at on state was raised by several times. In figure 4.2.2.1c, when drain voltage was fixed on 50 V, a little n-type behavior appeared with V_{min} at 88 V. When drain voltage was set at -50 V, in

figure 4.2.2.1d, ambipolar behavior with V_{min} of 12 V was observed. P-type FET mobility was calculated at $7.97 \times 10^{-7}\ cm^2V^{-1}s^{-1}$ and n-type mobility was calculated at $2.68 \times 10^{-7}\ cm^2V^{-1}s^{-1}$. Notice that ambipolar characteristics is not a normal behavior because doping on ordinary p-type FET devices will not induce n-type behavior. The drain voltage such as 50 V and -50 V influenced the gate field effect, since the source electrode is fixed at ground level.

Surface morphology was studied by AFM and the result is shown in figure 4.2.2.2., although it was somehow anticipated that no clear evidence of existing F_4TCNQ can be observed.

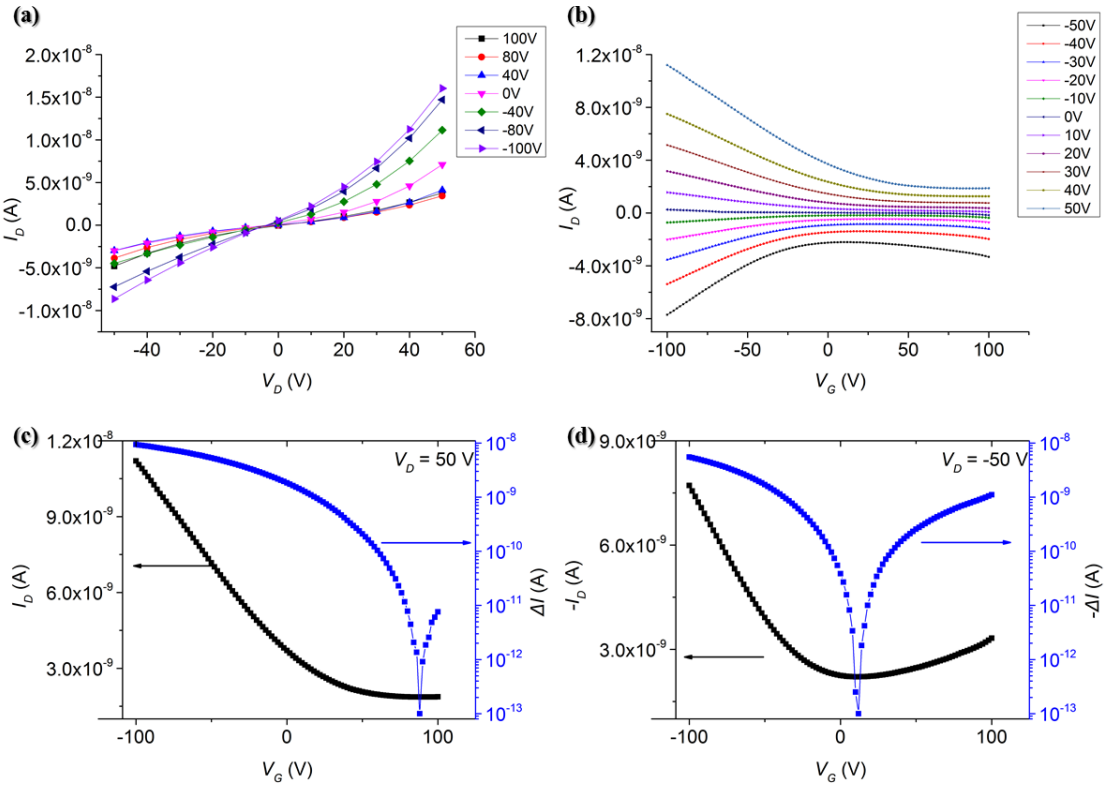

Figure 4.2.2.1: output characteristic curves (a) and transfer characteristic curves (b) of monolayer device fabricated by 10^{-3} M EDT-DMT-C_9-PA pure solution and doped by spin coating of 0.1 g/L F_4TCNQ solution. c) I_D-V_G curve and ΔI-V_G curve at drain voltage 50 V. d) I_D-V_G curve and ΔI-V_G curve at drain voltage -50 V.

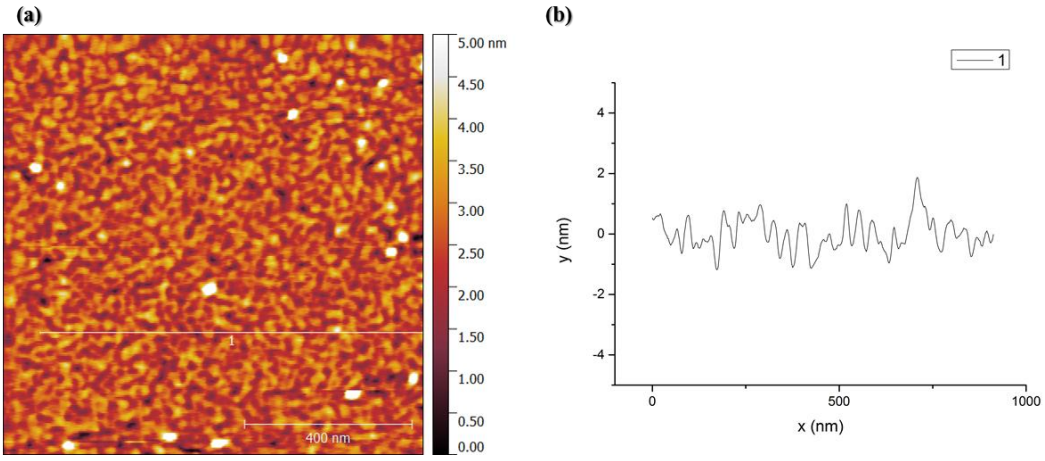

Figure 4.2.2.2: a) AFM image (1 μm × 1 μm) of device doped by 0.1 g/L F_4TCNQ solution. b) Cross sectional height profiles measured along the white line 1 in the AFM image.

4.2.3 Doping by 0.25 g/L F_4TCNQ solution

Further increase in the concentration of F_4TCNQ solution to 0.25g/L gave the FET performance a continued increase with both p- and n-type behavior. These can be observed clearly even when drain voltage was at positive region such as 50V. P-type mobility was calculated at $2.39 \times 10^{-6}\, cm^2V^{-1}s^{-1}$ and n-type mobility was calculated at $3.74 \times 10^{-6}\, cm^2V^{-1}s^{-1}$, which are slightly improved than the previous case. V_{min} appeared at 44 V and -2 V when drain voltage was fixed at 50 V and -50 V, respectively.

The performance seemed to be influenced by the time during which the device was paced under vacuum. One sample was kept under vacuum with a timer to check the time-dependence, whose results are shown in figure 4.2.3.3. Timer started from initiation of vacuum pumping. From 1 hour to 24 hours, p-type performance showed an increase which was probably due to the removal of surface impurity such as water molecule. Meanwhile, from 24 hours to 72 hours, the FET performance kept decreasing. ΔI-V_G curves clearly showed the shifting of V_{min} against time. Obviously, n-type kept shrinking and disappeared after 48 hours with V_{min} shifting towards positive direction region. Disappearance of n-type behavior could probably be attributed to the evaporation of F_4TCNQ under vacuum. This result determined that the sample dependence comes from not only spin coating process, but also the evaporation or deterioration of F_4TCNQ dopants.

Surface morphology was also studied by AFM and the result is shown in figure 4.2.3.2.

The surface was just like device doped by 0.1 g/L F_4TCNQ except that some islands appears with several nanometers in height.

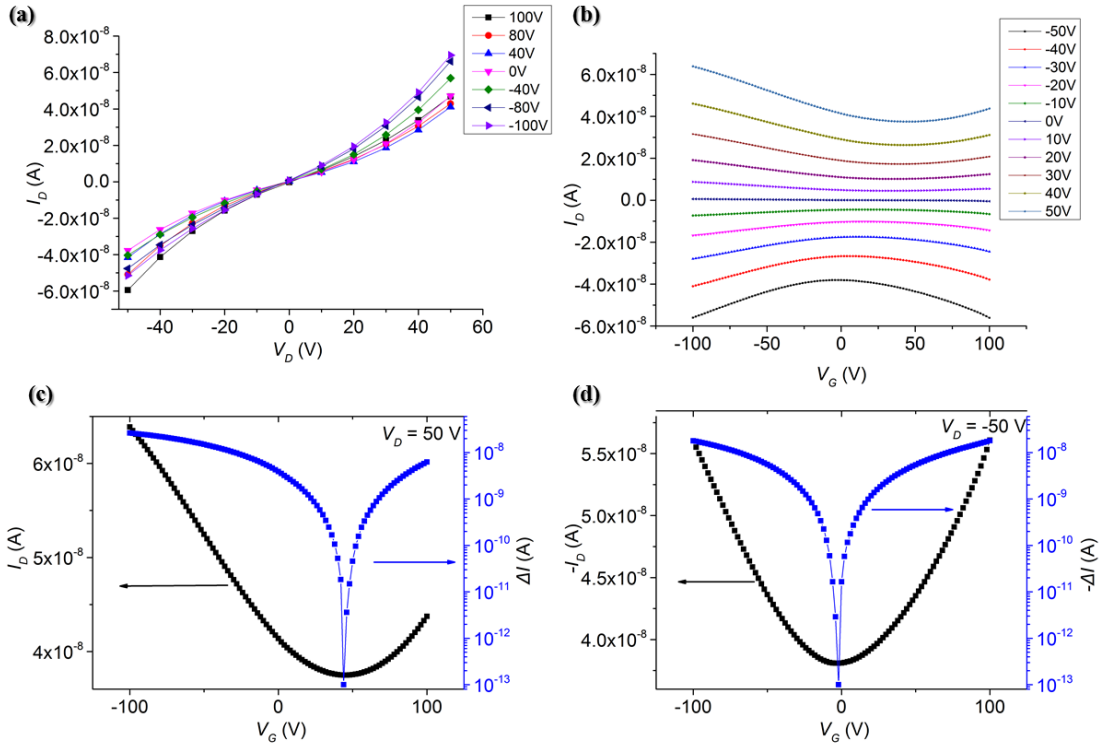

Figure 4.2.3.1: output characteristic curves (a) and transfer characteristic curves (b) of monolayer device fabricated by 10^{-3} M EDT-DMT-C_9-PA pure solution and doped by spin coating of 0.25 g/L F_4TCNQ solution. c) I_D-V_G curve and ΔI-V_G curve at drain voltage 50 V. d) I_D-V_G curve and ΔI-V_G curve at drain voltage -50 V.

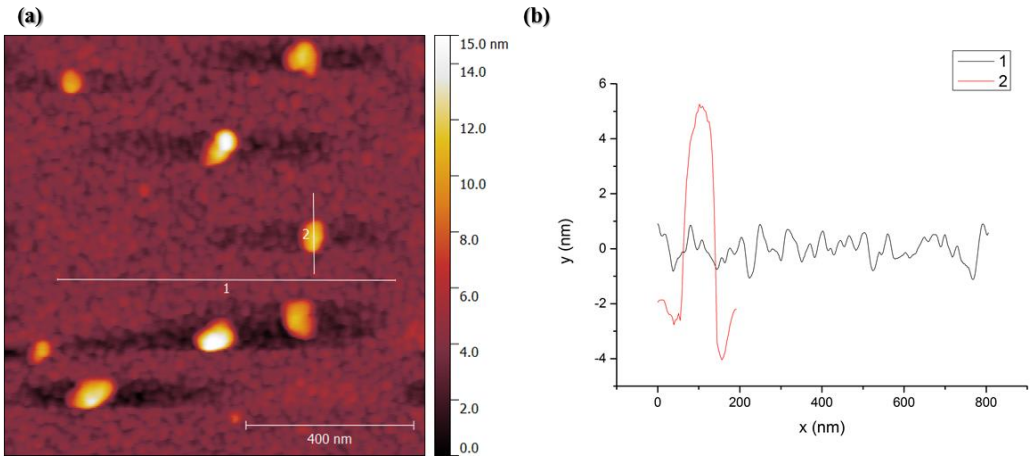

Figure 4.2.3.2: a) AFM image (1 μm × 1 μm) of device doped by 0.25 g/L F_4TCNQ. b) Cross sectional height profiles measured along the white line 1 and 2 in the AFM image.

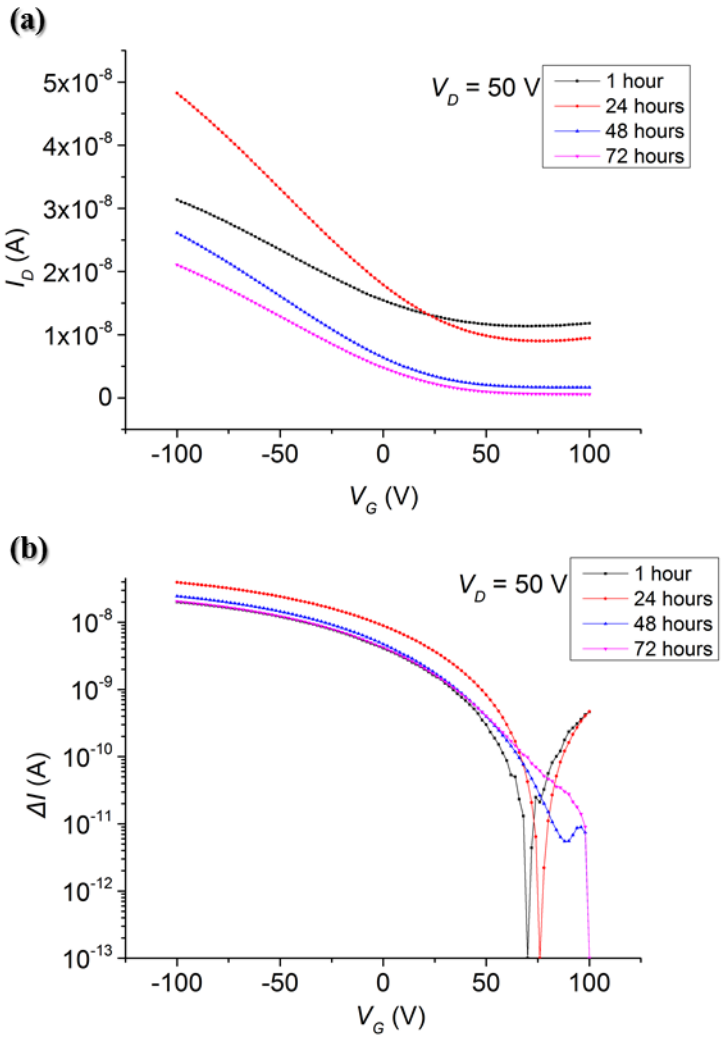

Figure 4.2.3.3: Time dependence of F_4TCNQ doped monolayer devices. (a) Transfer characteristic curves for 1 hour, 24 hours, 48 hours and 72 hours under vacuum. (b)V_g-ΔI curves of time dependence to mark the shift of threshold voltage.

4.2.4 Doping by 0.5 g/L F_4TCNQ solution

By increasing the concentration of F_4TCNQ solution to 0.5 g/L, the ambipolar FET behavior of doped devices became clearer. FET mobility and off current were increased at the same time. P-type mobility was calculated to be $5.22 \times 10^{-6}\ cm^2V^{-1}s^{-1}$ and n-type mobility was calculated to be $1.04 \times 10^{-5}\ cm^2V^{-1}s^{-1}$. At this doping concentration, V_{min} appears at 28 V and -12 V when drain voltage was fixed to 50 V and -50 V, respectively.

Since the carriers were injected not only from the gate electrode but also from drain electrode, "symmetric-gate" operations were helpful to combine the carrier injection effects from both electrodes, in which $U_g=V_G-V_D/2$. This treatment is already reported in analyzing behavior of BEDT-TTF-based organic Mott FETs[3].

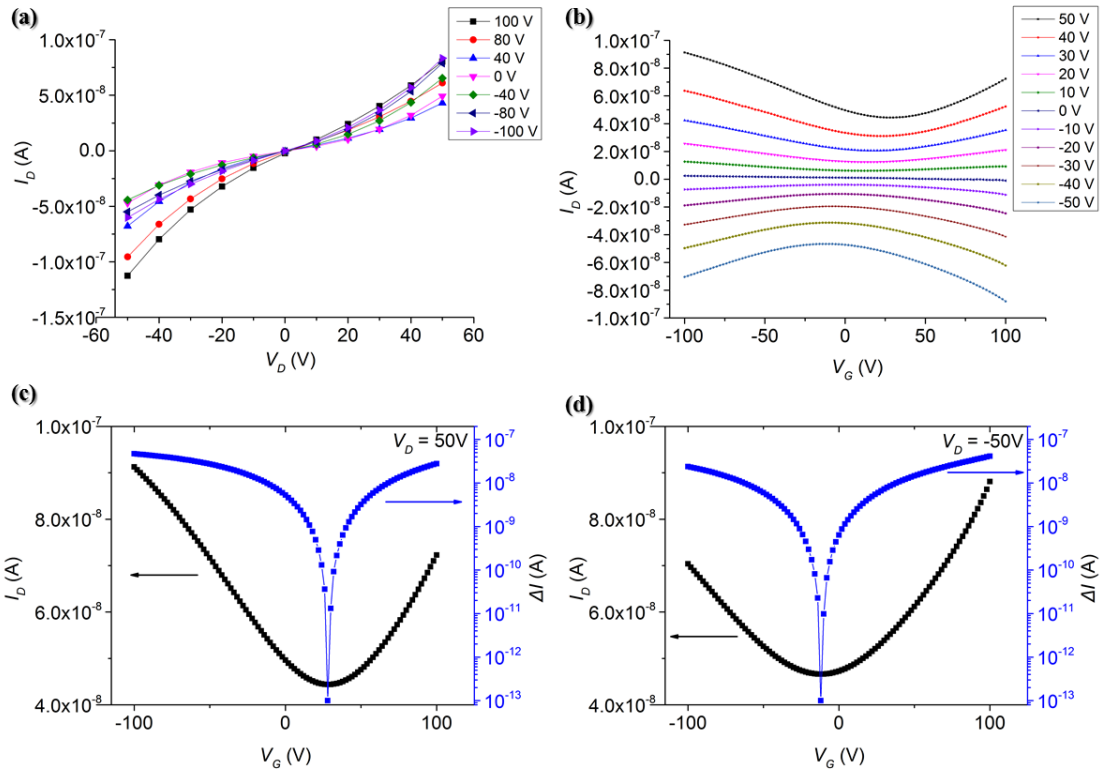

Figure 4.2.4.1: output characteristic curves (a) and transfer characteristic curves (b) of monolayer device fabricated by 10^{-3} M EDT-DMT-C_9-PA pure solution and doped by spin coat 0.5 g/L F_4TCNQ solution. c) I_D-V_G curve and ΔI-V_G curve at drain voltage 50 V. d) I_D-V_G curve and ΔI-V_G curve at drain voltage -50 V.

For example, with this operation, transfer curves of device doped by 0.5 g/L F_4TCNQ solution (Figure 4.2.4.1b) can be modified into figure 4.2.4.2. ΔI exhibits clear carrier injection with both positive and negative drain voltage. I_{min} dependence on V_D seems to be explained mostly from this effect since I_{min} for all the data appears around the same U_G. All doped monolayer devices can give a similar result.

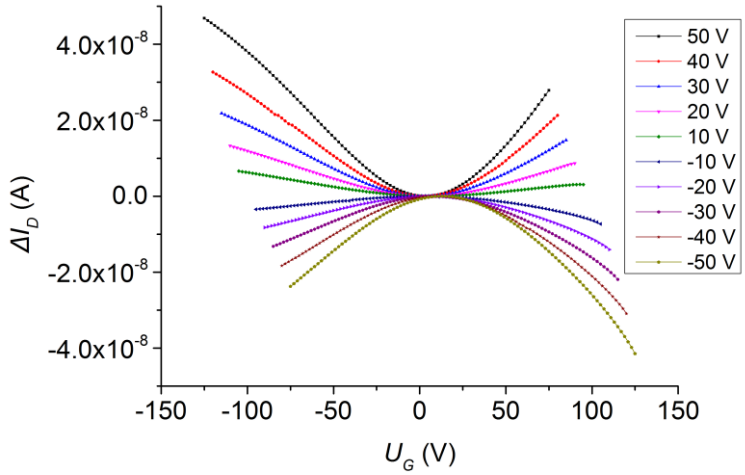

Figure 4.2.4.2: "Symmetric-gate" operated transfer characteristic curves of Figure 4.2.4.1b. ΔI was used to represent only field-induced current.

4.2.5 Doping by 1 g/L F_4TCNQ solution

Increasing the concentration of F_4TCNQ solution to 1 g/L led to a further increase of the performance of monolayer device together with an increased off current. On the surface of doped devices, very small crystals can be observed by optical microscope as shown in figure 4.2.5.1. At the same time, AFM images of doped device surface showed a flat surface with islands of several nanometers in height. This result indicated that the spin coated F_4TCNQ seemed not forming a film but gathered to form micro crystals, which implied that the doping of F_4TCNQ with spin coating method at this concentration was probably inhomogeneous. This pint will be discussed later.

Output and transfer characteristic curves of device doped by 1 g/L F_4TCNQ is shown in figure 4.2.5.2. Since the off current have been raised to several hundred nanoampere, FET switching current was not as obvious as devices doped by 0.5 g/L F_4TCNQ solution especially in p-type region. P-type mobility was calculated at $7.96 \times 10^{-6}\ cm^2V^{-1}s^{-1}$ and n-type mobility was calculated at $2.17 \times 10^{-5}\ cm^2V^{-1}s^{-1}$. V_{min} appeared at 18 V and -38 V when drain voltage was fixed on 50 V and -50 V, respectively.

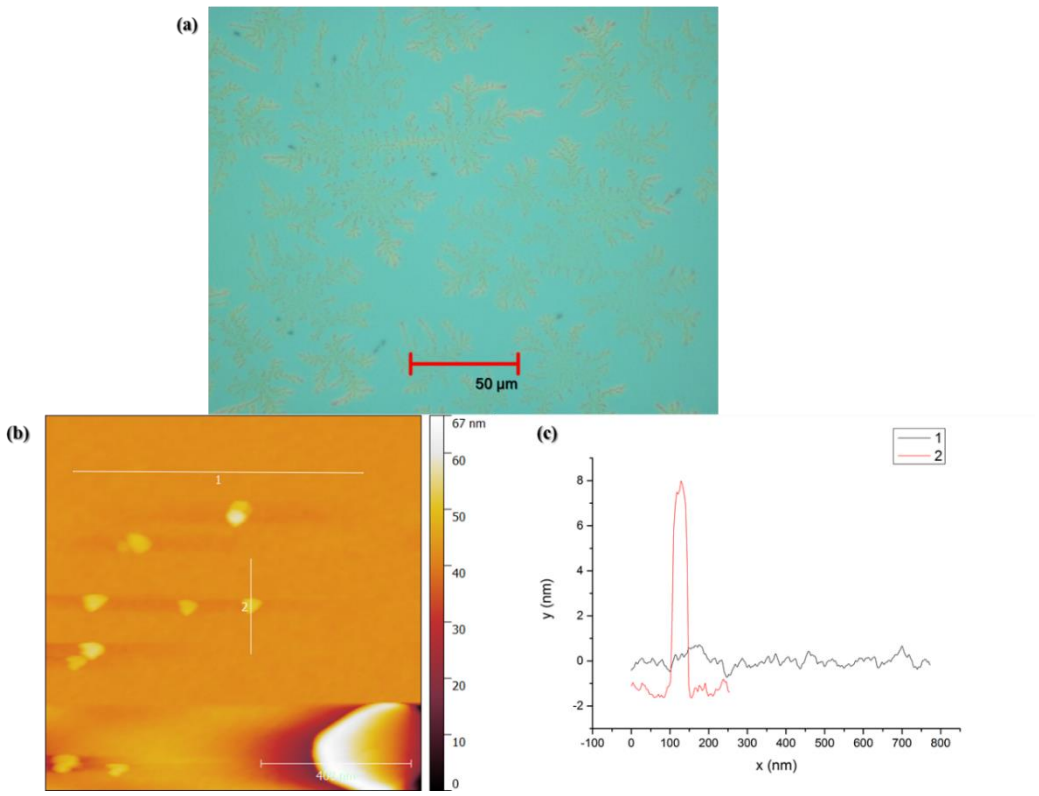

Figure 4.2.5.1: a) Crystals observed under microscope on the surface of device doped by 1 g/L F_4TCNQ solution. b) AFM image (1 µm × 1 µm) of device doped by 1 g/L F_4TCNQ. c) Cross sectional height profiles measured along the white line 1 and 2 in the AFM image.

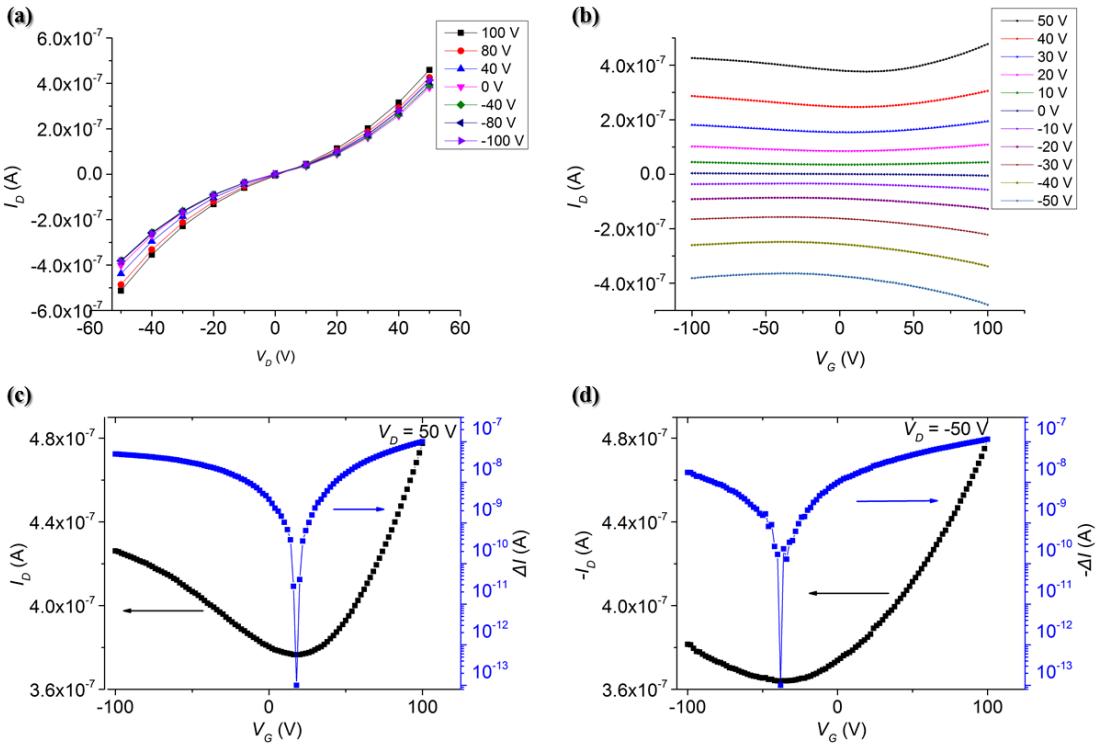

Figure 4.2.5.2: output characteristic curves (a) and transfer characteristic curves (b) of monolayer device doped by spin coating of 1 g/L F_4TCNQ solution after fabrication by 10^{-3} M EDT-DMT-C_9-PA pure solution. c) I_D-V_G curve and ΔI-V_G curve at drain voltage 50 V. d) I_D-V_G curve and ΔI-V_G curve at drain voltage -50 V.

4.2.6 Doping by 5 g/L F_4TCNQ solution

5 g/L F_4TCNQ solution was spin coated on the surface of monolayer devices to check the performance under highly 'doped' state. The result shown in figure 4.2.6.1 gave p-type mobility of $9.32 \times 10^{-6}\ cm^2V^{-1}s^{-1}$ and n-type mobility of $5.56 \times 10^{-5}\ cm^2V^{-1}s^{-1}$. The current rose to 10^{-6} A level while the mobility didn't rise very much, especially for p-type mobility. P-type performance almost disappeared in transfer characteristic curves.

In order to exclude the possibility of the n-type behavior from a pure F_4TCNQ layer, 0.1 g/L and 5 g/L F_4TCNQ was spin coated on bare alumina substrate to check the conductivity of F_4TCNQ itself. The transfer characteristic curves at drain voltage 50V are shown in figure4.2.6.2. Obviously, 0.1 g/L F_4TCNQ was not conductive and the measured current at this concentration was as low as 10^{-11} A. Device fabricated by 5 g/L F_4TCNQ solution offered a current up to 1.3×10^{-8} A at drain voltage of 50 V and

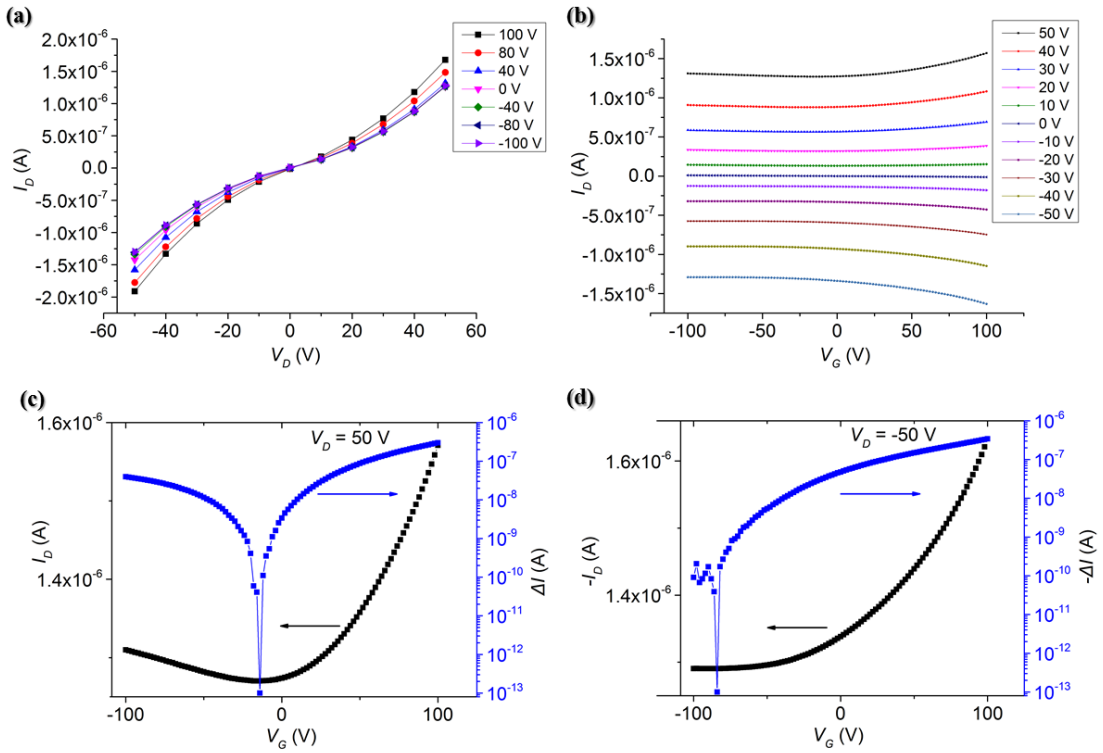

Figure 4.2.6.1: output characteristic curves (a) and transfer characteristic curves (b) of monolayer device fabricated by 10^{-3} M EDT-DMT-C_9-PA pure solution and doped by spin coating of 5 g/L F_4TCNQ solution. c) I_D-V_G curve and ΔI-V_G curve at drain voltage 50 V. d) I_D-V_G curve and ΔI-V_G curve at drain voltage -50 V.

gate voltage of 100 V. N-type mobility was calculated at $2.63 \times 10^{-7}\ cm^2V^{-1}s^{-1}$ from the slope of transfer characteristic curve. This value is even lower than the n-type mobility given by monolayer device doped by 0.1 g/L F_4TCNQ, which was $2.68 \times 10^{-7}\ cm^2V^{-1}s^{-1}$. Furthermore, 5 g/L F_4TCNQ doped monolayer device offered a current value up to 10^{-6} A, more than 100 times larger than that of F_4TCNQ itself. These results indicated the p- and n- type FET behavior of doped monolayer device did not come from the F_4TCNQ itself, but come from the doped monolayer.

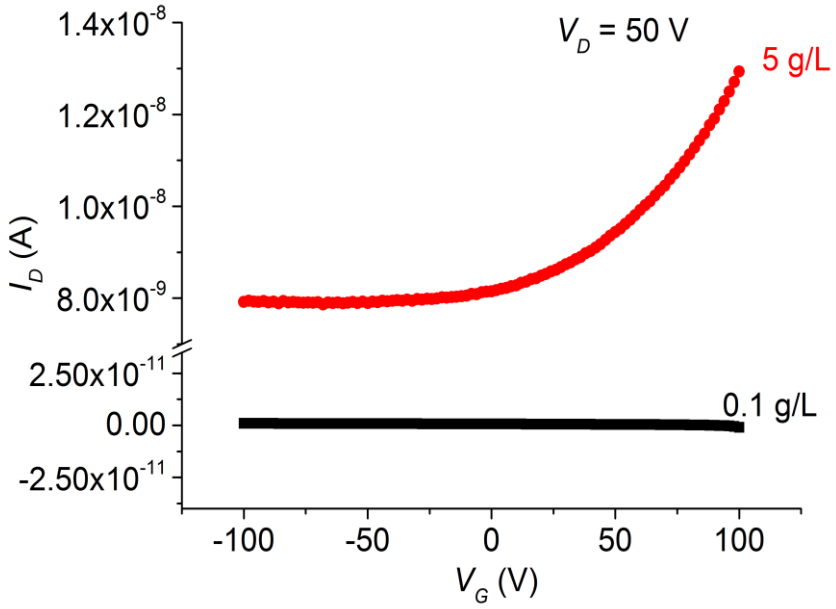

Figure 4.2.6.2: Transfer characteristic curves of devices fabricated by 0.1 g/L and 5 g/L F_4TCNQ solution on bare alumina substrate.

4.3 Doping by 0.5 g/L F4TCNQ solution on monolayer device made with TCNQ

Monolayer devices fabricated by solution containing both EDT-DMT-TTF-C_9-PA and TCNQ were also doped by 0.5 g/L F_4TCNQ solution to test the FET performance under F_4TCNQ doping. The output and transfer characteristic curves are shown in figure 4.3.1. Even the performance of these devices is much worse than monolayer devices fabricated by pure EDT-DMT-TTF-C_9-PA solution, the performance after doping was not so much different. P-type mobility was calculated at $2.12 \times 10^{-6}\ cm^2V^{-1}s^{-1}$ and n-type mobility was calculated at $9.57 \times 10^{-6}\ cm^2V^{-1}s^{-1}$. V_{min} appears at -32 V and -10 V for drain voltages -50 V and 50 V, respectively. Though the p-type mobility is lower than device fabricated by pure solution under the same doping concentration ($5.22 \times 10^{-6}\ cm^2V^{-1}s^{-1}$), the n-type mobility of this device is pretty close to that made from pure solution ($1.04 \times 10^{-5}\ cm^2V^{-1}$). This result indicates that the monolayer quality isn't so different from the monolayer fabricated by pure solution and the performance decrease of the undoped device should be attributed to the existing

TCNQ inside the monolayer, working as impurities. This impurity state seems to become insignificant when F_4TCNQ remove the electrons on TCNQ.

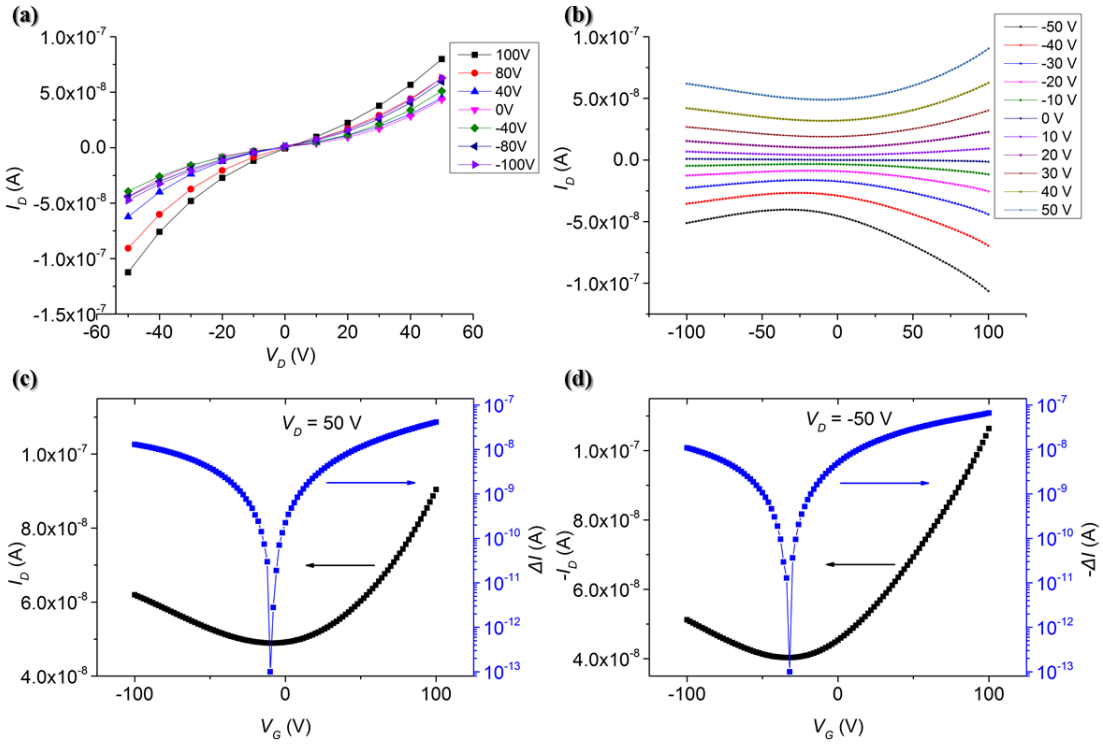

Figure 4.3: output characteristic curves (a) and transfer characteristic curves (b) of monolayer device fabricated by 10^{-3} M EDT-DMT-C_9-PA solution with TCNQ and doped by spin coating of 0.5 g/L F_4TCNQ solution. c) I_D-V_G curve and ΔI-V_G curve at drain voltage 50 V. d) I_D-V_G curve and ΔI-V_G curve at drain voltage -50 V.

4.4 Discussion

We know F_4TCNQ doping will induce charge-transfer and remove electrons from the monolayer. In other word, holes with positive charge will be injected into the monolayer. With significant number of holes existing in the monolayer device channel, the off-state will be hard to be achieved with gate electric field in a normal FET configuration.

F_4TCNQ have already been used as dopants for several p- and n-type OFET devices based on materials such as P3HT(Poly(3-hexylthiophene))[4], C8-BTBT(2,7-Dioctyl[1]benzothieno[3,2-b][1]benzothiophene)[5], pentacene and F16CuPc(Copper(II) -hexadecafluoro-29H,31H-phthalocyanine)[1]. In all these reports, F_4TCNQ doping to any of these p-type FETs did not induce n-type behavior. For instance, Yamagishi *et al.* reported the doping behavior of F_4TCNQ to p- and n- type FET devices made by

pentacene and F16CuPc[1]. In their experiment, for p-type FET devices fabricated by pentacene, increase of F_4TCNQ doping concentration enhanced the performance of FET device with threshold voltage shifting towards positive direction and no n-type behavior appeared. For n-type FET devices fabricated by F16CuPc, doping by F_4TCNQ decreased the performance of n-type device with threshold voltage again shifting towards positive direction. These doping effects are attributed to hole doping and electron trapping for p- and n-type devices, respectively. It is a common result that for both p- and n-type devices, doping by F_4TCNQ will shift the threshold voltage towards positive direction.

But for doped EDT-DMT-C_9-PA monolayer device, the same explanation doesn't

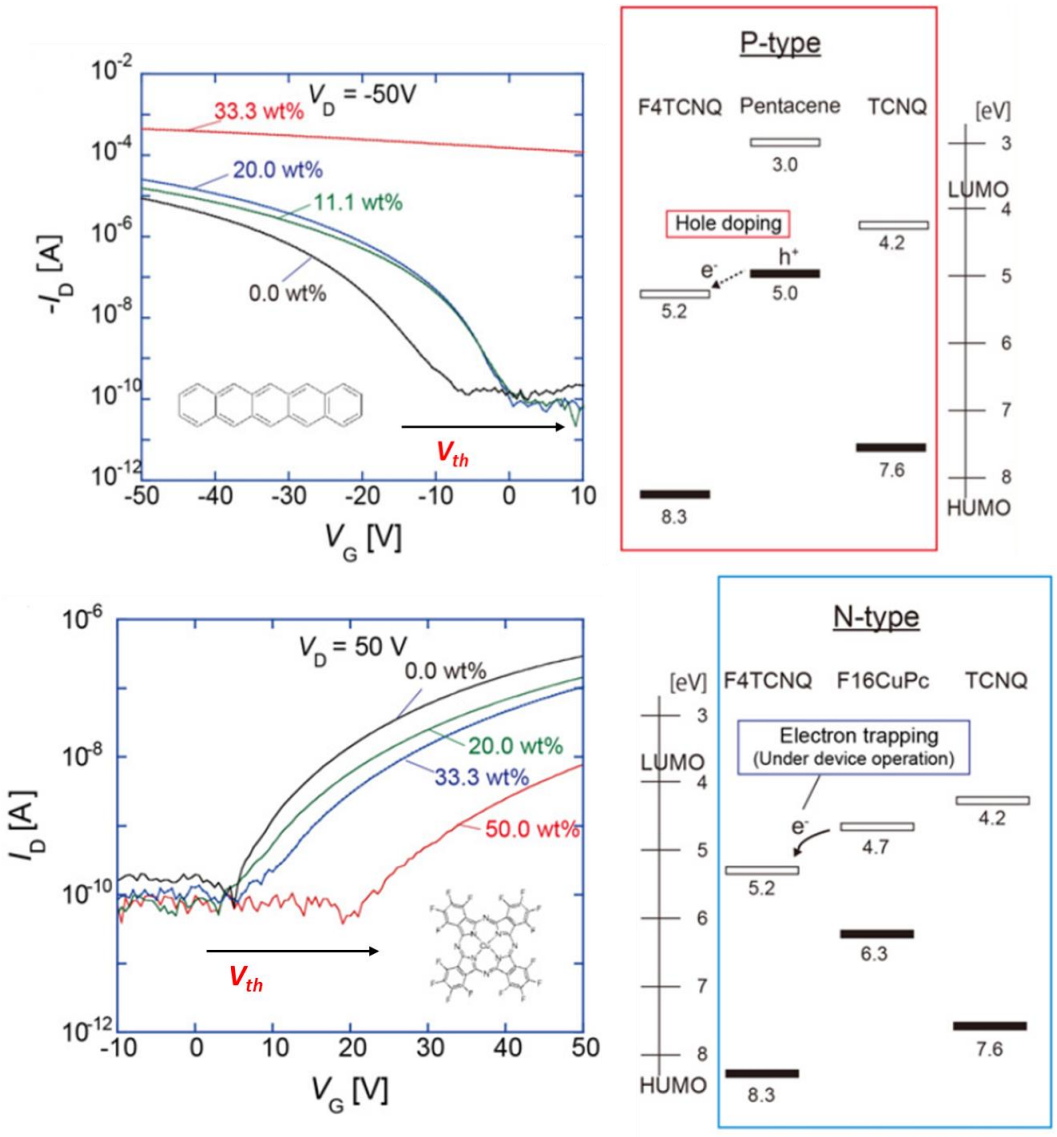

Figure 4.4.1: Doping effects of F_4TCNQ on p-type FET device fabricated by pentacene and n-type FET device fabricated by CuPc. The mechanism of these doping effects are shown by briefed energy diagram.[1]

work anymore. N-type behavior is not due to F_4TCNQ itself, because n-type FET behavior was observed even at a low doping concentration such as 0.1 g/L. V_{min} for each doping concentration is listed in table 4.4.1, and this V_{min} keeps shifting towards negative direction together with the increase of doping concentration, exactly the contrary to the doping behavior of normal semiconductor FET devices. These facts indicated the FET working mechanism should be different from ordinary semiconductor FET devices.

Table4.4.1: Threshold voltage at drain voltage 50 V and -50 V for different concentration of solution used for doping.

Doping solution concentration (g/L)	0.05	0.1	0.25	0.5	1	5
V_{min} (V) when V_D = 50 V	100	88	44	28	18	-14
V_{min} (V) when V_D = -50 V	78	12	-2	-12	-38	-84

Considering these monolayer FET channels are built with EDT-DMT-TTF monolayer and F_4TCNQ dopants that injects holes to the monolayer, a possible Mott-insulating state in this device can be discussed. In a Mott FET fabricated by κ-type BEDT-TTF cation radical crystals, hole carriers are existing in the conductive layer made of BEDT-TTF, but an insulating state is achieved at band filling of 0.5. Only at this band filling, the moving of carriers are stopped by Coulomb repulsion. It is plausible that Coulomb repulsion plays a similar role in the present doped monolayer FET devices and the ambipolar behavior comes from the Mott-insulating state, the same mechanism as Mott FET devices based on κ-type BEDT-TTF cation radical crystals. It seems that the present devices performance is coming from parallel and/or serial connection between non-doped p-type FET and doped Mott-FET moieties.

If the doped monolayer was homogeneous, Mott insulating state should be reached at some constant gate-voltage which was determined by band-filling. On the other hand, F_4TCNQ dopants cannot be observed as grains by AFM under all measured doping concentration, while micro crystals appeared at 1 g/L F_4TCNQ spin coated FETs and can be observed with microscope. This may indicate that the doping is not homogeneous, so that each doped monolayer device could be considered Mott FETs with different band-filling and this is connected to the absence of off state in a doped monolayer device. Since each small Mott FETs have different gate voltage which make

their band filling located at exact 0.5, V_{min} for every small Mott-FET is different to each other to result in a poor off state as a whole.

4.5 Summary

In this section, monolayer devices made by 10^{-3} M pure EDT-MDT-TTF-C_9-PA solution was doped by spin coating of F_4TCNQ solution with different concentrations. P-type FET behavior was enhanced and n-type behavior was induced by F_4TCNQ doping. This n-type FET behavior didn't come from the spin coated F_4TCNQ layer but come from the doped EDT-DMT-TTF monolayer.

When compared to F_4TCNQ doping effects on some reported devices made by organic semiconductor materials such as P3HT, C_8-BTBT, pentacene and F16CuPc, two important facts should be noticed as below:

1. The increase of doping concentration will shift the V_{min} towards *negative* direction, while in ordinary organic FETs it should shift towards positive direction.
2. N-type behavior appears at very low doping concentration such as 0.1 g/L, while in ordinary p-type organic FETs n-type behavior does not exist.

These two behaviors indicated this doped monolayer FET device must have a different working mechanism and this type of doped device could probably be a Mott FET.

4.6 Reference

(1) Yamagishi, Y.; Noda, K.; Yamada, H.; Matsushige, K. *Synthetic Met* **2012**, *162*, 1887.

(2) Sakai, M.; Sakuma, H.; Ito, Y.; Saito, A.; Nakamura, M.; Kudo, K. *Phys Rev B* **2007**, *76*, 045111.

(3) Hasegawa, T.; Mattenberger, K.; Takeya, J.; Batlogg, B. *Phys Rev B* **2004**, *69*, 245115.

(4) Lu, G.; Blakesley, J.; Himmelberger, S.; Pingel, P.; Frisch, J.; Lieberwirth, I.; Salzmann, I.; Oehzelt, M.; Di Pietro, R.; Salleo, A. *Nature communications* **2013**, *4*, 1588.

(5) Soeda, J.; Hirose, Y.; Yamagishi, M.; Nakao, A.; Uemura, T.; Nakayama, K.; Uno, M.; Nakazawa, Y.; Takimiya, K.; Takeya, J. *Adv Mater* **2011**, *23*, 3309.

Part 5 Temperature dependence

5.1 General introduction

Normally, in a semiconductor-based FET device, the resistance of device will decrease with increasing temperature. The reason is connected to the conduction mechanism: with higher temperature, more electrons (carriers) are excited by thermal energy to hop from valence band to conduction band and make the carrier number increase (resistance decrease). On the other hand, in a metal, since the resistance comes from the scattering of electrons, the temperature dependence of resistance shows opposite behavior. When temperature rises, increase of the kinetic energy of electrons and phonons will result in a higher scattering rate and create higher resistance. On the contrary, decreasing temperature will reduce scattering rate of electrons and result in decrease of resistance. These temperature dependent behaviors of semiconductor and metals are diametrically opposed to each other.

In reported organic Mott FETs fabricated with κ-type BEDT-TTF cation radical crystals, scientists are not only interested in the device performance, but also care about some fundamental physical behaviors. As mentioned in the first section, κ-Br crystals appear as an insulator at room temperature, and transfers into metal at about 50 K under ambient pressure. In reported devices, electrostatic doping by applying gate voltage can be used to modify this Metal-Insulator transition and insulator-superconductor transition[1-4].

Despite the direct metal/insulator behavior does not exist in the present device, measurement of the temperature dependence of resistance, which can be analyzed by Arrhenius plot to extract activation energy etc., is also meaningful. Such measurements can tell several fundamental physical issues of this doped monolayer FET device.

5.1.1 Arrhenius plot and Meyer-Neldel rule

In 1889, Swedish scientist Arrhenius proposed the Arrhenius equation to explain the temperature dependence of reaction rates:

$$k = Ae^{\frac{-E_a}{RT}} \tag{1}$$

or:

$$\ln(k) = \ln(A) - \frac{E_a}{R} \cdot \frac{1}{T} \tag{2}$$

,where k is rate constant, T is absolute temperature, A is a pre-exponential factor, E_a is activation energy and R is universal gas constant. Since universal gas constant R has a relationship with Boltzmann constant k_B, in which $R = N_A \cdot k_B$, the Arrhenius equation can be written as:

$$k = Ae^{\frac{-E_a}{N_A k_b T}} \tag{3}$$

or

$$\ln(k) = \ln(A) - \frac{E_a}{N_A \cdot k_B} \cdot \frac{1}{T} \tag{4}$$

,where N_A is Avogadro constant.

According to this equation, an Arrhenius plot requires a logarithm of kinetic constants as vertical axis and inverse of temperature as horizon axis. It is very useful to determine activation energy in a given process. In semiconductor materials, it can be used to trace the resistivity or conductivity and extract the activation energy. The equation can be write as:

$$\sigma = \sigma_0 e^{-\frac{E_a}{k_b} \cdot \frac{1}{T}} \tag{5}$$

Where σ is the conductivity and σ_0 is a constant. When T is infinite, $\lim_{T\to\infty} \frac{1}{T} = 0$ can be put forward, and $\lim_{T\to\infty} e^{\frac{-E_a}{N_A k_b} \cdot \frac{1}{T}} = 1$, to give $\sigma = \sigma_0$. This indicates that σ_0 is the conductivity minimum at high temperature limit.

In many real semiconductors, however, Arrhenius plot cannot be fitted and Meyer-Neldel rule which was pointed by Meyer for semiconducting oxides such as UO_2, Fe_2O_3, ZnO and TiO_2[5-8] can be applied:

$$\ln(A) = \alpha E_a + \beta \tag{6}$$

This relation is so called the Meyer-Neldel rule. Later research on organic semiconductors by Gutmann and Lyons in 1967 discussed the universality of this equation[9]. One year later, Rosenberg *et al.* integrated both (5) and (6) equations into:

$$\sigma = \sigma_{00} e^{\frac{E_a}{k_B T_{MN}}} e^{-\frac{E_a}{k_B T}} \tag{7}$$

and

$$\sigma_0 = \sigma_{00} e^{\frac{E_a}{k_B T_{MN}}} \tag{8}$$

,where σ_{00} is a constant pre-factor and T_{MN} is so called Meyer-Neldel temperature. Moreover,

$$E_{MN} = k_B T_{MN} \tag{9}$$

where E_{MN} is the Meyer-Neldel energy can be derived. In these equations, a

characteristic temperature T_{MN} with corresponding energy E_{MN} is introduced. A common cross point should exist when temperature T is equal to Meyer-Neldel temperature T_{MN}. Even though the Meyer-Neldel rule have been observed in "a wide variety of physical, chemical and biological processed"[10], the microscopic origin of Meyer-Neldel rule and the physical meaning of Meyer-Neldel energy are still under discussion. Despite these physical theories, Meijer *et al.* certificated the applicability of Meyer-Neldel rule in organic FETs.[10]

5.2 Temperature dependence

Three independent monolayer devices were doped by 0.5 g/L F_4TCNQ solution and cooled to 180 K. Transfer characteristic curve was measured at drain voltage 50 V with rising temperature by 10 K step. Generally, the devices were not conductive under 180 K. Metallic behavior was not observed at any range of temperature. This is probably due to the contact resistance between monolayer grains since the grain size is expected to be smaller than the channel length. Transfer characteristic curves of different temperature ranging from 180 K to 300 K are shown in Figure 5.2.1.

The performance of three devices were roughly similar, and the off current rose from 10^{-10} A to 10^{-7} A during a warming up process from 180 K to 300K. The FET behavior existed throughout the whole measurement area from 180 K to 300 K.

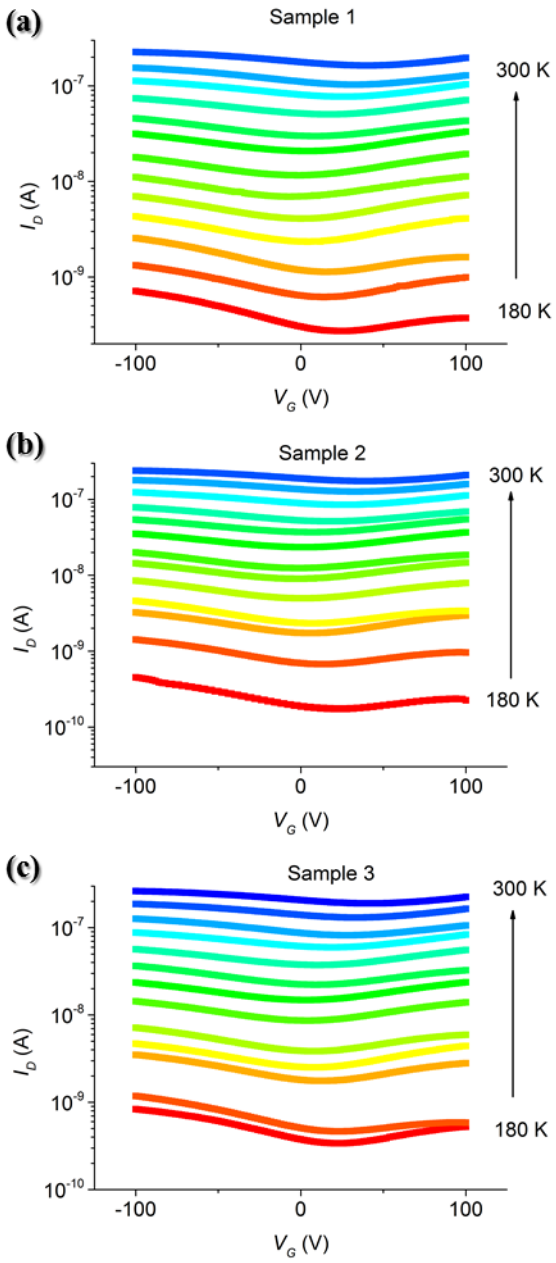

Figure 5.2.1: Temperature dependent transfer characteristic curves of three different monolayer devices doped by 0.5 g/L F_4TCNQ solution under drain voltage 50 V. All these devices showed semiconductor behavior.

5.3 Results of Arrhenius plot and Meyer-Neldel rule

5.3.1 Results of Arrhenius plot and Meyer-Neldel rule in p-type region

According to all three plots, gate voltage ranging from 20 V to -100V were considered on p-type region, and 30V to 100 V were considered n-type. With these three samples, Arrhenius plot were performed in p-type region. Results of three different samples are shown in figure 5.3.1.1. Though we could not get rid of the off current which made the fitting lines densely located with each other, a clear common crossing point were observed for all samples, which indicated Meyer-Neldel rule is suitable for p-type region. Common crossing points for 3 samples were located at about 416K, 444K and 437K. Thus, Meyer-Neldel energy were calculated at 36meV, 38 meV and 38 meV for sample 1, 2 and 3, respectively. These value were very close to reported OFET materials such as dihexyl-sexithiophene (E_{MN}≈43 meV)[11], pentacene (38 meV[10] or 34 meV[12]), PTV (poly(thiophenevinylene)) (42 meV[10] or 35 meV[12]) and C_{60} (E_{MN} ≈ 36 meV)[13,14].

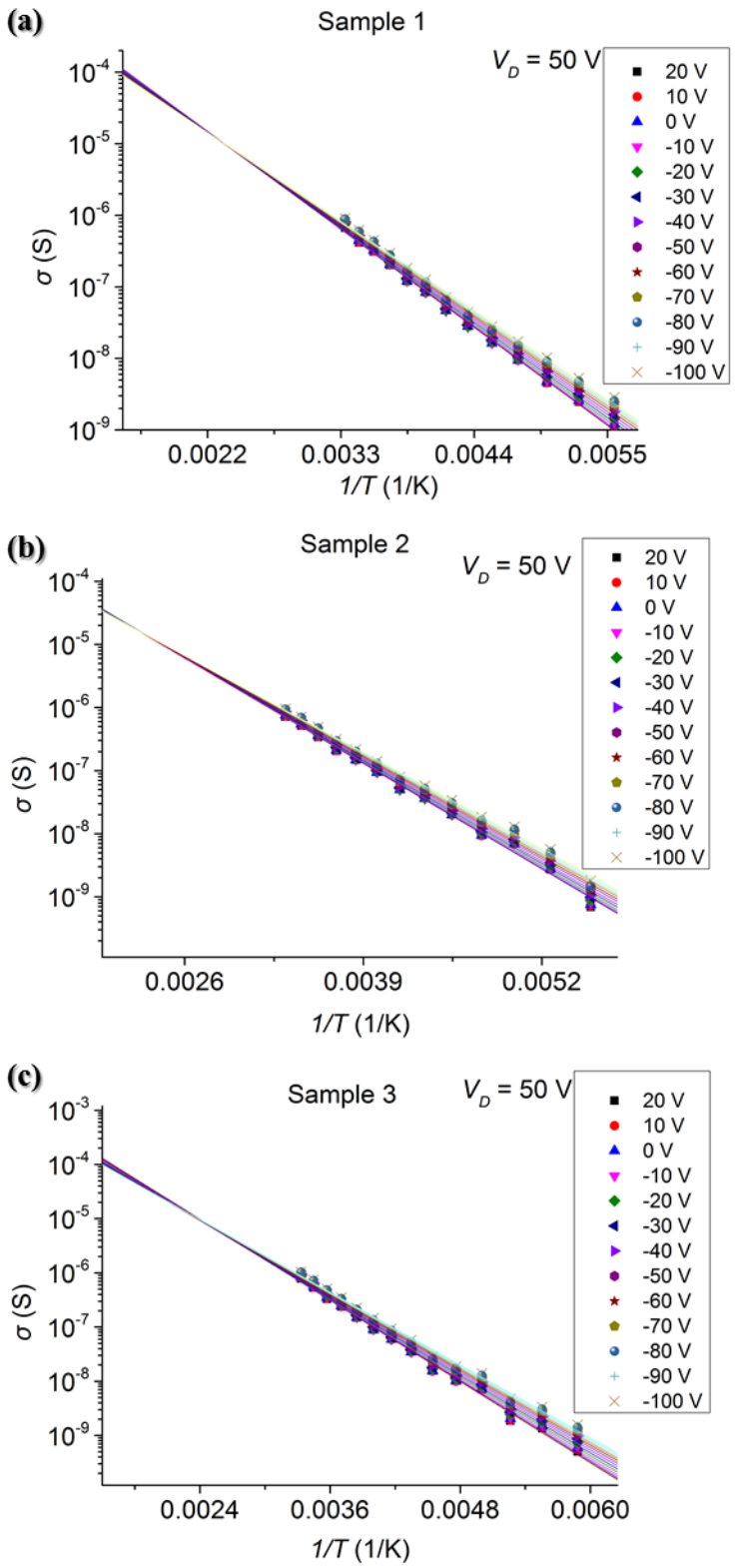

Figure 5.3.1.1: To three independent samples Arrhenius plot were investigated for p-type region. Common cross point can be observed in all three plots.

5.3.2 Result of Arrhenius plot and Meyer-Neldel rule in n-type region

With the three samples, Arrhenius plot was also performed in n-type region with drain voltage of 50 V. Results of three different samples are shown in figure 5.3.2.1.

In all cases, no common crossing point can be observed, which indicated Meyer-Neldel rule seems not applicable to n-type region.

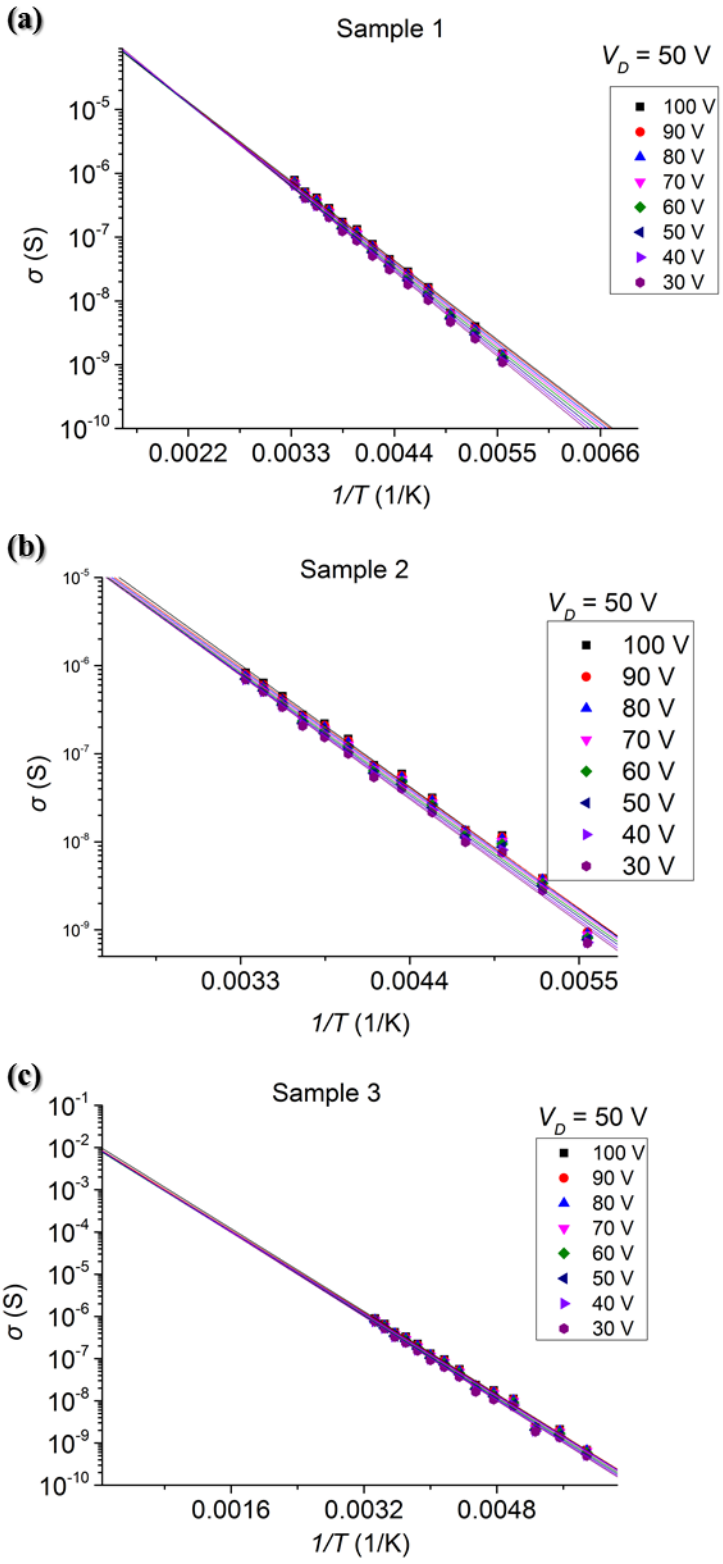

Figure 5.3.2.1: To three independent samples Arrhenius plots were investigated for n-type region. No common cross point can be observed in all three plots.

5.3.3 Activation energy and conductivity limit

Since the Meyer-Neldel rule was not suitable for n-type region, conductivity limit σ_0 and activation energy E_a were extracted and plotted against gate voltage, whose results are shown in figure 5.3.3.1. For all three samples, σ_0 and E_a exhibit a peak at gate voltage of about 10 V, 0 V and 20 V for sample 1, 2 and 3, respectively. For p-type region, both conductivity limit σ_0 and activation energy E_a kept decreasing with increasing gate voltage. But for n-type region, both of them decreased and then turned to increase for all three samples.

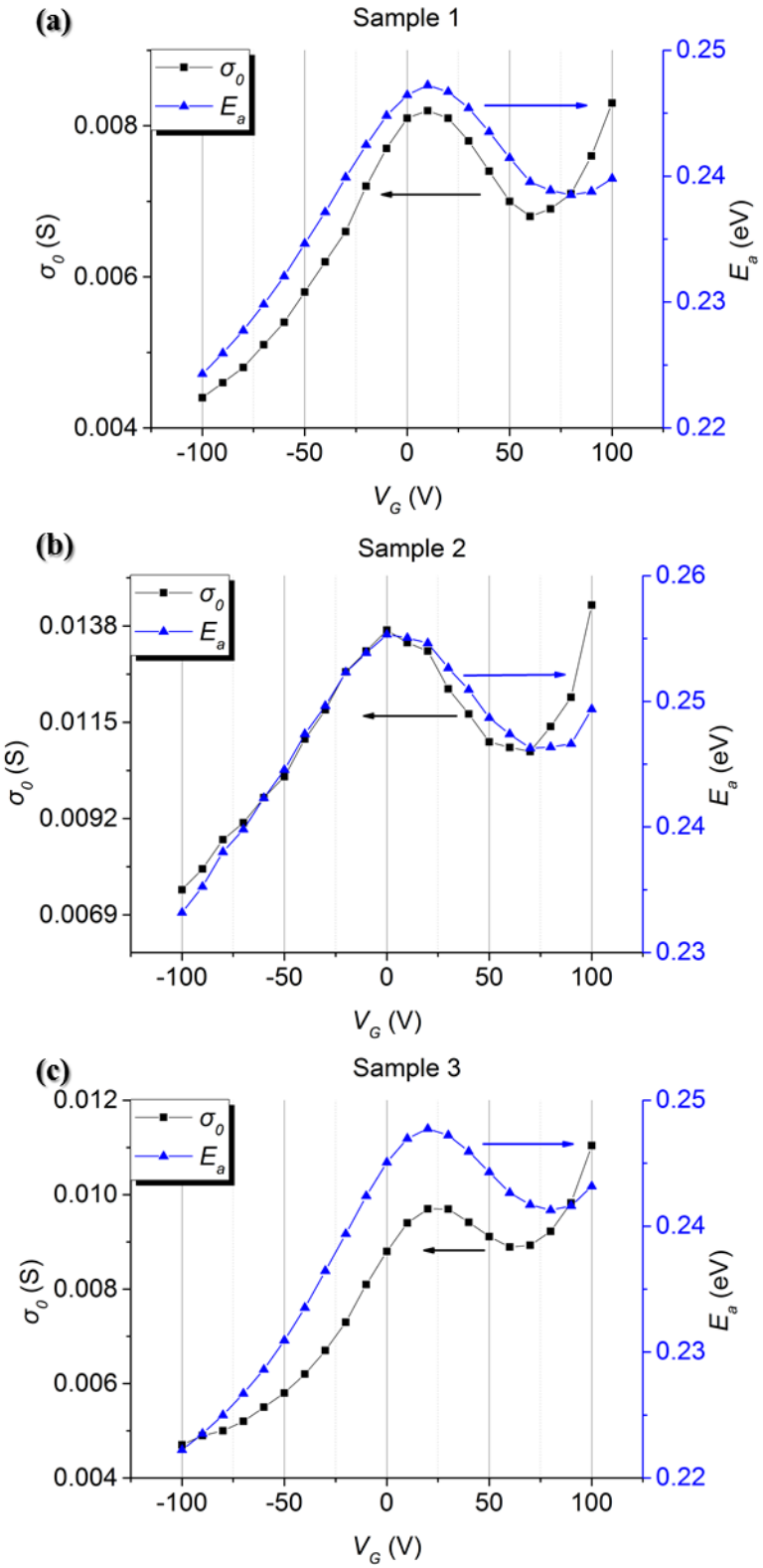

Figure 5.3.3.1: Gate voltage related conductivity limit σ_0 and activation energy E_a extracted from Arrhenius plots of three independent samples.

5.4 Discussion

All three samples showed similar behavior, indicating the analyzed features are not related to sample dependence but are connected to the fundamental issues of this type of device.

For an organic semiconductor-based FET device, the conducting mechanism is normally based on hopping of carriers, and the activation energy is determined by the energy difference between HOMO or LUMO energy level and Fermi level for p- and n-type FETs, respectively. It is understood that in an ordinary FET device, activation energy should keep decreasing with the continually increasing of gate voltage.

On the other hand, in a FET device using Mott insulator as channel, the half-filled conduction band separated into Upper Hubbard band and Lower Hubbard band because Coulomb repulsion forms the insulating phase. Application of gate voltage will inject carriers into the insulating channel, and the band-filling changes from 0.5. This band filling change is known to induce a phase-transition to merge Upper Hubbard band and Lower Hubbard band into one. With band-filling shifting, the Coulomb repulsion will be effectively suppressed, and UHB and LHB will also be affected. This behavior is known to create a pseudo gap. In 2016, Kawasugi *et al.* reported the existence of pseudo gap in a κ-type BEDT-TTF salt[15]. As this pseudo gap is changing its shape during electronic doping, the noncompliance of Meyer-Neldel rule in n-type region could be associated with this phenomenon, if this doped monolayer in FET device is a doped Mott insulator. Since the precondition of Meyer-Neldel rule is the stationary band structure during electronic doping, band structure of Mott-insulating monolayer with pseudo gap will not satisfy the requirement for Meyer-Neldel rule.

Figure 5.3.4.1 showed the expected working mechanism of this type of monolayer device. For an undoped monolayer device, the EDT-DMT-TTF core should have fully-occupied HOMO band and empty LUMO band (band insulator). Doping with F_4TCNQ to this monolayer will remove electrons from the HOMO band. If the every two EDT-DMT-TTF cores are forming a dimer in which the HOMO band will separated into antibonding orbital and bonding orbital, a Mott-insulating state will be realized with +0.5 valent molecule. Since the energy level of antibonding orbital is higher than bonding orbital, one electron in antibonding orbital will first be extracted and a half-filled antibonding band will be formed. The Coulomb repulsion separates this antibonding orbital into UHB and LHB, and create a Mott insulating phase. If EDT-DMT-TTF appears independently as monomer, giving out one electron to F_4TCNQ will also create a half-filled HOMO band, to make the Coulomb repulsion separate this half-filled HOMO band into UHB and LHB again. In both dimer and monomer case, to

realize the Mott insulating phase, precise control of the molecular oxidation state to be homogeneous is very important. In this doped monolayer device, since we could not perfectly control the doping to be homogeneous, off state as a Mott insulator was not realized in all area of the channel at the same time. The whole device was considered made up of several small Mott FETs with different band-filling and the ambipolar behavior comes from the shift of band-filling during electrostatic doping.

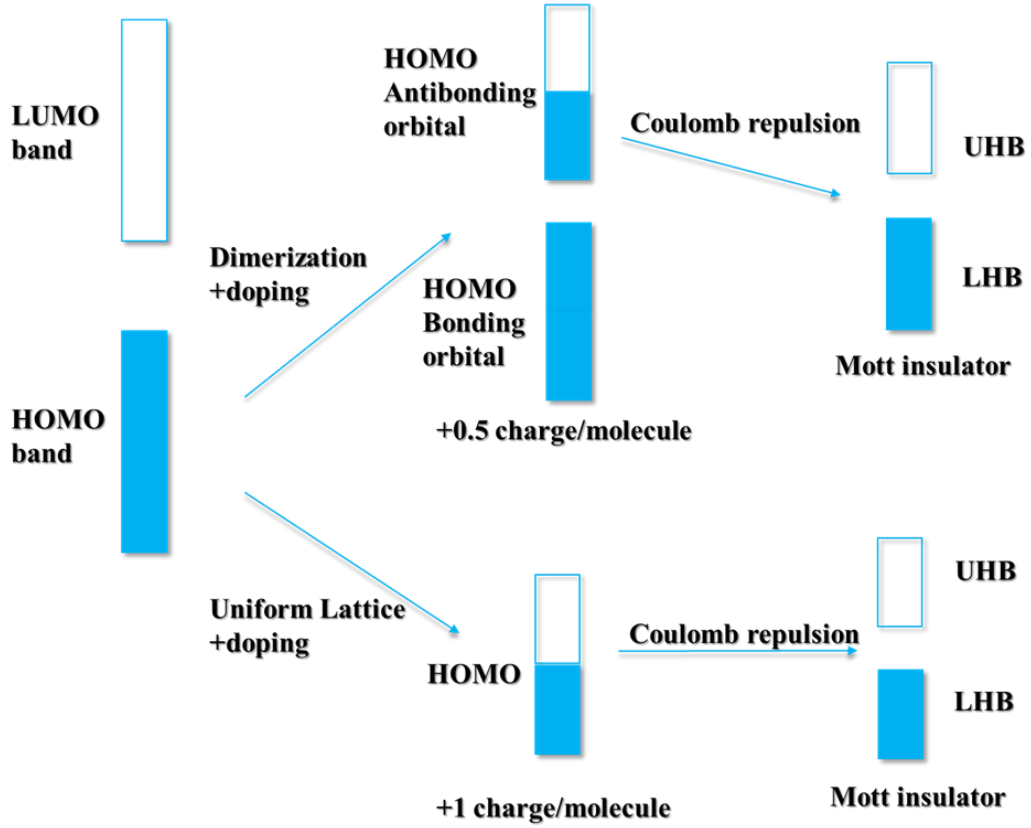

Figure 5.3.4.1: Electronic energy diagram of this type of device.

If one considers the relationship between activation energy and valence of EDT-DMT-TTF core (band filling), a neutral monolayer is a semiconductor (band insulator) at the beginning. Doping to this monolayer will reduce the activation energy because the Fermi energy will approach the mobility edge. On the other hand, when the band filling gets close to + 0.5 value, a Mott insulating phase will become another cause of an activation energy increase. Further doping to empty band, will result in another band insulator (semiconductor) phase when the two electrons in the antibonding orbital of HOMO band are removed. A brief relationship between band filling and activation energy is drawn as figure 5.3.4.2. For the three devices measured, since n-type electronic doping will increase the activation energy at higher gate voltages, the valence of EDT-DMT-TTF core may be located in areas to the left part of valence between 0 and 0.5.

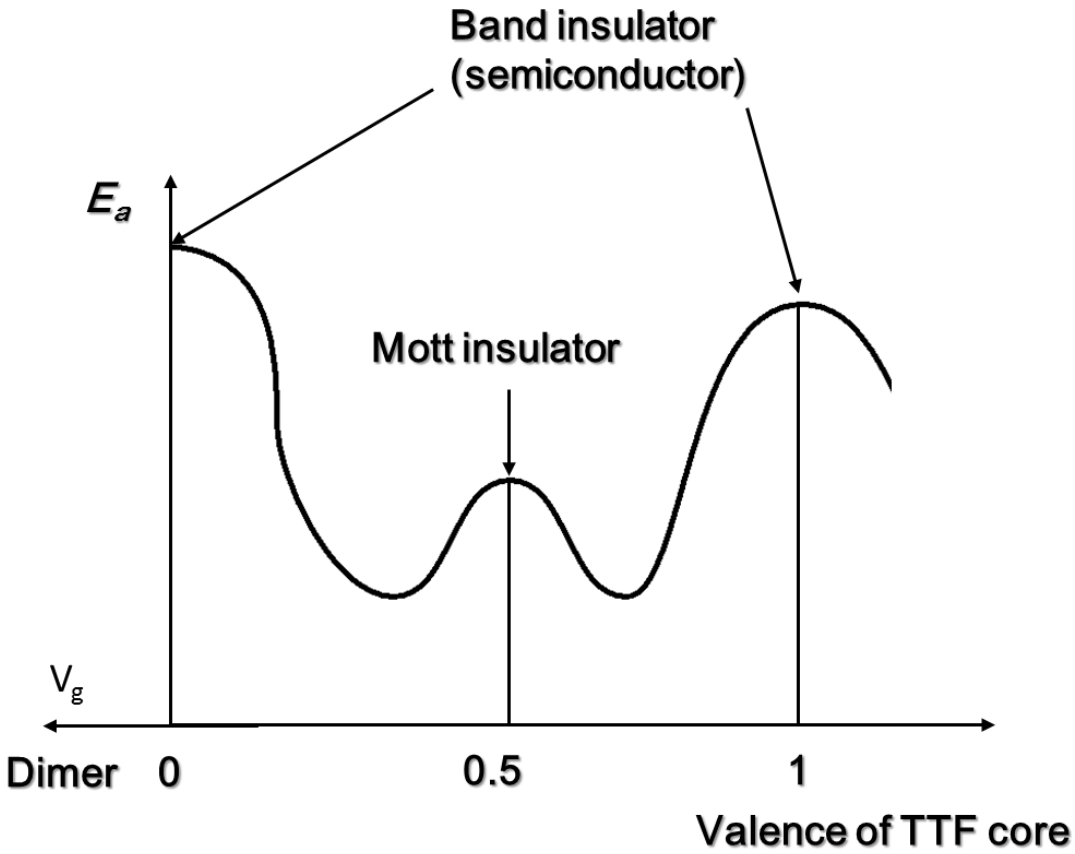

Figure 5.3.4.2: Brief phase diagram of band filling and activation energy for dimerized monolayer.

5.5 Summary

In this part, temperature dependencies of the resistance for three independent monolayer devices doped by 0.5 g/L F_4TCNQ solution were measured. Arrhenius plots were performed to extract the conductivity limit σ_0 and activation energy E_a. In all three samples, Arrhenius plots on n-type region didn't follow Meyer-Neldel rule, indicating the absence of a stationary energy band, which could probably be attributed to pseudo gap behavior. Since pseudo gap was calculated to be existing in κ-type BEDT-TTF cation radical crystals, the doped monolayer was also expected to be a Mott insulator with pseudo gap at n-doped region. In gate voltage dependencies of activation energy curves, activation energy turned to increase in high positive gate voltage region. This can be also explained by the same picture. The designed working mechanism of this doped monolayer device has been reviewed and a brief and hypothetical diagram of molecular valence and activation energy was drawn for understanding of the present system.

5.6 Reference

(1) Yamamoto, H. M.; Nakano, M.; Suda, M.; Iwasa, Y.; Kawasaki, M.; Kato, R. *Nat Commun* **2013**, *4*, 2379.

(2) Suda, M.; Takashina, N.; Namuangruk, S.; Kungwan, N.; Sakurai, H.; Yamamoto, H. M. *Adv Mater* **2017**.

(3) Suda, M.; Kato, R.; Yamamoto, H. M. *Science* **2015**, *347*, 743.

(4) Sato, Y.; Kawasugi, Y.; Suda, M.; Yamamoto, H. M.; Kato, R. *nano lett*, **2017**, *17*, 708.

(5) Meyer, W. *Z. Physik* **1933**, *85*, 278.

(6) Meyer, W. *Z Tech Phys* **1935**, *16*, 355.

(7) Meyer, W.; Neldel, H. *Z. tech. Phys* **1937**, *18*, 588.

(8) Meyer, W. *Z. Elektrochem.* **1944**, *50*, 274.

(9) Gutmann, F.; Lyons, L. E. *Organic semiconductors*; Wiley, 1967.

(10) Meijer, E.; Matters, M.; Herwig, P.; De Leeuw, D.; Klapwijk, T. *Appl Phys Lett* **2000**, *76*, 3433.

(11) Horowitz, G.; Hajlaoui, R.; Delannoy, P. *Journal de Physique III* **1995**, *5*, 355.

(12) Brown, A.; Jarrett, C.; De Leeuw, D.; Matters, M. *Synthetic Met* **1997**, *88*, 37.

(13) Wang, J.; Chen, Y. *Appl Phys Lett* **1998**, *73*, 948.

(14) Paloheimo, J.; Isotalo, H.; Kastner, J.; Kuzmany, H. *Synthetic Met* **1993**, *56*, 3185.

(15) Kawasugi, Y.; Seki, K.; Edagawa, Y.; Sato, Y.; Pu, J.; Takenobu, T.; Yunoki, S.; Yamamoto, H. M.; Kato, R. *Nature communications* **2016**, *7*, 12356.

Part 6 Concluding remarks

In this thesis, fabrication of a monolayer Mott FET which is mimicking a single layer of κ-type BEDT-TTF crystal has been described.

In part 1, the research background and future prospects of organic semiconductors are described together with a brief introduction of an organic Mott insulator such as κ-type BEDT-TTF cation radical crystal. Normal and Mott-insulating organic materials are both able to be utilized in FET devices, but the switching mechanisms of these type of devices are quite different. The objective of this research, creating a monolayer Mott insulator FET device which works at room temperature, has been discussed.

In part 2, the molecular design to fabricate a self-assembled monolayer was described. To an EDT-DMT-TTF skeleton a C_9 alkyl chain with phosphonic acid was connected. This designed molecule was synthesized and reacted with alumina substrate to form a monolayer under various conditions. The monolayer fabrication process was discussed. Pre-doped monolayer fabrication was also attempted.

In part 3, the FET performance of fabricated monolayer device was checked. An undoped monolayer FET device offered a low hole mobility of $5.54 \times 10^{-7}\ cm^2V^{-1}s^{-1}$. In pre-doped monolayer device, both TNCQ and F_4TCNQ doping made the performance of the fabricated monolayer device even worse. Mott insulator phase could not be realized by this pre-doping.

In part 4, acceptor molecule F_4TCNQ was used to dope the monolayer devices and ambipolar behavior was induced by this F_4TCNQ doping. This ambipolar FET device was found to be different from ordinary semiconductor FETs for two reasons. First, doping to a p-type FET induced ambipolar behavior, which has never been seen in other p-type organic FETs. Second, the V_{min} which is the separation point of p- and n-type behavior was shifting towards negative direction with increasing dopant amount, which is exactly on the contrary to ordinary organic FET devices. These facts indicated that the doped monolayer device was not a normal FET device but was showing a different switching mechanism to ordinary semiconductor FETs.

In part 5, temperature dependence was checked. In all three independent monolayer devices doped by 0.5 g/L F_4TCNQ solution, the same temperature dependent behavior was observed. Although the data quality was moderate, the reproducibility of this result indicated that the observed feature was a common behavior of this doped monolayer device. Unlike FETs based on cation radical crystals made of BEDT-TTF, metallic-behavior was not observed even at low temperature, probably because of the large trap state density and contact resistance of monolayer grains. Arrhenius plots

afforded gate-voltage dependency of the conductivity limit and activation energy. In all three devices, these two parameters increased in highly positive gate voltage region, which cannot be explained by traditional band theories. At the same time, the data did not obey Meyer-Neldel rule, indicating a non-stationary band structure changing with electronic doping which could probably be attributed to a pseudo gap formation. Since pseudo gap is a typical phenomenon for doped Mott-insulators such as κ-type BEDT-TTF–based FETs, the present results are indicating that doped monolayer device is a Mott FET. The large off current can be attributed to the inhomogeneous doping since the band-filling of every single molecule in the active layer cannot be precisely controlled at exactly 0.5.

Throughout these works, a monolayer which could be doped into a doped Mott insulator was achieved. These results would provide possibilities to observe clear Mott transition and even superconducting transition in such kind of monolayer devices in the future.

List of publications

Chapter 1-6

Fabrication and Operation of Monolayer Mott FET at Room Temperature.

Yang F.; Suda M. and Yamamoto H. M. *Bull. Chem. Soc. Jpn.* **2017**, 90, 1259-1266.

Acknowledgement

This doctoral thesis is a summary of author's study that have been carried out under the supervision of Prof. Dr. Hiroshi Yamatomo at Research Center of Integrative Molecular Systems (CIMoS), Institute for Molecule Science.

My heartfelt appreciation goes to Prof. Dr. Hiroshi Yamatomo who guided me to a fruitful academic life with appropriate advices and a deep understanding.

I deeply thank to Assistant Prof. Dr. Masayuki Suda (Research Center of Integrative Molecular Systems, Institute for Molecule Science) whose kind assistance and suggestions made a large contribution to my work.

I feel a deep gratitude to Assistant Prof. Dr. Kenta Kawaguchi (Research Center of Integrative Molecular Systems, Institute for Molecule Science) for his kind discussion into some physical problems.

And I thank to Dr. Mikio Uruichi (Research Center of Integrative Molecular Systems, Institute for Molecule Science) for measurements of some single crystals and Raman spectra.

I would like to express my deep thanks to Prof. Dr. Ikuyoshi Tomita (Electronic Chemistry, Tokyo Institute of Technology) for his help of the student status. I also deeply thank to Prof. Dr. Yoshiro Yamashita (Electronic Chemistry, Tokyo Institute of Technology, retired) for he kindly educated my synthetic technique that was helpful to advance my study.

I very thank to all members of our laboratory for their kind assistance and warm encouragement.

Finally, I would like to express my sincere gratitude to my wife, Weiyi Li who constantly encouraged me. Her support made it possible to complete this work.

November 20, 2017

Fan Yang